Multidisciplinary Analysis and Optimization under Uncertainty

By

Chen Liang

Dissertation

Submitted to the Faculty of the

Graduate School of Vanderbilt University

in partial fulfillment of the requirements

for the degree of

DOCTOR OF PHILOSOPHY

in

Civil Engineering

May, 2016

Nashville, Tennessee

Approved: Date:

_____ _____
Professor Sankaran Mahadevan

_____ _____
Professor P. K. Basu

_____ _____
Professor Mark N. Ellingham

_____ _____
Professor Mark P. McDonald

_____ _____
Professor Dimitri Mavris

_____ _____
Professor Roger Cooke

To my father Dehong, mother Shiping and cousin Yingli

ACKNOWLEDGEMENT

I would like to express my utmost gratitude to my adviser Professor Sankaran Mahadevan, for his knowledge, insight and work ethic that have been a great value to my dissertation and graduate life. He showed me how to think, work, write and talk professionally, which is a tremendous inspiration and invaluable guidance for my future career. I am thankful for his indescribable patience and enormous support, and am looking forward to continuing our relationship during my professional career.

I would like to convey my sincere appreciation to my committee members, Professors Prodyot Basu, Mark Ellingham, Mark McDonald, Dimitri Mavris and Roger Cooke. Their knowledge, lectures, insights and feedback have motivated me and offered precious contributions to this dissertation. I would also like to express my gratitude to Dr. Anca Hanea from University of Melbourne and Dan Ababei at LightTwist Software for the gracious time and effort they spent passing on their wealth of knowledge about copulas.

I am grateful to have the opportunities to work with several brilliant students and postdoctoral fellows at Vanderbilt. In particular, I thank Dr. Sirisha Rangvajhala for mentoring me and offering me her profound knowledge in optimization and aeroelasticity. I thank Dr. Shankar Sankararaman for his outstanding mentorship in multidisciplinary analysis and uncertainty quantification. I thank Dr. You Ling for his generous academic help and personal friendship. I also thank Dr. Vadiraj Hombal for teaching his programming expertise.

This dissertation could not have been accomplished without the unconditional love and support from my father, my mother and all family members. I am also thankful for the friendships I made with Ghina Nakad, Josh Mullins, Erin Decarlo, Chenzhao Li, Lindsay Jenkins, Tong Hui, Bethany Burkhardt, Lyndsey Fyffe, Hao Yan, Long Wang, Muqun Li, Johnny Pryor, Alyson Dickson,

Geoff Macdonald and many others at Vanderbilt. Finally, I would like to offer my special appreciation to Greg and Katherine Letterman and their family, for their unselfish love and help throughout years, which makes Nashville my second home.

This study was supported by funds from several sources: (1) NASA Langley Research Center under a Hypersonics NRA project (Cooperative Agreement No. NNX08AF56A1, Technical Monitor: Lawrence Green), (2) Sandia National Laboratories, and (3) Department of Civil and Environmental Engineering at Vanderbilt University. The support is gratefully acknowledged. The licenses of the software UNINET by LightTwist Inc. and VisualDOC by Vanderplaats R&D Inc. were graciously offered by the product owners. The numerical studies were conducted using the computational resources of the Advanced Computing Center for Research and Education (ACCRE) at Vanderbilt University

TABLE OF CONTENTS

LIST OF TABLES

LIST OF FIGURES

CHAPTER 1

INTRODUCTION

1.1. OVERVIEW

Many engineering system analyses are composed of multiple disciplinary analyses that are governed by different physics. Interaction between individual disciplines is typically modeled by exchanging physical quantities between individual analyses (e.g., displacements and pressures exchanged between fluid and structural analyses as shown in **Figure 1.1** in order to model fluid-structure interaction). In many problems, computational models are available for individual disciplinary analyses, but not for coupled system analysis; even if the latter exists, the computational cost of the coupled analysis is usually quite high.

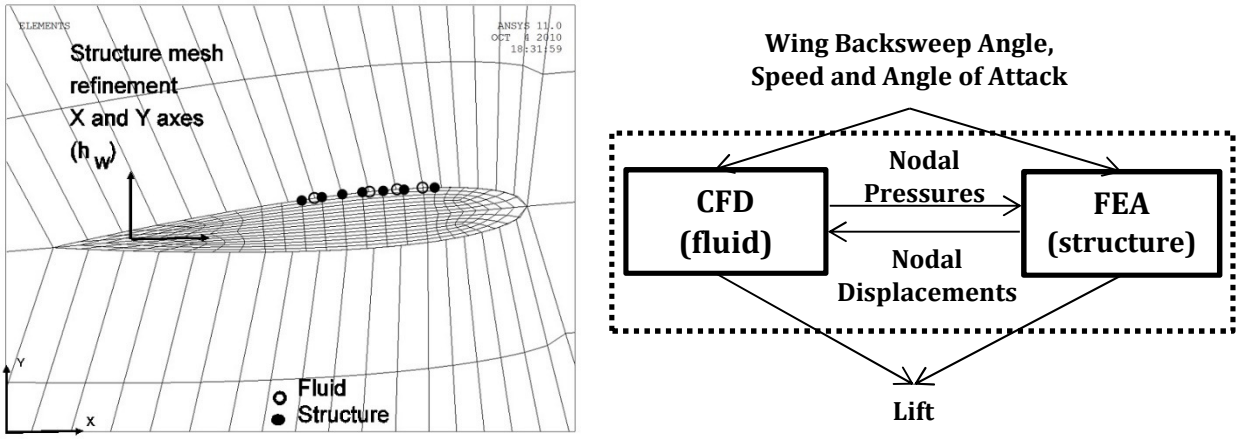

(a) Airfoil structural and fluid meshes **(b) Relationships between two analyses**

Figure 1.1. Aero-elastic analysis: feedback coupled structural and fluid dynamic analyses

Note that the fluid analysis is accomplished by computational fluid dynamics (CFD) and the structural analysis is done using FEA (finite element analysis). Multi-disciplinary analysis (MDA) and multidisciplinary design optimization (MDO) techniques have been studied during the past three decades to develop computational methods [1, 2] for systems that involve multiple coupled disciplines, analyses or subsystems in various applications such as fluid-structure interaction [3], thermal-structural analysis [4], fluid-thermal-structural analysis [5], etc. The performance of a multidisciplinary system is determined by individual disciplines as well as the interactions between them. The increasing dimensionality with analysis and design variables accumulated from multiple disciplines presents serious computational challenges in MDA and MDO [6].

The consideration of uncertainty sources further increases the computational effort, since probabilistic assessment requires repeated runs of the deterministic analysis. A simple approach to extend the deterministic multidisciplinary analysis (MDA) to

nondeterministic MDA is by conducting Monte Carlo sampling outside the deterministic analysis. This can be unaffordable when computationally expensive codes (e.g., high-fidelity CFD and FEA [6] that model the system in **Figure 1.1**) are used for individual disciplinary analyses. Therefore, efficient approaches need to be developed for MDA and MDO under uncertainty.

Three types of uncertainty sources need to be considered in design optimization: physical variability, data uncertainty and model uncertainty. Physical variability (aleatory uncertainty) in loads, system properties, etc., is irreducible and is commonly represented through probability distributions. Data uncertainty (epistemic) may be caused by sparse and/or imprecise data, and can be reduced by collecting more information. Model uncertainty (epistemic) arises from the model used to approximate the physics, and can be attributed to three types of sources: uncertain model parameters (due to limited data), numerical errors (i.e., solution approximations due to limited computational resources), and model form error (due to the assumptions made in the model) [7]. The propagation of aleatory uncertainty is well-studied in the literature, and can be accomplished by Monte Carlo sampling or First/Second-Order Reliability Methods (FORM/SORM) [8]. However, epistemic uncertainty (lack of knowledge) is an active research topic, and needs careful treatment due to its variety of sources and representation formats.

In the context of MDA under uncertainty, several studies have particularly focused on reliability analysis for multidisciplinary systems. Du and Chen [9] included the disciplinary constraints in the most probable point (MPP) estimation for reliability analysis. Mahadevan and Smith [10] developed a multi-constraint FORM approach for MPP estimation. Sankararaman and Mahadevan [11] proposed a likelihood-based approach for

MDA (known as the LAMDA approach). This methodology estimates the PDF of the coupling variables by calculating the probability of satisfying interdisciplinary compatibility, and obtains a theoretically exact solution while preserving the functional dependence between the coupling variables. Liang et al. [12] extended the LAMDA method to include model uncertainty, by using an auxiliary variable approach. The majority of these existing approaches convert the stochastic MDA into a few deterministic MDA problems through linear approximations, solved by a gradient-based method (i.e., FORM). This approximation is beneficial in terms of computational efficiency. However, the existing methods are only suitable for low-dimensional coupling, and are found to be inefficient when solving MDA with a large number of coupling variables.

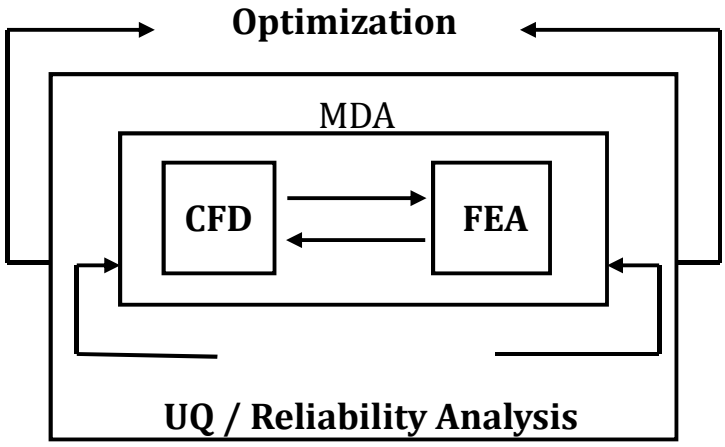

Figure 1.2 Optimization for MDA under uncertainty

Optimization methods under uncertainty within engineering design have generally been pursued in two directions: (1) reliability-based design optimization (RBDO), where

the focus has been on achieving desired reliability levels for constraints [13, 14, 15], and (2) robust design optimization (RDO), where the primary focus has been on minimizing objective function variations, typically quantified by their respective variances [16, 17, 18]. The components for MDO under uncertainty diagram are shown in **Figure 1.2**. In each design cycle, the optimizer passes a set of design values to the inner loop, where the MDA under uncertainty is implemented, and the output will be used for further design.

Efficient uncertainty propagation strategies have be proposed by several researchers considering different sources of uncertainty, but only in MDO settings with low-dimensional coupling. Gu et al. [19] proposed a worst case uncertainty propagation method using derivative-based sensitivities. Li and Azarm [20] developed a multi-objective collaborative robust optimization approach that considers interval uncertainty and both continuous and discrete design variables for multidisciplinary problems. Jiang et al. [21] proposed a spatial-random-process approach for both aleatory and epistemic uncertainty propagation in low-dimensional multidisciplinary analysis. Little work has been found focusing on the efficient optimization under uncertainty for high-dimensional coupled analysis.

Non-probabilistic approaches such as fuzzy set theory [22, 23] and evidence theory [24] have also been studied in the literature. Similar to the existing MDA approaches, these methods adopt either linear approximation and/or gradient-based algorithm when solving the optimization problem, and thus suffer from the curse of dimensionality. In another category of approaches, surrogate models have often been used for individual disciplinary analyses when the original disciplinary analysis codes are expensive [25]. Based on surrogate modeling (or metamodeling), Kokkolaras et al. [26] developed an advanced mean

value method, which was extended by Liu et al. [27] by using moment-matching and considering the first two moments. Surrogate models such as Kriging models [28], neural networks [29] etc. can be expensive to train, since fully converged analysis of the physics model is required for each training point. Thus, many surrogate models become unreliable for high-dimensional problems in feedback-coupled MDA and MDO.

1.2. RESEARCH OBJECTIVES

The overall goal of the proposed research is to develop an efficient framework for multidisciplinary analysis and optimization with the consideration of both aleatory and epistemic uncertainty. As mentioned earlier, the previous implementation of LAMDA which uses the FORM approach is only suitable for low-dimensional coupling. Therefore this dissertation aims to extend the LAMDA concept to high-dimensional coupling, and investigates the use of Bayesian network for this purpose. Once the uncertainty propagation methodology is developed, next an optimization under uncertainty framework is developed, also using the Bayesian network, to implement multi-disciplinary and multi-objective design under uncertainty.

Specifically, four objectives are pursued, two related to MDA and two related to MDO. The first objective addresses the propagation of epistemic uncertainty — data uncertainty and model error — through multidisciplinary analysis. When the individual disciplinary analyses are connected using a large number of coupling variables, approaches dealing with low-dimensional problems may not be applicable any more [30]. Therefore,

the second objective is to investigate a methodology for uncertainty propagation in a high-dimensional coupled system. The third objective aims at developing a framework to incorporate different sources of uncertainty in single disciplinary design optimization, considering multiple objectives. The fourth objective investigates a Bayesian methodology for the design optimization of multidisciplinary systems with feedback coupled analyses.

1.3. ORGANIZATION OF THE DISSERTATION

The subsequent chapters are arranged to address the four research objectives.

Chapter 2 presents a probabilistic framework to include the effects of both aleatory and epistemic uncertainty sources in feedback-coupled multi-disciplinary analysis. A previously developed likelihood-based approach is extended in this chapter to incorporate the effects of epistemic uncertainty arising from data uncertainty and model errors. Global sensitivity analysis is extended to quantify the contribution of model uncertainty in feedback-coupled MDA.

Chapter 3 develops a novel approach for efficient uncertainty quantification and propagation in multidisciplinary analysis (MDA) with a large number of coupling variables. A Bayesian network approach is proposed for probabilistic MDA, i.e., inference of distributions of the coupling variables by enforcing the interdisciplinary compatibility condition (which is treated similarly to data for updating). A copula-based approach is employed for efficient sampling from the joint and conditional distributions. Further

computational efficiency is achieved through dimension reduction using principal component analysis.

Chapter 4 develops a probabilistic graphical modeling approach for multi-objective optimization under uncertainty. Given paired samples of the inputs and outputs from the system analysis model, a Bayesian network is constructed to represent the joint probability distribution of the inputs and outputs. This Bayesian network is then exploited as a surrogate model in reliability-based design optimization (RBDO). The joint probability of multiple objectives and constraints is included in the formulation. The Bayesian network along with conditional sampling is also exploited to select training points that enable effective construction of the Pareto front.

Chapter 5 proposes a comprehensive framework for the optimization of multidisciplinary systems with feedback coupling between the individual disciplines. The proposed framework is composed of four elements: multidisciplinary analysis, Bayesian network, vine copula-based sampling and design optimization. The Bayesian network is pursued in two directions: (1) probabilistic multidisciplinary analysis (MDA), as in Chapter 3, and (2) probabilistic surrogate modeling, as in Chapter 4. The copula-based sampling technique is employed for efficient sampling from the joint and conditional distributions. The proposed Bayesian network surrogate is then used for efficient reliability assessment within an optimization framework. This leads to simultaneous interdisciplinary compatibility enforcement and the objectives/constraints evaluation within MDO. The proposed MDO methodology is implemented within a framework of reliability-based design optimization.

CHAPTER 2

MDA UNDER ALEATORY AND EPISTEMIC UNCERTAINTY

2.1. INTRODUCTION

As mentioned in Section 1.1, multidisciplinary analysis requires the collaboration of multiple individual disciplinary analyses. Based on the direction of information flow, the coupling between two individual disciplinary analyses can be either uni-directional (feed-forward) or bi-directional (feedback). The focus of this dissertation is on feedback coupling which is more complex due to the iterations between two analyses to achieve interdisciplinary compatibility. Computational methods for feedback-coupled MDA can be classified into three different groups: (1) Field elimination methods [31], (2) monolithic methods [32], and (3) partitioned methods [33]. The field elimination and monolithic methods tightly couple the disciplinary analyses together, while the partitioned method does not. The well-known fixed point iteration method (repeated analysis until convergence of coupling variables) and the staggered solution approach [31, 33] for time-dependent problems are examples of partitioned methods.

An important factor in the analysis and design of multi-disciplinary systems is the presence of uncertainty in the system inputs and the models used for each analysis. In this chapter, we consider the three sources of uncertainty mentioned in Section 1.1, which are: (1) Natural variability (aleatory), (2) data uncertainty (epistemic), and (3) model

uncertainty (epistemic). The representation and propagation of these types of uncertainty in multi-disciplinary analysis is the focus of this chapter.

Methods for the representation and the propagation of aleatory uncertainty in a monolithic or feed-forward system are well established. Aleatory uncertainty has been modeled through random variables with fixed probability distributions and distribution parameters. A variety of approaches such as Monte Carlo Methods, first-order reliability method (FORM), second-order reliability method (SORM), etc. are available for the propagation of aleatory uncertainty through monolithic or feed-forward analysis [8]. However, only a small number of studies have addressed the propagation of both aleatory uncertainty and epistemic uncertainty in single disciplinary analysis [34,35, 36, 37, 38, 39, 40, 41, 42]. Studies on uncertainty propagation through feedback-coupled MDA are even fewer [9, 10, 11, 26, 19], and have only addressed aleatory uncertainty.

The input variables in an analysis could be deterministic or stochastic, and epistemic uncertainty may be present regarding both types of inputs (due to lack of information, referred here generally as data uncertainty). For example, an input variable may be a fixed but unknown constant, and the information may be available as an interval from an expert. Or an input variable may have natural variability (aleatory), but due to lack of data, its distribution type and/or parameters may be uncertain. Epistemic uncertainty regarding the inputs has been addressed through evidence theory [35, 36], possibility theory [43], fuzzy sets [23], imprecise probabilities [44], p-boxes [40], aleatory-like but conservative treatment [41], likelihood-based probabilistic approaches [42, 45], etc., but has been mostly applied to feed-forward or monolithic problems.

Model errors can generally be categorized into two types [7]: (1) model form errors which are due to assumptions about system behavior, boundary conditions, operating conditions and model parameters; and (2) numerical solution errors, which arise from the solution process adopted to solve the mathematical model, and include discretization error, surrogate model error, truncation error (e.g., lower-order approximations), etc.. Liang and Mahadevan [46] considered a detailed treatment of model errors due to both model form assumptions and numerical solution approximations, and developed a methodology to systematically quantify and aggregate the uncertainty due to multiple error sources. Kennedy and O'Hagan [47] quantified model error in monolithic or feed-forward analysis using Bayesian calibration. To the best of our knowledge, no work has been reported in uncertainty quantification that includes model errors within feedback-coupled MDA.

The aforementioned sources of uncertainty (variability, data uncertainty and model errors) cause the output of MDA to be uncertain. Non-deterministic MDA in the presence of variability can be solved by SOFPI (i.e., Monte Carlo sampling loop outside the deterministic fixed-point-iteration analysis). However, such analysis is computationally prohibitive. Therefore, efficient alternatives, in the presence of aleatory uncertainty alone, have been investigated by several researchers [9, 10, 11, 22, 23, 24] (see Section 1.1).

Review of these studies reveals that the existing methods for MDA under uncertainty either require considerable computational effort or introduce several approximations to reduce the computational effort. For example, in the decoupled approach adopted by Du and Chen [9] and Mahadevan and Smith [10], the probability density functions (PDF) of the coupling variables are calculated by Taylor series-based first-order second moment approximation. These approaches improve the efficiency by

trading off the accuracy since they ignore the dependence between the coupling variables. To include dependence between the coupling variables, a likelihood-based MDA (LAMDA) approach was proposed by Sankararaman and Mahadevan [11]. In this method, the probability of satisfying the inter-disciplinary compatibility is calculated using the principle of likelihood, which is then used to estimate the PDF of the coupling variables. This approach requires no coupled system analysis and yet is theoretically exact, thereby preserving the functional dependence between the individual disciplinary analyses.

In [11], only aleatory uncertainty was considered. In this chapter, the LAMDA method is extended to include epistemic uncertainty (i.e., data uncertainty and model errors) in multidisciplinary analysis. A likelihood-based approach is employed to represent the effect of data uncertainty (sparse and/or imprecise data) through either parametric families of distributions [48] or non-parametric distributions [34] for the input variables. The presence of model uncertainty makes the output of analysis uncertain even for a fixed input, and model error usually varies with the input. This presents a serious challenge for non-deterministic MDA, since previously available methods have only considered models with deterministic output for a particular input realization. A novel approach is developed in this chapter to include model error in MDA using the concept of an auxiliary variable defined through the probability integral transform.

The system output uncertainty is due to the contribution of different sources of variability, data uncertainty and model uncertainty. The identification of the dominant contributors of uncertainty can be realized using probabilistic sensitivity analysis. A global sensitivity analysis (GSA) approach [49] which explores the entire space of input factors is considered in this chapter. However, previous work in GSA has only considered

deterministic feed-forward or monolithic models with only *aleatory* inputs; this chapter extends GSA to *feedback-coupled* MDA under *both* aleatory and epistemic uncertainty.

In the following sections, the basic LAMDA framework is briefly introduced first. Then a likelihood-based approach is proposed to include data uncertainty within the LAMDA framework. After that, the consideration of model uncertainty in MDA is addressed through a novel auxiliary variable approach, based on the probability integral transform. Using the auxiliary variable concept, a global sensitivity analysis approach for feedback-coupled MDA is proposed also. A mathematical example and an electronic packaging problem are used to demonstrate the proposed methodology.

2.2. LIKELIHOOD-BASED APPROACH FOR MULTIDISCIPLINARY ANALYSIS (LAMDA)

This section briefly introduces the likelihood-based approach for MDA. **Figure 2.1** is a diagram of a multidisciplinary system which consists of three analyses. A feedback analysis is required between analyses 1 and 2. The input vector is $\boldsymbol{x} = \{\boldsymbol{x_1}, \boldsymbol{x_2}, \boldsymbol{x_s}\}$ where $\boldsymbol{x_1}$ and $\boldsymbol{x_2}$ are the input vectors for each individual analysis, and $\boldsymbol{x_s}$ is shared by both analyses. Given a realization of $\boldsymbol{x}$, the interdisciplinary analysis between analyses 1 and 2 is conducted; the coupling variables, i.e. $\boldsymbol{u_{12}}$ and $\boldsymbol{u_{21}}$, will converge to particular values. A simplistic implementation of this iterative analysis is fixed point iteration (FPI). After convergence, each disciplinary analysis releases a subsystem output, i.e., g_1 and g_2, to analysis 3 to evaluate the system level output, i.e., f.

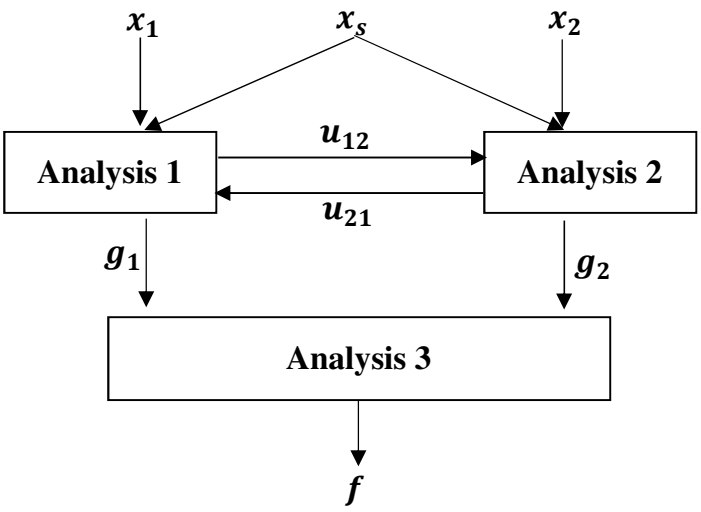

Figure 2.1. Multidisciplinary system

Figure 2.2 shows one iteration of the feedback coupled analysis. This single iteration is denoted by a function G whose input is u_{12} and output is U_{12}, i.e.,

$$U_{12} = G(u_{12}, \boldsymbol{x}) = A_1(u_{21}, \boldsymbol{x}) \tag{2.1}$$

where $u_{21} = A_2(u_{12}, \boldsymbol{x})$. The input variable u_{12} is yielded by "Analysis 1" from the previous iteration, and the output U_{12} is the input of "Analysis 2" in the following iteration. Inter-disciplinary compatibility is satisfied when $u_{12} = U_{12}$.

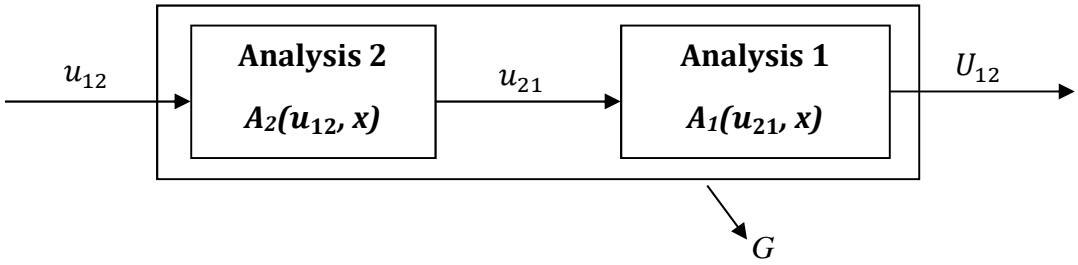

Figure 2.2 Multidisciplinary system: partially decoupled

For a given value of u_{12}, when input variability is considered, the output U_{12} can be denoted by a probability density function: $f_{U_{12}}(U_{12}|u_{12})$. It is desired to calculate $P(U_{12} = u_{12} \mid u_{12})$, which is the probability of satisfying the interdisciplinary compatibility conditioned on u_{12}. This is similar to the definition of a likelihood function in parameter estimation problems where $P(y = y_{obs}|\theta)$ indicates the probability of observing the output to be equal to some value y_{obs} conditioned on the value of the parameter of interest θ. Thus here the likelihood of u_{12} may be defined as:

$$L(u_{12}) \propto P(U_{12} = u_{12}|u_{12}) \tag{2.2}$$

Note that likelihood is only meaningful up to a proportionality constant. The probability in Eq. (2.2) can be approximated by integrating the conditional PDF $f_{U_{12}}(U_{12}|u_{12})$ over an infinitesimal window around the conditional value of u_{12}:

$$P(U_{12} = u_{12}|u_{12}) = \frac{1}{\sigma}\int_{u_{12}-\frac{\delta}{2}}^{u_{12}+\frac{\delta}{2}} f_{U_{12}}(U_{12}|u_{12})dU_{12} \tag{2.3}$$

where δ is the length of the window. In Ref [11], the integration in Eq. (2.3) is estimated by the first-order reliability method (FORM). FORM calculates the probability that a performance function $H \equiv h(\boldsymbol{x})$ is less than or equal to h_c, given stochastic input variables $\boldsymbol{x}$, which is equivalent to calculating the cumulative probability density (CDF) of H at $H=h_c$ [8]. Using this idea, FORM analyses are applied to calculate the integral in Eq. (2.3) at the upper and lower bounds, i.e., $h_u = F_{U_{12}}(U_{12} = u_{12} + \frac{\delta}{2}|u_{12})$ and $h_l = F_{U_{12}}(U_{12} = u_{12} - \frac{\delta}{2}|u_{12})$, which are essentially the probability of $(U_{12} < u_{12} + \frac{\delta}{2})$ and $(U_{12} < u_{12} - \frac{\delta}{2})$ respectively. Note that in implementing FORM for each u_{12}, only the feed-forward analysis of **Figure 2.2**

is needed to estimate G and its derivatives $\nabla G(\boldsymbol{x})$; i.e., in each iteration of FORM, only $\boldsymbol{x}$ is changing, not u_{12}. The likelihood of u_{12} is approximated by:

$$L(u_{12}) \propto \frac{h_u - h_l}{\delta} \tag{2.4}$$

The likelihood function only needs to be evaluated at a few points. Then the PDF of u_{12} can be evaluated as:

$$f(u_{12}) = \frac{L(u_{12})}{\int L(u_{12}) du_{12}} \tag{2.5}$$

A recursive adaptive version of Simpson's quadrature [50] can be used to evaluate the integral in Eq. (2.5). After evaluating the PDF for a few values of u_{12}, the entire PDF is approximated by interpolation. The LAMDA method is theoretically exact; but approximations are introduced in the numerical implementation by using FORM to calculate the CDF values in Eq. (2.3). However, the LAMDA framework is not dependent on FORM; if the analysis is nonlinear, SORM or one of several methods of Monte Carlo sampling can be used instead. The key point is that LAMDA only needs a single run through the two analyses for each realization of u_{12} and not an iterative analysis to convergence for each u_{12}.

Once the PDF of the converged value of u_{12} is constructed, the feedback-coupled analysis of **Figure 2.1** can be replaced by a unidirectional coupled analysis as shown in **Figure 2.3**. The coupling variable u_{12} is brought to the same level with the input variable $\boldsymbol{x}$; both $\boldsymbol{x}$ and u_{12} can be treated as the input variable to this partially decoupled system. The uncertainty of the subsystem level and system level output can be characterized by sampling $\boldsymbol{x}$ and u_{12}; for each sample of input and u_{12}, only one function evaluation of Analyses 1 and 2 is required to compute g_1 and g_2. The results are then used to calculate f.

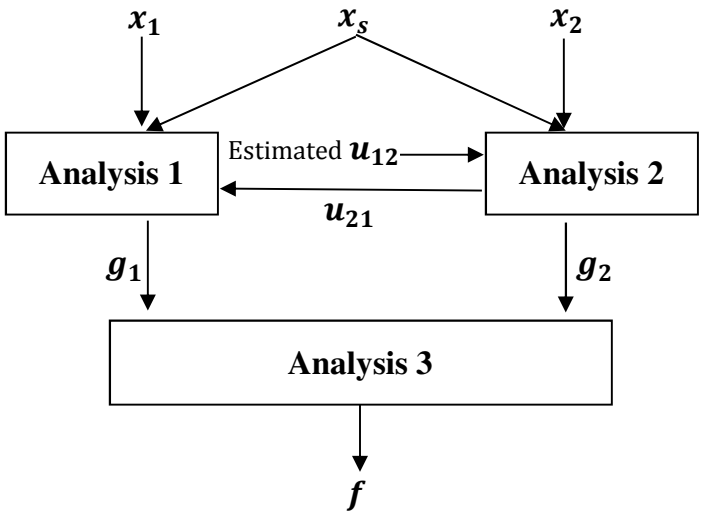

Figure 2.3 Multidisciplinary system: partially decoupled

Note that the LAMDA approach is general, and is equally applicable to correlated or uncorrelated $\boldsymbol{x}$. The focus of this chapter is on coupling between disciplines, and the input correlation is not considered in the numerical examples. However, the problem of correlated input random variables has been solved long ago, and does not present any new challenge. When input correlation is considered, the input random variables can be transformed into a space of uncorrelated variables [8], after which FORM can be used to evaluate the likelihood.

2.3. INCLUSION OF DATA UNCERTAINTY IN MDA

This section develops a likelihood-based approach to include data uncertainty regarding the input variables (due to sparse and/or imprecise data) within MDA.

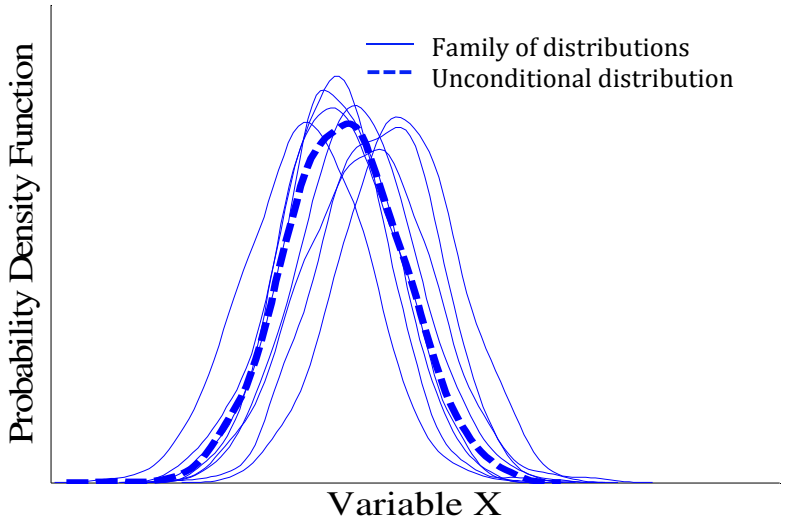

Figure 2.4 Family of distributions

Data uncertainty can be regarding a stochastic or deterministic quantity. This chapter focuses on the first type of uncertainty, i.e., only sparse and/or interval data is available on an input random variable. An enhanced LAMDA method that accounts for epistemic uncertainty regarding the input random variables is proposed here. This method combines data uncertainty due to sparse point data and interval data and develops a probabilistic representation for this uncertainty through a nonparametric PDF [34].

Suppose the available information for a random variable X is a combination of m data intervals: $\{[a_1, b_1], \dots [a_m, b_m]\}$, and n data points $\{s_1, \dots s_n\}$. Based on the principle of likelihood, two approaches can be pursued to represent this type of uncertainty: parametric [48] and non-parametric [34]. In the parametric approach, a discrete random variable D and a random variable vector $\boldsymbol{\theta}$ are assumed to denote the distribution type and the distribution parameters respectively. Randomly sampling D and $\boldsymbol{\theta}$ will result in a family

of probability distributions as shown in **Figure 2.4**. This family of distributions is used to fit the data interval and data points of $\boldsymbol{X}$, and the likelihood of D and $\boldsymbol{\theta}$ is given by:

$$L(D, \boldsymbol{\theta}) \propto \prod_{j=1}^{m} \left[F_X\left(b_j | D, \boldsymbol{\theta}\right) - F_X(a_j | D, \boldsymbol{\theta}) \right] \prod_{i=1}^{n} f_X(s_i | D, \boldsymbol{\theta}) \tag{2.6}$$

D and $\boldsymbol{\theta}$ may be estimated by maximizing the likelihood function in Eq. (2.6) (note that D is discrete). The candidate distribution types can sometimes be selected based on prior knowledge or physical considerations; in other cases, however, the choice of distribution type candidates may be difficult.

To avoid the assumption of distribution type, a non-parametric approach [34] can be adopted. Consider the variable $\boldsymbol{X}$ with m interval and $n$point data. The maximum and minimum values in this data are used as the upper and lower bounds of X. The entire domain is then uniformly discretized by a set of points q_i ($i = \{1, \dots Q\}$). Let p_i denote the PDF value at the i^{th} point, i.e., $f_X(x_i = q_i) = p_i$; the PDF over the entire domain can be constructed by interpolating these PDF values. Let $\boldsymbol{p}$ denote the vector of the PDF values, i.e., $\boldsymbol{p} = (p_1, \dots p_Q)$; the likelihood function of $\boldsymbol{p}$, which is defined as the probability of observing the given data (point values and data intervals) given $\boldsymbol{p}$, can be written as:

$$L(\boldsymbol{p}) \propto \prod_{j=1}^{m} \left[F_X\left(b_j | \boldsymbol{p}\right) - F_X(a_j | \boldsymbol{p}) \right] \prod_{i=1}^{n} f_X(s_i | \boldsymbol{p}) \tag{2.7}$$

The value of $\boldsymbol{p}$ can be estimated by maximizing the likelihood$L(\boldsymbol{p})$ using the optimization problem in Eq. (2.8). The three constraints for the optimization are: (1) the vector $\boldsymbol{p}$ (PDF values at the discretized points) needs to be positive; (2) the PDF value over the entire domain of X needs to be positive; and (3) the integrated area under the PDF curve must be unity. A Gaussian Process (GP) interpolation technique is employed in this

chapter to fit the entire PDF curve based on $[p_1, \dots p_Q]$; however, other interpolation techniques may also be used.

$$\begin{gathered} \max_{\boldsymbol{P}} L(\boldsymbol{P}) \\ \text{s.t. } p_i \geq 0 \text{ for } \forall\, p_i \in \boldsymbol{P} \\ f_x(x) \geq 0 \text{ for } \forall\, x \\ \int f_x(x)dx = 1 \end{gathered} \tag{2.8}$$

The above likelihood-based method is exploited to fit a non-parametric probability distribution to include the effect of data uncertainty due to sparse and interval data. It avoids assumptions on the distribution type or distribution parameter. The resulting probability distribution can be easily applied to uncertainty propagation with Monte Carlo sampling or FORM.

2.4. INCLUSION OF MODEL UNCERTAINTY IN MDA

2.4.1. MODEL ERROR QUANTIFICATION

Liang and Mahadevan developed approaches for model error quantification in feed-forward computational models [46]; however, the propagation of model error through multiple models is not straightforward in feedback-coupled MDA. Model errors can be classified into two categories: (1) model form error caused by simplifications or assumptions about the physics of the problem, and (2) numerical errors due to the solution

process, such as discretization error, error due to limited sampling, etc. The quantification methods for different types of model errors are distinct from each other. Model form error can be estimated using actual experimental data; and numerical solution error can be calculated using the result of model verification. When input variability and data uncertainty are considered, the model errors need to be quantified at each input realization. This section focuses on the inclusion of model error within MDA in a generalized manner that includes both model form error and numerical solution errors.

A simple way to handle input-dependent model error is to use an additive model discrepancy term and include it in subsequent analysis. Kennedy and O'Hagan [47] used Bayesian calibration to quantify this model discrepancy term. Mahadevan and Rebba [51], and Chen [52] included the additive model error term in reliability-based design optimization. However, when multiple sources contribute to model error, and when these sources do not combine in a simple manner, the additive term approach is not easy to use. Sankararaman et. al [53] used a Bayesian network approach to combine multiple sources of model error. However, complication arises in feedback-coupled MDA if the model error term has to be added after each iteration of individual disciplinary analyses. Also, model error is a function of the input and this function is not generally known; thus, it is not straightforward to include the additive model error term in feedback-coupled MDA.

In many problems, the original disciplinary analyses may be expensive, and may need to be replaced by surrogate models. Many types of surrogate modeling techniques are available (e.g., Gaussian process models [47], polynomial chaos expansion [54], support vector regression [55], artificial neural network [56], etc.). A review of state-of-the-art modeling techniques for solving different types of optimization problems is provided in

[56]. Use of a surrogate model introduces error in the prediction, which has two components: bias and variance. A leave-one-out cross validation approach can be used to estimate bias with an existing number of training points [57], and sequential training point selection techniques have been proposed in the literature for bias reduction [57, 58]. Expressions for the variance of surrogate model prediction are also available in the literature (for example, variance is readily available for Gaussian process and polynomial chaos expansion models; see [46]).

Regardless of whatever individual or multiple sources contribute to the model error, the output of a model due to the presence of model error is a probability distribution even for a fixed value of the input. Note that some errors are deterministic (e.g. discretization error) and some are stochastic (e.g. surrogate model error); their combined effect makes the model output stochastic even for a fixed input. This presents an interesting challenge. Only aleatory uncertainty was considered in the original LAMDA method (Section 2.2). Therefore, for a given value of u_{12} and $\boldsymbol{x}$, the output U_{12} was a deterministic value. However, in the presence of model error, the output U_{12} becomes a probability distribution. This makes it difficult to evaluate Eq. (2.2): How can we talk about the probability of a distribution being equal to a particular value? The likelihood in Eq. (2.2) can only be calculated when the output U_{12} is a deterministic value for a given value of u_{12} and $\boldsymbol{x}$. An auxiliary variable method is proposed below to overcome this challenge.

2.4.2. AUXILIARY VARIABLE METHOD

For the sake of illustration, consider a normal random variable X with uncertain parameters. Assume that the parameters of X, i.e. μ_X and σ_X, have normal distributions; the uncertainty of X is therefore denoted as: $X \sim N(\mu_X(\mu_\mu, \sigma_\mu), \sigma_X(\mu_\sigma, \sigma_\sigma))$, where $\mu_\mu, \sigma_\mu, \mu_\sigma$ and σ_σ are deterministic values based on sources such as expert opinion. Given a realization of μ_X, and σ_X, X is a distribution. Let P denote an auxiliary variable, defined by the probability integral transform [59] as

$$P = \int_{-\infty}^{x} f_X(X|\mu_X, \sigma_X)dX \tag{2.9}$$

where x is a generic realization of X. $P \in [0,1]$ is the CDF value. For a realization of μ_X and σ_X, the well-known inverse CDF method of Monte Carlo simulation taken over a realization of P from a uniform distribution gives a fixed value of $\boldsymbol{x}$. Therefore, $\boldsymbol{x}$ can be written as:

$$\boldsymbol{x} = F^{-1}_{X|\mu_X,\sigma_X}(p) \text{ or } \boldsymbol{x} = H'(p, \mu_X, \sigma_X) \tag{2.10}$$

where p is a realization of P. Thus by introducing the auxiliary variable P, we get a unique value of X for a given value of μ_X and σ_X. The probability integral transform helps to define the auxiliary variable P, and will be used to include the stochastic model error in coupled MDA.

Note that this approach can also be extended to handle the case when a parametric family of distributions is used to represent an input random variable due to data uncertainty. In that case, if a discrete variable D represents the distribution type, and Θ

represents the vector of distribution parameters, then a unique value of x can be obtained for a realization of D, θ and P as:

$$x = H'(p, d, \theta) \tag{2.11}$$

Note that H' is not the same in Eqs. (2.10) and (2.11).

2.4.3. REPRESENTATION OF MODEL UNCERTAINTY

For a given value of u_{12} and input $\boldsymbol{x}$, the output U_{12} follows a probability distribution due to model error. This distribution can be represented by a conditional PDF $f_{U_{12}}(U_{12}|u_{12}, \boldsymbol{x})$. Let auxiliary variable P denote the conditional CDF at $U_{12} = u_{12}$ given u_{12} and $\boldsymbol{x}$, i.e.,

$$P = \int_{-\infty}^{u_{12}} f_{U_{12}}(U_{12}|u_{12}, \boldsymbol{x}) dU_{12} \tag{2.12}$$

where $P \in [0,1]$. For a given value of input $\boldsymbol{x}$ and u_{12}, when a single value of P is sampled from $U(0,1)$, a unique value of U_{12} can be obtained through the inverse CDF method. Hence $U_{12} = H'(p, u_{12}, \boldsymbol{x})$, which is deterministic, can now be used to evaluate the likelihood in Eq. (2.2) using FORM, as shown in **Figure 2.5**. With a unique value of U_{12} defined as above, two evaluations of FORM are implemented at $C = u_{12} + \frac{\delta}{2}$ and $C = u_{12} - \frac{\delta}{2}$ to get h_u and h_l respectively. In FORM, $Prob(H' - C \leq 0) = \Phi(-\beta)$.

Given PDFs of $\boldsymbol{x}, P$

Min $\beta = \boldsymbol{u}^T\boldsymbol{u}$

s.t. $H'(\boldsymbol{p}, \boldsymbol{x}, u_{12}) - C = 0$

where standard normal $\boldsymbol{u} = T(p, \boldsymbol{x})$

Figure 2.5 FORM with auxiliary variable

The PDF of u_{12} can then be obtained using Eq. (2.4) and Eq. (2.5).

The auxiliary variable approach to include model error in MDA offers several benefits: (1) the auxiliary variable *P* represents the overall effect of model error in a generalized manner; no matter how different types of model errors are combined, it considers the overall distribution of the output as a result of these error sources for a fixed input. (2) The use of the auxiliary variable provides an elegant method to include model error in the LAMDA method, and the challenge of accumulating model error through multiple iterations of MDA is bypassed due to the single iteration strategy of LAMDA. (3) The use of the probability integral transform to define the auxiliary variable provides a theoretically exact way to include model error in feedback-coupled MDA. (4) Representation of the model error through a random variable *P* brings x and *P* on the same level, and facilitates a single loop approach to implement FORM, thus providing computational efficiency. In contrast, a sampling-based approach to include model error would need an additional nested loop of analysis.

2.5. GLOBAL SENSITIVITY ANALYSIS IN FEEDBACK-COUPLED MDA

Uncertainty propagation analysis is often accompanied by sensitivity analysis to identify the significant contributors to the model output uncertainty. Several benefits are possible such as: (1) reduction of number of uncertainty sources considered in the analysis and design optimization; (2) guidance in resource allocation for data collection; and (3) guidance in model refinement. Global sensitivity analysis has been used to calculate the effect of the variability of an input quantity on the variance of the output quantity [49]. Consider a model given by:

$$Y = G(X_1, X_2 \dots X_n) \tag{2.13}$$

where X_i and Y are input-output pairs of a generic model. The first-order sensitivity indices are estimated as:

$$S_i^1 = \frac{V_{X_i}(E_{X_{\sim i}}(Y|X_i))}{V(Y)} \tag{2.14}$$

where the notation $E_{X_{\sim i}}(Y|X_i)$ denotes the expectation of output Y given a particular value of variable X_i and considering the random variations of all other variables except for X_i (denoted by $X_{\sim i}$). The symbol V_{X_i} represents the variance of the aforementioned expectation over multiple samples of X_i. The first-order sensitivity index indicates the contribution of uncertainty due to a particular individual variable, regardless of its interactions with other variables. The evaluation of Eq. (2.14) can be accomplished by either double-loop or single-loop Monte Carlo sampling. The sum of first-order indices of all variables is always less than or equal to unity.

A total effects index is also calculated to account for the uncertainty contribution of X_i in combination with all other variables:

$$S_i^T = \frac{E_{X_{\sim i}}(V_{X_i}(Y|X_{\sim i}))}{V(Y)} = 1 - \frac{V_{\sim i}\left(E_{X_i}(Y|X_{\sim i})\right)}{V(Y)} \tag{2.15}$$

where $V_{X_i}(Y|X_{\sim i})$ denotes the variation of output Y at a fixed realization of all variables except X_i , over multiple samples of X_i only; $E_{X_{\sim i}}$ calculates the expectation of this variation over multiple samples of $X_{\sim i}$. The sum of the total effects indices of all variables is always greater than or equal to unity.

Previous work in GSA has only considered aleatory uncertainty in the input variables [46]. When model output uncertainty is caused by input variability, data uncertainty and model errors, the contribution of all the sources needs to be quantified. The sensitivity to the input variable distributions is straightforward to calculate by using sampling techniques. However, when uncertainty caused by stochastic model errors is considered, the GSA cannot be directly implemented due to the lack of a deterministic input-output transfer function.

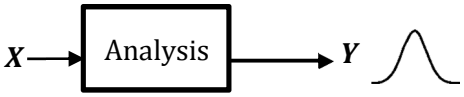

Figure 2.6 Output uncertainty due to model errors

Figure 2.6 shows the stochastic functional relation between input $\boldsymbol{X}$ and output $\boldsymbol{Y}$. Consider Eq. (2.14) and Eq. (2.15), in which the inner loops of sampling calculate $E_{X_{\sim i}}(Y|X_i)$

and $V_{X_i}(Y|X_{\sim i})$ respectively; both evaluations require deterministic function output. In the presence of model uncertainty, the output $\boldsymbol{Y}$ is a distribution even for a fixed input $\boldsymbol{X}$. Therefore, a new auxiliary variable is introduced to explicitly include model uncertainty in sensitivity analysis. Consider the model in Eq. (2.1). Suppose model output has a distribution D at a given input $\boldsymbol{X}$; this can be denoted as: $Y \sim D(\mu_{pred}(\boldsymbol{X}), \sigma_{pred}(\boldsymbol{X}))$, where μ_{pred} is the predicted mean function value and σ_{pred} is the standard deviation that represents the uncertainty in the prediction due to model uncertainty.

Let U_Y denote the auxiliary variable which is defined as $U_Y = \int_{-\infty}^{y} f_Y(Y|\boldsymbol{X})dY$, where $\boldsymbol{X}$ is one realization of the input and f_Y is the PDF of Y conditioned on $\boldsymbol{X}$. The individual and total effects of U_Y are:

$$S_{U_Y}^1 = \frac{V_{U_Y}(E_X(Y|U_Y))}{V(Y)} \tag{2.16}$$

$$S_{U_Y}^T = \frac{E_X(V_{U_Y}(Y|X))}{V(Y)} = 1 - \frac{V_{U_Y}\left(E_X\left(Y|X_{U_Y}\right)\right)}{V(Y)} \tag{2.17}$$

Thus, the use of the auxiliary variable method in variance-based GSA provides an explicit means to quantify the contribution of the stochastic model error to the system level output variance. It represents the effect of model uncertainty through the auxiliary random variable U_Y, and brings model uncertainty to the same level of analysis as input uncertainty. The sensitivity of U_Y given in Eq. (2.16) and Eq. (2.17) can be regarded as an index of the contribution of model error to the overall output uncertainty.

Note that Eq. (2.15) to (2.17) are often used in the context of feedforward analyses. In the LAMDA approach, after the distribution of the coupling variable is obtained, uncertainty propagation is implemented with the partially decoupled analysis in **Figure**

2.2, which is essentially a feedforward analysis. Therefore, the above sensitivity analysis can also be applied in the context of feedback coupled analysis, with the help of LAMDA.

In summary, Sections 2.3 to 2.5 introduced the representation and the propagation of data uncertainty and model uncertainty in coupled MDA. Likelihood-based parametric and non-parametric approaches to handle data uncertainty were presented. Model error sources result in a stochastic model output; and an auxiliary variable method is introduced to account for the model error through a random variable which provides a breakthrough in the implementation of both LAMDA and GSA to feedback coupled MDA. Since variability and data uncertainty of a random variable are together represented by a non-parametric distribution, the combined effect of aleatory and epistemic uncertainty in each input random variable is identified by a single sensitivity index. However, if a variable has a significant impact on the output uncertainty, and separation of the effects of aleatory and epistemic uncertainty is desired, then a parametric distribution can be used for this variable, with uncertain distribution type and parameters. See [45, 60] for details of such analysis.

2.6. NUMERICAL EXAMPLES

A mathematical MDA example is considered in this section first. Two assumptions for model error are made for the sake of illustration and propagated using the enhanced LAMDA approach. Next, an electronic packaging example is used to demonstrate the

quantification and propagation of different sources of uncertainty in MDA using the proposed approach.

2.6.1. MATHEMATICAL MDA PROBLEM

The mathematical example shown in **Figure 2.7** consists of 3 analyses. A feedback coupling exists between "Analysis 1" and "Analysis 2", and the coupling variables are denoted as u_{12} and u_{21}. Then the subsystem output g_1 and g_2 are calculated and used as the inputs to analysis 3 to compute the system level output f. The input variables x_1, x_2 and x_3 are assigned normal distributions: $N(1,0.1)$. x_4 is characterized by a lognormal distribution: $LogN(1,0.1)$.

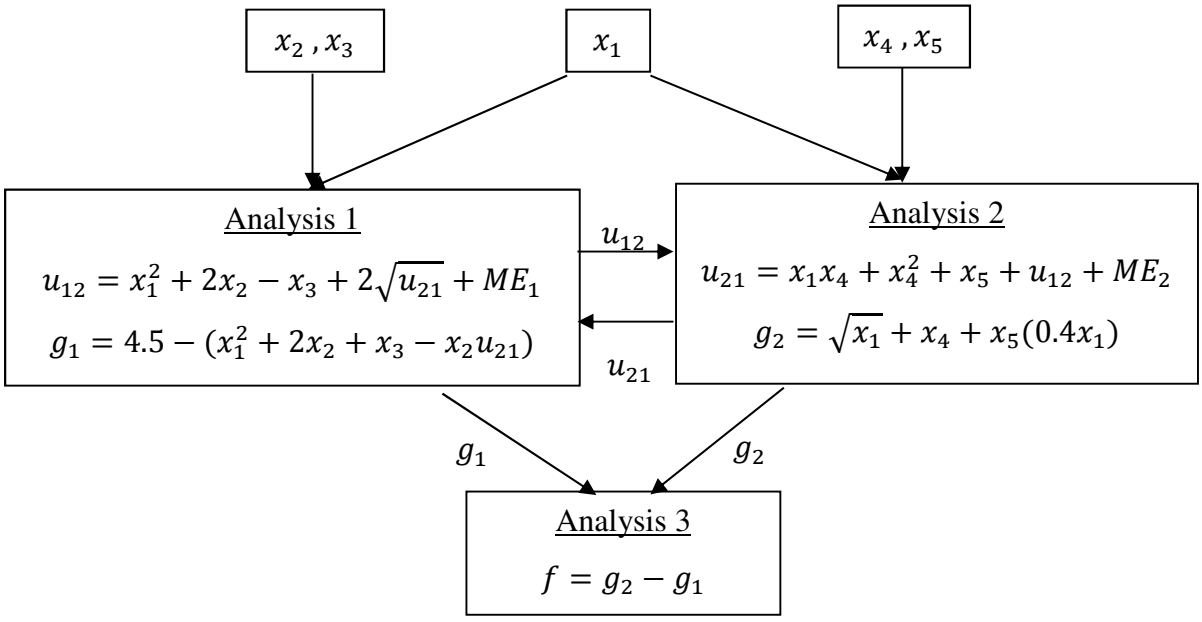

Figure 2.7 Functional relations of the mathematical MDA model

2.6.1.1. Epistemic Uncertainty Due to Insufficient Data

Epistemic uncertainty is assumed for x_5. The data is available in the form of 3 intervals {[0 2], [0.02 1.97], [0.14 1.89]} and 2 point values {0.99, 1.02}. The domain bounded by the maximum and minimum available values of the available data is divided into 10 equally spaced points, with PDF values $P_i, i = 1 \dots 10$. The optimization framework in Eq. (2.8) is then adopted to estimate the optimal P_i that maximizes the likelihood function constructed using Eq. (2.7). A cubic spline technique is employed to interpolate the likelihood and construct the non-parametric PDF presented in **Figure 2.8**.

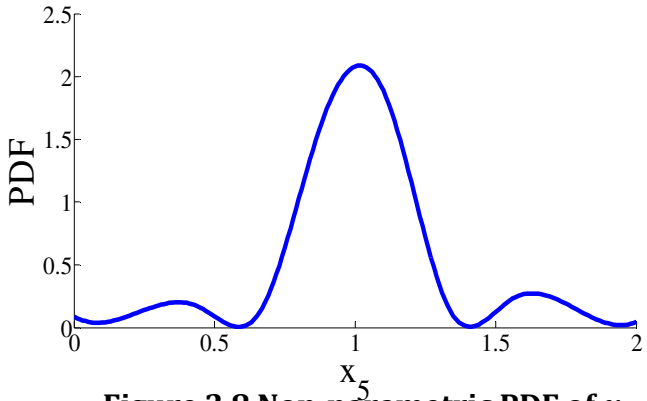

Figure 2.8 Non-parametric PDF of x_5

2.6.1.2. Epistemic Uncertainty Due to Model Errors

For the sake of illustration, model errors ME_1 and ME_2 are assumed in "Analysis 1" and "Analysis 2" respectively as functions of the input and coupling variables. Two cases of

model error are addressed: (1) deterministic model error, and (2) stochastic model error. The assumed mathematical forms of the model errors are listed in **Table 2.1**. Additionally, results are also computed for the case with no model error, for the sake of comparison.

Table 2.1 Model errors in coupled analysis

Model Error	Deterministic Model Errors	Stochastic Model Errors
ME_1	${ME_1}^D = 0.05x_2 + 0.1(u_{21})^{\frac{1}{4}}$	$\mu({ME_1}^S) = {ME_1}^D$ $\sigma({ME_1}^S) = 0.15 * {ME_1}^D$
ME_2	${ME_2}^D = 0.1\sqrt{u_{12}} + 0.2x_5$	$\mu({ME_2}^S) = {ME_2}^D$ $\sigma({ME_2}^S) = 0.15 * {ME_2}^D$

2.6.1.3. Uncertainty Quantification of the Coupling Variables

For each coupling variable in both cases, the entire PDF is estimated by interpolating 15 integration points, each of which has been evaluated by LAMDA (Eq. 1). The propagation of variability and data uncertainty for deterministic model errors can be fulfilled by the original LAMDA method. In the stochastic error scenario, the proposed auxiliary variable method is used to address the model error. Two auxiliary variables h_1 and h_2, representing the CDFs of the model errors respectively, are introduced; both are uniformly distributed from 0 to 1 based on the probability integral transform (Section 2.4.2). The resultant PDFs of the coupling variables with deterministic and stochastic model errors and without error are shown in **Figure 2.9**. The mean and standard deviation

of u_{12} and u_{21} are calculated and listed in **Table 2.2**. SOFPI is implemented with 20,000 samples of the input as the benchmark solution.

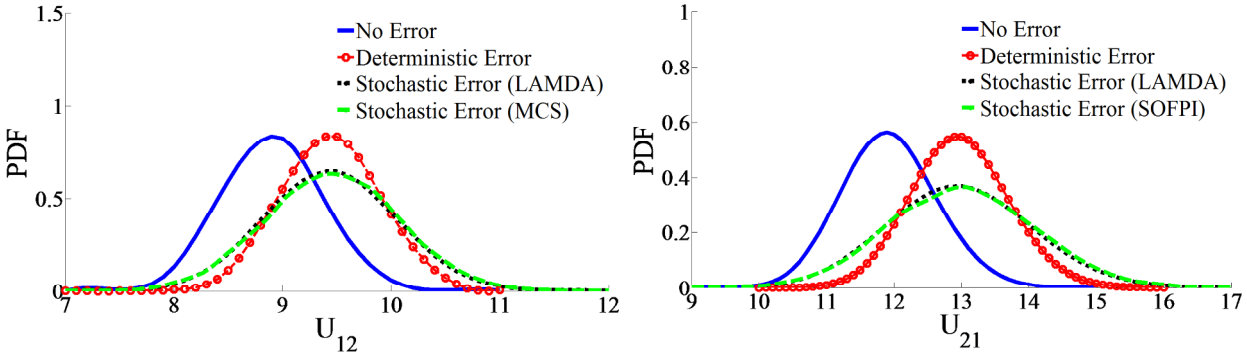

Figure 2.9. PDFs of coupling variables U_{12} (left) and U_{21} (right)

Table 2.2 Mean and standard deviation of coupling variables

Case No.	Type		u_{12}	u_{21}	No. of Function Evaluations
1	No model error	μ_N	8.95	11.94	572
		σ_N	0.49	0.72	
2	Deterministic model error	μ_D	9.40	12.99	594
		σ_D	0.48	0.73	
3	Stochastic model error (LAMDA)	μ_L	9.45	12.98	768
		σ_L	0.62	1.08	
4	Stochastic model error (SOFPI)	μ_S	9.46	13.03	379,246
		σ_S	0.62	1.10	

The following observations are drawn from **Table 2.2**:

(1) The PDFs of u_{12} and u_{21} for cases 1 and 2 have almost the same shape and standard deviation, and are only separated by the deterministic model error value.

(2) Including the stochastic model error increases the computational effort by 34.3% comparing with the "No model error" case, and 26.3% with the "Deterministic model error" case. This is because the introduced auxiliary variables increase both the dimension and the nonlinearity of the problem. This case can be finished in less than 1 second using LAMDA method. On the other hand, 20,000 SOFPI evaluations take 493.1 seconds and 379,246 function evaluations.

(3) Once the PDF of the coupling variable is calculated, the scheme in **Figure 2.3** can be used for uncertainty propagation and estimate the PDF of the individual disciplinary and system outputs: g_1, g_2 and f. Note that this does not require the iterative analysis between Analyses 1 and 2, therefore becomes a simpler uncertainty propagation through a feed-forward analysis. For the sake of illustration, Monte Carlo sampling is used to estimate the PDF of the system output. Following the scheme in **Figure 2.3** the analysis in the other direction is retained. The PDFs of the inputs $\boldsymbol{x}$ and u_{12} are used first in "Analysis 2" to estimate u_{21} and g_2, and then in "Analysis 1" to estimate g_1, followed by the overall system output f. **Table 2.3** lists the mean values and standard deviations of the outputs in different cases.

Table 2.3 Mean and standard deviation of g_1, g_2 and f

		g_1	g_2	f
No Model Error	μ	12.50	2.41	-10.1
	σ	1.2	0.16	1.18
Deterministic Case	μ	13.52	2.41	-11.11
	σ	1.26	0.16	1.23
Stochastic (LAMDA)	μ	13.60	2.43	-11.17
	σ	1.42	0.16	1.40
Stochastic (MCS)	μ	13.49	2.41	-11.08
	σ	1.60	0.15	1.55

(4) It could be argued that in the presence of expensive disciplinary computational models, SOFPI could be used with surrogate models. However, building the surrogate model has significant computational expense. In the mathematical example, an average of 19 function evaluations is needed for deterministic MDA to converge at each input. To obtain the training points for the surrogate model, such coupled analysis needs to be evaluated at multiple realizations of the input. The number of training points can be very high if the input is high-dimensional and the model is highly nonlinear. Therefore, the total number of function evaluations will still be large. Thus the computational effort in building the surrogate model should also be considered in such comparisons.

Global sensitivity analysis is conducted to quantify the sensitivity of the system level output f to the uncertain inputs and model errors from both analyses. The auxiliary variables h_1 and h_2 denote the uncertainty introduced by the model errors. The input, coupling and auxiliary variables are sampled, then the decoupled analysis is executed to evaluate the output uncertainty. Therefore, the total number of function evaluations equals the number of variables (input/coupling/ auxiliary) times the sample size (1,000 samples

are used), which equals 8,000. The first-order sensitivity indices and the total-effect indices are shown in **Table 2.4**.

Table 2.4: Global sensitivity indices

	x_1	x_2	x_3	x_4	x_5	h_1	h_2
First-Order	0.007	0.670	0.019	0.036	0.019	0.039	0.180
Total Effect	0.007	0.681	0.019	0.037	0.021	0.041	0.184

The index for h_2 indicates that the stochastic model error from "Analysis 2" has a large impact on the uncertainty of the final system output, while model error from "Analysis 1" has a small effect. The use of the auxiliary variable method enabled the sensitivity analysis to include uncertainty contributions from model errors. It replaced the double-loop approach with a single-loop calculation, thus greatly reducing the computational effort. According to **Table 2.4**, it can be observed that the first-order and total effect sensitivity indices of the corresponding variables are quite similar. Since the total effect reflects the uncertainty significance of a variable from both its individual variation and its interactive effect with other variables, the result indicates that the collaborative effect of the variables is insignificant.

2.6.2. ELECTRONIC PACKAGING EXAMPLE

The electronic packaging problem [61] is a two-discipline analysis with feedback coupling between the electrical and thermal analyses. The system is composed of a circuit with a single resistor and a heat sink on which the resistor is mounted. A diagram of the heatsink is shown in **Figure 2.10(a)**.

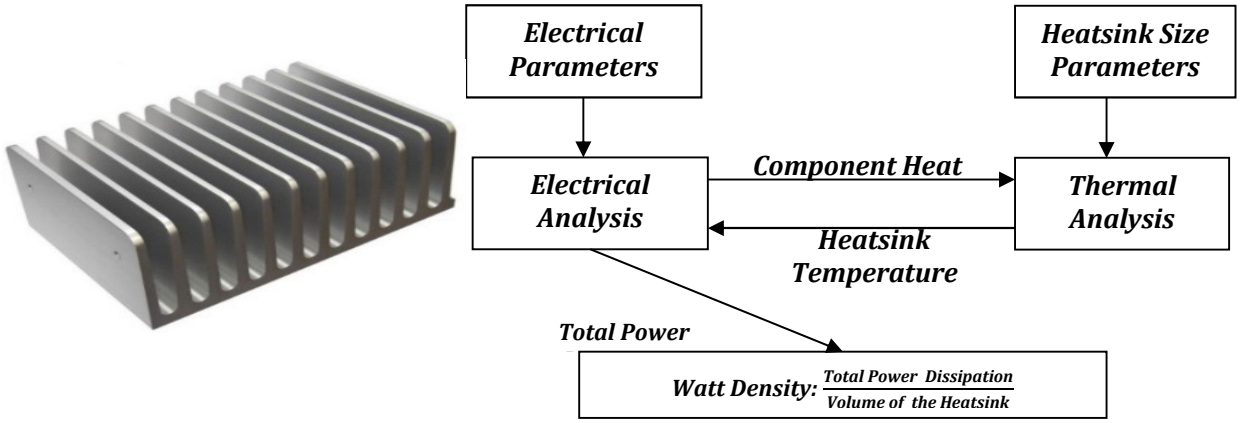

(a) Geometry of a regular heatsink **(b) Disciplinary analyses and coupling variables**

Figure 2.10 Electronic packaging problem: feedback coupled MDA.

When the circuit is turned on, the resistor generates heat that is dissipated by the heatsink. The component resistance is affected by the operating temperature, while the temperature depends on the heat produced by the resistor. The interdisciplinary relationships are shown in the **Figure 2.10(b)**. The electronic analysis is computed

algebraically, whereas the thermal analysis needs to solve a 2D heat transfer problem through finite difference method.

The deterministic parameters are: Voltage = 10.0 volts and room temperature $T = 20.0°C$. The random variables together with their uncertainty are listed in **Table 2.5**. The state variables are defined by the relations: $y_1 = \frac{y_5}{y_7}$; $y_2 = x_5(1 + x_6(y_5 - T))$; $y_3 = \frac{Voltage}{y_2}$; $y_4 = y_3^2 y_2$; $y_5 = Thermal(y_4, x_1, x_2, x_3, x_4)$, y_5 is an implicit function of the geometric parameter of the heatsink and the power dissipation in resistor, it needs to be computed through the finite difference method, and $y_6 = x_1 x_2 x_3$.

In this example, geometric parameters x_1, x_2, x_3 and x_4 are appointed as the design variables, of which the upper and lower bounds are [0.15, 0.15, 0.08, 0.05] and [0.05, 0.05, 0.02, 0.01]. The design variables are assumed to have variability. x_5 and x_6 are additional uncertain variables. The distribution types and parameters are assumed to be precisely known forx_5, whereas the distribution characteristic of x_6 are uncertain due to the availability of only interval data and sparse point data (epistemic uncertainty). A non-parametric PDF is constructed using the likelihood-based approach [34] for a combined representation of the aleatory and epistemic uncertainty regarding x_6. Details about the uncertain variables are provided in **Table 2.5**.

The coupling variables are component heat (due to power dissipation in resistor) computed in the electrical analysis, and component temperature y_5 estimated in the thermal analysis. The system output power density is the ratio between total power dissipated and the volume of the heatsink.

Table 2.5 Parameters of the electronic packaging system

Parameter		Parameter (Unit)
Input Variables and Associated Uncertainty	x_1	Heat sink width (m) $\sim N(0.1,0.01)$
	x_2	Heat sink length (m) $\sim LogN(0.1,0.01)$
	x_3	Fin length (m) $\sim N(0.05,0.005)$
	x_4	Fin width (m) $\sim N(0.025,0.0025)$
	x_5	Nominal resistance at temperature T° (W) $\sim N(10,0.1)$
	x_6	Temperature coefficient of electrical resistance (°K^{-1}) data Intervals: [0.004,0.009],[0.0043,0.0085],[0.0045,0.0088] data Points: {0.0055, 0.0057}
Thermal and Electrical State Variables	y_1	Power density (watts/m^3)
	y_2	Resistance at temperature T_1 (W)
	y_3	Current in resistor (amps)
	y_4	Power dissipation in resistor (watts)
	y_5	Component temperature (T_1) of resistor (°C)
	y_6	Heat sink volume (m^3)

2.6.2.1. Model Error Quantification

The two disciplinary analyses (electrical and thermal) are evaluated using two different mathematical models. The electrical analysis is solved algebraically based on electrical circuit analysis and the computational process is straightforward. In the thermal analysis, the component temperature y_5 is retrieved by numerically solving a two-dimensional heat transfer differential equation using a finite difference method. Due to limited computational resources for solving the continuum problem, assume that only a

coarse mesh can be used, causing discretization error. Meshes are only required for x and y directions (heat transfer in the thickness direction is ignored for the thin plate). A Gaussian Process-based technique is used to estimate discretization error [62] in FDA/FEM analysis as an enhancement of the traditional Richardson extrapolation method. The basic theory of the Gaussian Process (GP) technique is provided in Appendix I on page 150. The GP approach to quantify discretization error is briefly summarized below:

For a given input x_n, T mesh tests : h_{set}= $\{h^1, \ldots h^T\}$ are conducted, where h^i denotes a particular mesh size combination. The associated model outputs, i.e. g_{raw} = $\{g_{raw}(x_n, h^1), \ldots, g_{raw}(x_n, h^T)\}$, are then collected. A GP model is constructed using the mesh sizes and the corresponding outputs $\{h_{set}; g_{raw}\}$. The corrected estimate of the function value at input x_n is then predicted at h = 0, i.e., the function value is estimated at an infinitesimal mesh size. In the electronic packaging application, the finest affordable mesh size 0.005; Therefore, three mesh tests: h_{set} = {0.007, 0.006, 0.005} (same mesh in both x and y directions) are conducted; the mesh sizes together with the output component temperatures are used to train the GP model; after that, the heatsink temperature at h=0 is predicted using this GP model. **Figure 2.11** is a demonstration of GP getting trained by three data points (circle dot) and prediction at $h = 0$. The red square dot represents the mean prediction by the GP model and the green dashed lines are the 95% bounds. The Richardson extrapolation method is also applied under three mesh tests: h_R = {0.0072, 0.006, 0.005} (the mesh refinement ratios need to be constant), and its result denoted by the blue square dot agrees well with the GP prediction. Even though the true function value is deterministic, the GP prediction quantifies the uncertainty in estimating it. This

uncertainty is epistemic uncertainty due to the finite number of training points; as the number of training point increases, this uncertainty will be reduced.

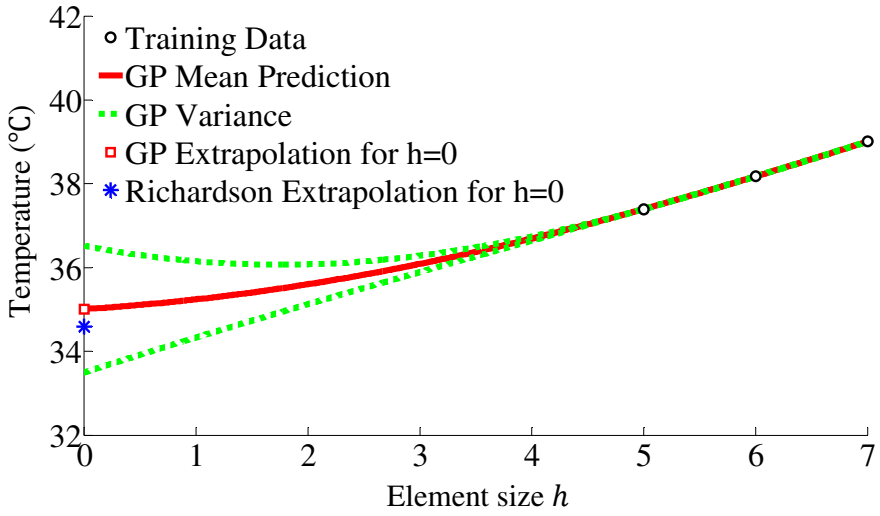

Figure 2.11 Mean and 95% bound of GP prediction, accounting for discretization error (Thermal analysis)

In stochastic MDA, discretization error needs to be quantified at each input realization using GP extrapolation. As mentioned above, the predictions of GP at mesh size $h = 0$ include a predicted mean value, and variance that indicates the uncertainty in the prediction as shown in **Figure 2.11**. The presence of the stochastic model prediction even for a single fixed input value poses a challenge for uncertainty propagation in coupled MDA. Consider one iteration of the coupled analysis in **Figure 2.10(b)**. Given one realization of the inputs $\boldsymbol{x}$, the output temperature $y_5 = Thermal(y_4, \boldsymbol{x})$ must be deterministic where T denotes the thermal analysis; however, when y_5 is evaluated using a GP, the outcome will

be accompanied with variability; the mean and standard deviation of the output, which are determined using Eq. (A1.4) and (A1.5), are functions of $\mathbf{x}$ and y_4:

$$f(y_5|\boldsymbol{x}) \sim N(\mu(\boldsymbol{x}, y_4), \sigma(\boldsymbol{x}, y_4)) \tag{2.18}$$

For each realization of $\boldsymbol{x}$ and y_4, the epistemic uncertainty due to model error will lead to a family of distributions for y_5. Since FORM requires a deterministic output from the performance function, the stochastic GP prediction cannot be directly used in the LAMDA method.

Therefore an auxiliary variable $P_h \sim U[0,1]$ is defined. With the auxiliary variable P_h, a unique value of the prediction can be determined through inverse CDF. Therefore, the model output becomes a deterministic function of $\boldsymbol{x}$, y_4 and h and the LAMDA approach can be implemented using FORM as in Eq. (2.8). Two different cases, with different model error assumptions are considered:

Case 1 (No model error): No assumption of model error is made for the electrical analysis; and for the thermal analysis, the temperature value is evaluated using the finest mesh within the limitation of computation resources. The uncertainty sources are only the six input variables; note that x_6 has both aleatory and epistemic uncertainty, whereas x_1 to x_5 have only aleatory uncertainty (fixed distribution type and distribution parameters).

Case 2 (Stochastic model error): The discretization error of thermal analysis is quantified using GP. The resulting uncertainty is then included in LAMDA using an auxiliary variable. The sources of uncertainty being considered are 5 aleatory inputs, 1 input with both aleatory and epistemic uncertainty, and the model prediction uncertainty due to discretization error. Note that the discretization error is actually deterministic, but there is uncertainty in estimating it because of a small number of mesh sizes tested. This

uncertainty is expressed by the variance of the GP prediction of temperature at $h = 0$. And in the MDA and sensitivity analysis, this uncertainty is represented by the auxiliary variable P_h.

2.6.2.2. PDF of the coupling variables and system output

The PDFs of temperature and component heat are estimated for both cases and are shown in **Figure 2.12**. The system level output, power density, is calculated as:

$$Power\ density = \frac{Component\ Heat\ (y_4)}{Heatsink\ Volume\ (x_1 \times x_2 \times x_3)} \tag{2.19}$$

where x_1, x_2, x_3 are the geometric parameters. Its distribution is evaluated using Monte Carlo simulation for illustration. Samples of component heat y_4 together with x_1, x_2 and x_3 are generated independently and used to calculate power density using Eq. (2.19). **Figure 2.12** compares the marginal PDFs of temperature and component heat under two model error assumptions; the PDFs of power density are compared in **Figure 2.13**. The first and second moments of the PDF are compared in **Table 2.6.**

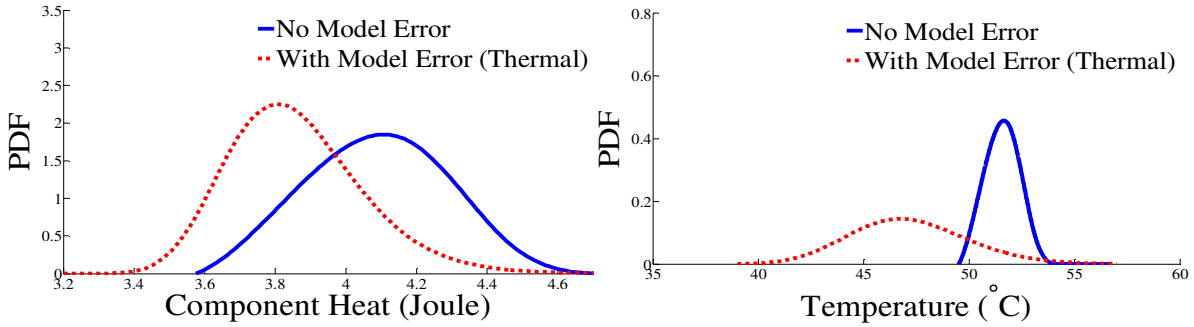

Figure 2.12 PDF of coupling variables: component heat y_4 (left) and temperature y_5 (right)

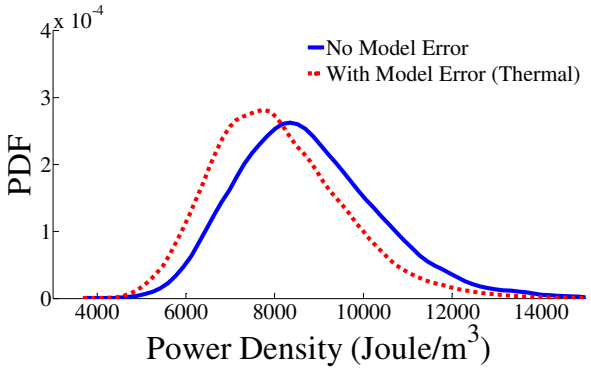

Figure 2.13 PDF of system output: power density

Table 2.6 Mean and standard deviation of temperature and power density

		Temperature	Component Heat	Power Density
No Model Error	**Mean**	52.24	4.13	8757.82
	STD	1.06	0.21	1618.00
Stochastic Model Error	**Mean**	47.13	3.98	8080.00
	STD	2.80	0.23	1507.09

The number of function evaluations in the LAMDA method when considering the model error and stochastic model output is 1219, whereas 910 evaluations are needed when no error is considered. When the disciplinary analyses are computationally cheap, SOFPI can be used to generate the benchmark solution (the entire PDF) for LAMDA to compare with, as shown in the earlier mathematical example. However, when the disciplinary analyses are expensive, it may not be affordable to generate the entire PDF using SOFPI. In such a situation, SOFPI could be run for a few samples of input realizations, and the SOFPI outputs can be compared against the PDF generated by LAMDA.

Figure 2.14 compares SOFPI results for 35 input realizations against the LAMDA-generated PDF for the coupling variables and the system level output. It is seen that the SOFPI results are within the range of the LAMDA-generated PDF. In addition to a graphical comparison, model validation techniques can also be used for a quantitative comparison; several such techniques are well studied in the literature [42, 43].

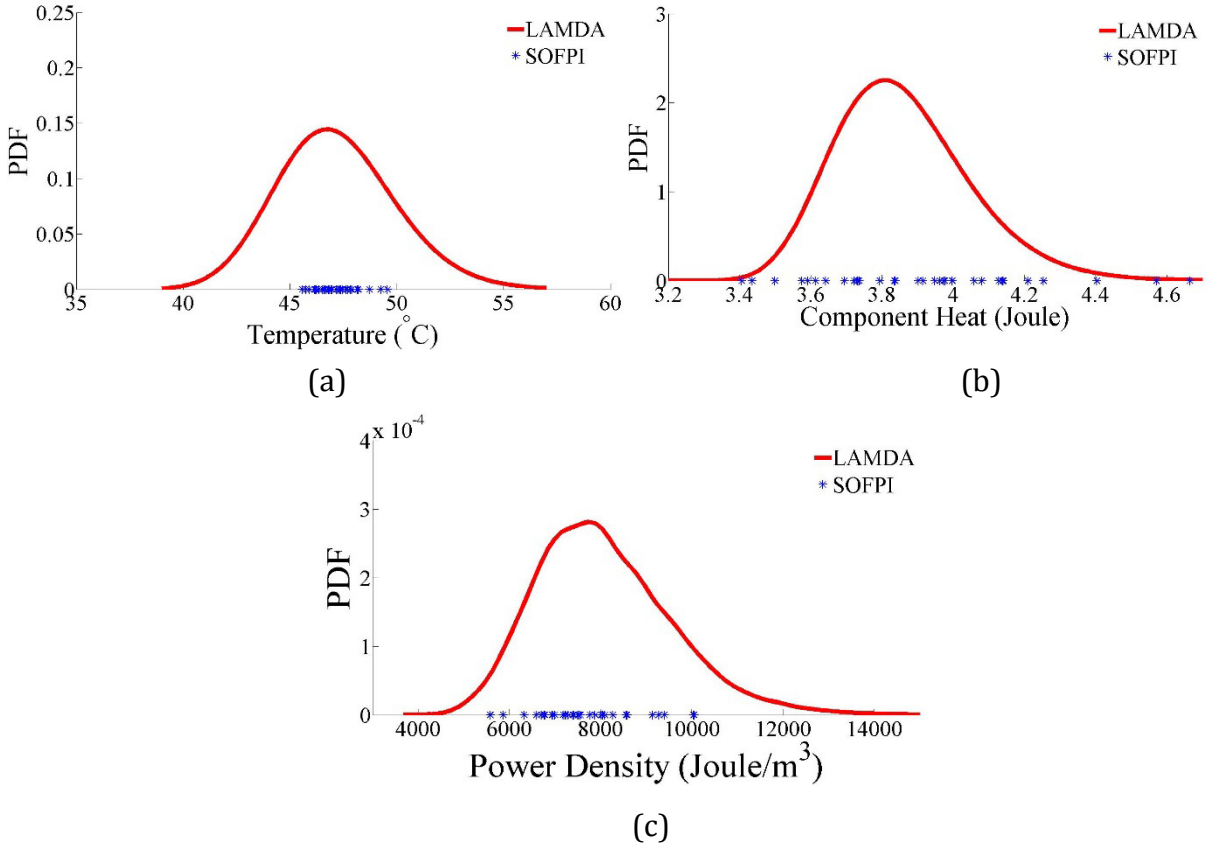

Figure 2.14: Comparison of results from LAMDA and SOFPI for (a) Temperature, (b) Component heat, and (c) Power density

2.6.2.3. Results and discussion

According to **Figure 2.11**, for a given input $\{x_1 \dots x_6\}$, the predicted temperature from thermal analysis decreases as the mesh becomes finer. This phenomenon agrees well with the PDFs of the temperature in **Figure 2.12**, where the distribution for the stochastic model error case shifts to the left compared with the no model error case. When model error is included, all subsystem outputs have greater variances as expected. In addition, the model error appears to cancel the effect of input variability and data uncertainty and lead to a smaller final output uncertainty. A GSA is implemented to quantify the sensitivity of heat to the input uncertainty and model error. The auxiliary variable P_h represents the uncertainty due to the GP-based estimation of discretization error (i.e., discretization error in thermal analysis). The total number of function evaluations mostly depends on how fast FORM converges. When the number of input, coupling and auxiliary variables is small, and if the analysis is linear, FORM converges quickly and the number of function evaluations is small. On the other hand, if the input and coupling variables are high dimensional, and if more auxiliary variables are used (i.e., more models with stochastic model error), or if the decoupled analysis is highly nonlinear, more function evaluations are expected for FORM to converge. The first-order sensitivity indices and the total-effect indices are given in **Table 2.7**.

Table 2.7: Sensitivity indices of electronic packaging problem

	x_1	x_2	x_3	x_4	x_5	x_6	P_h
First-Order	0.362	0.228	0.327	0.000	0.037	0.046	0.048
Total- Effect	0.371	0.236	0.333	0.000	0.038	0.049	0.053

In **Table 2.7**, variables x_1 to x_5 have aleatory uncertainty, x_6 has both aleatory and epistemic uncertainty, and P_h is epistemic uncertainty due to model error. The global sensitivity analysis is able to include both types of uncertainty by using the auxiliary variable approach. It is observed that in this example, three aleatory variables - length (x_1) and width (x_2) of the heatsink and the length of the fin (x_3) - have a dominant impact on the output variance, whereas the other uncertainty sources only have a small influence. Similarly to Table 2.4, the difference between the first-order and total effect is very small, which means the collaborative effect between the variables is negligible.

2.7. SUMMARY

This chapter proposed a methodology to include input variability, data uncertainty, and model errors within feedback-coupled MDA. Data uncertainty in the input random variables (due to sparse and/or imprecise data) is represented through non-parametric distributions using a likelihood-based approach. The effect of stochastic model error is considered by an auxiliary variable method based on the probability integral transform. These developments bring the epistemic uncertainty to the same level of analysis as input variability such that the propagation of both aleatory and epistemic uncertainty can be

implemented in a single loop manner. The auxiliary variable approach also provides a way for including epistemic uncertainty within global sensitivity analysis, which previously could only be applied to aleatory uncertainty sources. The proposed methodology thus provides a general formulation to include input data uncertainty, model form error and numerical errors (e.g., discretization error, surrogate model error, etc.) within feedback coupled MDA.

Based on the concept of likelihood, the next chapter investigates a novel approach to expand the scalability and solve MDA problems with a large number of coupling variables.

CHAPTER 3

STOCHASTIC MDA WITH HIGH-DIMENSIONAL COUPLING

3.1. INTRODUCTION

The problems addressed in the LAMDA approach and the methodology developed in Chapter 2 only contains one coupling variable in each direction. In reality, the number of coupling variables can be very large. For example, in the areoelasticity analysis of **Figure 1.1,** the nodal pressures and nodal displacements exchanged by CFD and FEA are both vectors of large size. In this scenario, the computational effort for even a first-order approximation increases dramatically with the dimension, while the solution accuracy drops even faster. Further, the disciplinary simulation models are computationally expensive, hence the function evaluations demanded by the LAMDA method is quite prohibitive.

Due to the scalability challenges posed by such problems, this chapter focuses on developing efficient methods for the uncertainty quantification for high-dimensional feedback coupled analysis. The LAMDA concept discussed in Chapter 2 is implemented using a Bayesian network, using samples of input, output and coupling variables from one iteration of feedback coupled MDA.

A Bayesian network (BN) is essentially the representation of a multivariate distribution through a directed acyclic graph which represents variables with nodes and

their dependence relationships with edges. Within mechanical systems, it has been used for system reliability assessment [63], model validation under uncertainty [64], diagnosis [65] and uncertainty quantification [66]. The Bayesian network is capable of incorporating a large number of variables and exhibits strong capability for uncertainty integration from multiple aleatory and epistemic sources [67, 68]. A Bayesian network can be created using multivariate samples to describe the statistical dependence among the variables and updated using available data. In this chapter, the satisfaction of the interdisciplinary compatibility is shown to be mathematically similar to updating with observed data, and thus the joint PDF of the coupling variables can be computed using the Bayesian updating process.

The estimation of the posterior distribution in Bayesian updating requires an appropriate sampling technique. Common algorithms such as Markov Chain Monte Carlo (MCMC) sampling [69] and expectation maximization [70] are computationally prohibitive for large size problems. To overcome this challenge, a copula-based sampling technique is introduced in this chapter to efficiently generate samples from the Bayesian network. A copula is a function that relates the joint CDF of multiple variables to their marginal CDFs and their correlations [71, 72]. The copula has been used to obtain the joint CDF in many fields such as actuarial science and statistics [72], and in investigating reliability analysis and RBDO for correlated [15] and non-Gaussian [73] input random variables. In this chapter, given interdisciplinary compatibility, the copula is conditionally sampled [67] to estimate the conditional joint distribution of all the variables.

Generating samples from a Bayesian network using a copula-based approach is quite general. However, if a joint Gaussian copula is assumed, then the conditional joint

updating and conditioning of the BNs can be accomplished analytically [74], providing tremendous computational efficiency.

In the aeroelasticity problem, the coupling variables in each direction (e.g., pressure, displacement) are correlated to each other. This issue leads to difficulty in the numerical implementation because the quantities at neighboring nodes are highly correlated, causing singularity in the covariance matrix of the copula. Therefore, a principal component analysis (PCA) [75] is adopted to capture the dominant variance in the data and reduce the dimensionality, and the Bayesian network is built in the principal component space.

The contributions of this chapter can be summarized as follows:

1. Develop a Bayesian network approach for stochastic MDA with feedback coupling;
2. Use copula-based sampling for efficient construction of the joint PDF of coupling variables that satisfy interdisciplinary compatibility; and
3. Use principal component analysis to reduce the dimension of the Bayesian network.

The proposed approach consisting of the above three contributions is referred to as BNC-MDA (Bayesian Network and Copula-based Multi-Disciplinary Analysis) in this dissertation. BNC-MDA is basically the implementation of the LAMDA concept using a Bayesian network, which facilitates scaling up to high-dimensional problems. The proposed method is illustrated using a mathematical MDA problem first, and later using an aircraft wing aeroelastic analysis problem.

The rest of the chapter is organized as follows. Section 3.2 discusses the difficulty of LAMDA in solving high-dimensional coupled MDA. Section 3.3 develops the proposed BNC-MDA methodology. Two numerical examples - a mathematical example and an aeroelastic

problem - are presented in Section 3.4 to demonstrate the proposed methodology. Section 3.5 provides concluding remarks.

3.2. CHALLENGES POSED BY HIGH-DIMENSIONAL COUPLING

This section briefly analyzes the difficulty in applying FORM-based LAMDA (Chapter 2) to problems with a large number of coupling variables.

In the LAMDA approach, for a given instance of the coupling variable, the integral in Eq. (2.3) is computed by taking the finite difference of two FORM analyses. This calculation needs to be repeated for multiple instances of the coupling variable to construct its PDF using Eq. (2.5).

In high-dimensional coupled problems where the coupling quantities are large in number, each individual discipline accepts and yields a large number of coupling variables as inputs and outputs respectively (e.g., displacements and pressures at a large number of nodes in coupled FEA/CFD analyses). In this case, the joint distribution of the coupling variables needs to be evaluated. Consider a problem with two coupling variables in each direction as shown in **Figure 3.1(a)**. A single iteration is shown in **Figure 3.1(b)**. To estimate the joint distribution of $\boldsymbol{U_{21}}$ and $\boldsymbol{V_{21}}$ under interdisciplinary compatibility, suppose a first-order approximation of the bivariate joint distribution is adopted [76].

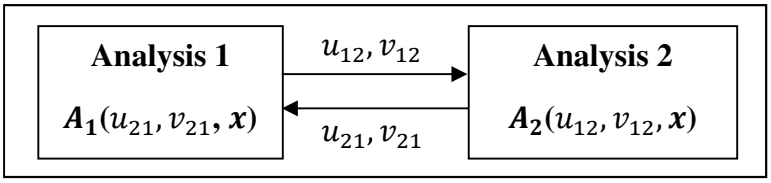

(a) Coupled analysis with two coupling variables in each direction

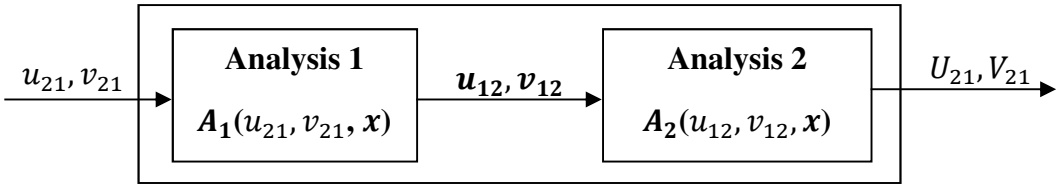

(b) One iteration of the coupled analysis

Figure 3.1 Two-dimensional coupled analysis and one iteration representation

The coupling variables from "Analysis 2" to "Analysis 1" are denoted by $\boldsymbol{u_{21}}$ and $\boldsymbol{v_{21}}$. To evaluate the joint PDF value at an instantiation of (u_{21}, v_{21}), the FORM analysis needs to be conducted to compute four joint CDFs F_1 at $(u_{21} + \delta_1, v_{21} + \delta_2)$, F_2 at $(u_{21} + \delta_1, v_{21} - \delta_2)$, F_3 at $(u_{21} - \delta_1, v_{21} + \delta_2)$ and F_4 at $(u_{21} - \delta_1, v_{21} - \delta_2)$. Then finite difference can be used to obtain the joint PDF value at (u_{21}, v_{21}):

$$f(u_{21}, v_{21}) = \frac{F_1 - F_2 - F_3 + F_4}{4\delta_1\delta_2} \tag{3.1}$$

As the number of coupling variables increases, the number of function evaluations required by the above finite difference procedure becomes very large. For example, consider 2 disciplinary analyses coupled by n variables in each direction. If 10 integration points are taken for each variable, 10^n points will need to be evaluated in the n-dimensional hypercube. At least $2n + 1$ FORM analyses need to be executed at each point for the finite difference analysis. Assuming m function evaluations are required for each

FORM analysis to converge (on average), the total number of function evaluations is: $10^n \times (2n+1) \times m$. As n increases, the number of function evaluations will become enormous, resulting in prohibitive computational effort. In addition, since FORM is a first-order approximation, the nonlinearity of the function G may also affect the accuracy, and the approximation may get worse as the dimension becomes higher. Consequently, the problems that can be solved by the original LAMDA approach (implemented using FORM and finite difference) are confined to low-dimensional coupling where the functions are inexpensive to evaluate and not highly nonlinear. Therefore, Section 3.3 develops a Bayesian network-based approach to implement the LAMDA concept for high-dimensional problems.

3.3. BAYESIAN NETWORK AND COPULA-BASED SAMPLING

The Bayesian network approach is investigated in this section, together with a copula-based sampling technique, to overcome the challenges of high-dimensional coupling discussed above. Given samples of coupling variables yielded by individual disciplinary analyses in two consecutive iterations, a Bayesian network is constructed to represent the joint distribution of these coupling variables. Next, a copula-based sampling technique is used to generate samples of the coupling variables that satisfy interdisciplinary compatibility.

3.3.1. BAYESIAN NETWORK FOR COUPLING VARIABLES DISTRIBUTION

A Bayesian network (BN) is a probabilistic graphical model that represents a multivariate joint distribution (nodes) through univariate distributions and conditional probabilities (edges). A common usage of the Bayesian network is to infer the posterior distribution of the nodes given observed data (evidence). The posterior probability of event U given evidence e could be evaluated using Bayes' theorem as:

$$P(U|e) = \frac{P(U,e)}{P(e)} = \frac{P(U,e)}{\sum_U P(U,e)} \tag{3.2}$$

In a coupled analysis, the uncertainty regarding the coupling variables in MDA can be represented by their probability distributions conditioned on interdisciplinary compatibility. The Bayesian network for the two-discipline analysis of **Figure 3.1**, regarding two coupling variables in one direction is shown in **Figure 3.2**. In this network, u_{21} and v_{21} represent the coupling variable values generated from the i^{th} iteration, while U_{21} and V_{21} are the corresponding values from the $(i+1)^{th}$ iteration. $\varepsilon_{u_{21}}, \varepsilon_{v_{21}}$ represent the differences of the corresponding variable values between the two iterations, i.e.,

$$\varepsilon_{u_{21}} = U_{21} - u_{21},\ \varepsilon_{v_{21}} = V_{21} - v_{21} \tag{3.3}$$

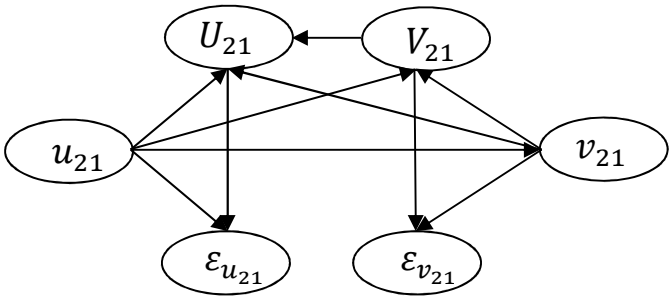

Figure 3.2 Bayesian network connecting coupling variables in two successive iterations

Due to the input uncertainty, the coupling variables and the difference terms are all stochastic quantities. The Bayesian network can be trained using samples of these variables, generated by first generating samples of input variables $\boldsymbol{x}$ and executing the $(i-1)^{th}$ and the i^{th} iterations of the coupled analysis. Note that the $\boldsymbol{x}$ variables are not included in the BN, since our interest is in connecting the coupling variables in two consecutive iterations for the same $\boldsymbol{x}$. The evidence *e*, which is interdisciplinary compatibility being satisfied, can be represented as $\left[\varepsilon_{u_{21}}, \varepsilon_{v_{21}}\right] = [0,0]$. Therefore, the joint PDF of U_{21}, V_{21}, u_{21} and v_{21} given the compatibility condition is:

$$f_{U_{21},V_{21},u_{21},v_{21}}\left(U_{21},V_{21},u_{21},v_{21}|U_{21}=u_{21},V_{21}=v_{21}\right) = f_{f_{U_{21},V_{21},u_{21},v_{21}}}\left(U_{21},V_{21},u_{21},v_{21}|\varepsilon_{u_{21}}=0,\varepsilon_{v_{21}}=0\right) \tag{3.4}$$

This formulation could be easily extended to coupled analyses with higher dimensions. The accuracy of the Bayesian network depends on the number of training samples. In the Bayesian network in **Figure 3.2**, the samples of the coupling variables used to construct the Bayesian network are obtained from two consecutive iterations of the original coupled analysis. Since a full convergence analysis is not required, collecting a

large number of samples of the coupling variables becomes more affordable for high-fidelity models.

To evaluate the joint posterior distribution in Eq. (3.4), a proper sampling technique is required. Markov Chain Monte Carlo (MCMC) sampling is frequently used in Bayesian updating [77]; however, this technique is usually time-consuming. Therefore, a vine copula-based sampling technique is employed here to estimate the joint PDF in an efficient manner.

Details of Bayesian network and vine copula-based sampling are provided in Appendix II.

3.3.2. DIMENSION REDUCTION OF THE BAYESIAN NETWORK

The technique of BNC-MDA could be used for both the forward problem, i.e. uncertainty propagation, and the inverse problem, i.e. Bayesian inference. The size of the Bayesian network for a high-dimensional problem increases as the number of variables increases. For example, in the aeroelastic problem shown in **Figure 1.1**(and later discussed in Section 3.4.2), the FEA mesh has 258 nodes. Each node has 1 nodal pressure and 3 nodal displacements (along each coordinate). Therefore, it leads to a coupled system with 258 nodal pressures as coupling variables in one direction, and 774 nodal displacements as coupling variables in the other. Using the proposed decoupled approach, we can simplify the problem by only looking at the direction with fewer coupling variables. Nevertheless, it still requires us to build a BN similar to **Figure 3.2** but with 258 nodes each for the nodal pressure at the $(i-1)^{th}$ iteration, the i^{th} iteration and the difference between them (thus

774 nodes in one BN). This will cause a tremendous amount of work constructing the network. Meanwhile, the nodal pressures in adjacent nodes are highly correlated with each other. This may lead to a singular covariance matrix affecting the sampling.

Therefore, principal component analysis (PCA) is adopted for the purpose of reducing the dimensionality of the BN. PCA, also known as Karhunen-Loeve expansion or proper orthogonal decomposition [75] depending on the field of application, maps correlated variables to an uncorrelated space using an orthogonal transformation. The resulting uncorrelated variables are referred to as principal components. Each principal component is a linear combination of the original variables; all the principal components are orthogonal to each other, hence no redundant information is stored. The number of principal components is as large as the original set of variables, but the first few principal components may capture a large fraction of the total variance of the original data if the original variables have strong correlation. Therefore, use of PCA helps to reduce the number of variables (i.e., first few principal components) while including most of the variance in the problem.

In the context of high-dimensional coupled MDA, coupling variables in each direction constitute a vector. Considering one iteration of the coupled analysis as shown in **Figure 3.3**, assume that the input coupling variable $\boldsymbol{u_{21}}$ is a vector consisting of N components; so is the output $\boldsymbol{U_{21}}$. Considering the variability in input $\boldsymbol{x}$, if we draw M random samples of $\boldsymbol{x}$, then each component of the vectors $\boldsymbol{u_{21}}$ and $\boldsymbol{U_{21}}$ has the corresponding M samples.

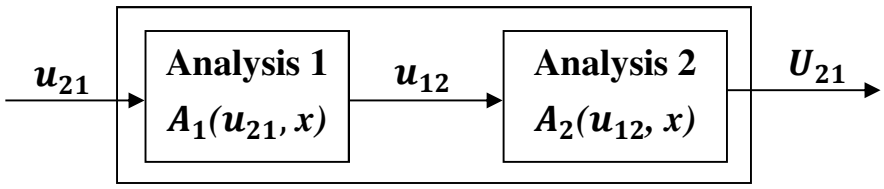

Figure 3.3 One iteration of a high-dimensional coupled system

The M pairs of $\boldsymbol{u_{21}}$ and $\boldsymbol{U_{21}}$ are first merged into a single $2M \times N$ matrix: the first M rows as samples of input $\boldsymbol{u_{21}}$ and last M rows as samples of output $\boldsymbol{U_{21}}$, and each column representing one component of the vector $\boldsymbol{u_{21}}$(and the corresponding component of $\boldsymbol{U_{21}}$). We denote this $2M \times N$ data matrix by $\boldsymbol{X}$. The singular value decomposition is denoted as $\boldsymbol{X} = \boldsymbol{U\Sigma V}^T$, where $\boldsymbol{\Sigma}$ is a $2M \times N$ rectangular diagonal matrix with $\sqrt{\lambda_i}$, $(i = 1 \dots N)$ at the first N diagonal entries, and zeros at the rest. $\boldsymbol{V}$ is the $N \times N$ matrix of the eigenvectors of $\boldsymbol{X^T X}$, and $\boldsymbol{U}$ is a $2M \times 2M$ matrix of vectors, each of which is calculated as $\boldsymbol{u_i} = \frac{\mathbf{1}}{\sqrt{\lambda_i}} \boldsymbol{X v_i}$. The PCA transformation of $\boldsymbol{X}$ with preserved dimensionality is given by:

$$\boldsymbol{Y}^T = \boldsymbol{X}^T \boldsymbol{U} = \boldsymbol{V\Sigma}^T \boldsymbol{U}^T \boldsymbol{U} = \boldsymbol{V\Sigma}^T \tag{3.5}$$

where each row of $\boldsymbol{Y}$ is a linear transformation of the corresponding row in $\boldsymbol{X}$. Since:

$$\boldsymbol{X} = \boldsymbol{UY} \tag{3.6}$$

If $\boldsymbol{W}$ denotes the first l rows of $\boldsymbol{U}$, and $\boldsymbol{Z}$ denotes the first l columns of $\boldsymbol{Y}$, then approximation of $\boldsymbol{X}$ by $\widetilde{\boldsymbol{X}}$ is achieved as:

$$\widetilde{\boldsymbol{X}} = \boldsymbol{WZ} \tag{3.7}$$

l is the selected number of principal components (PCs). The number of PCs required is determined by the amount of variance captured. Note that the matrix $\boldsymbol{Z}$ consists of two parts: the top M rows are the principal components for input $\boldsymbol{u_{21}}$, i.e., $PC^j_{\boldsymbol{u_{21}}}, j = 1 \dots l$, whereas the bottom M rows are the principal components for output $\boldsymbol{U_{21}}$, i.e., $PC^j_{\boldsymbol{U_{21}}}, j = 1 \dots l$. After PCA, the differences between the corresponding principal components of $\boldsymbol{u_{21}}$ and $\boldsymbol{U_{21}}$ are calculated as:

$$\boldsymbol{\varepsilon^j_{PC} = PC^j_{u_{21}} - PC^j_{U_{21}}} \tag{3.8}$$

and a Bayesian network is built with the quantities in Eq. (3.8). The resulting Bayesian network has $3l$ nodes. A simplifying approximation is also possible, by assuming the uncorrelated nodes to be separated (no edges). In that case, the full Bayesian network is decomposed into l smaller Bayesian networks with 3 nodes each. The smaller Bayesian network for the i^{th} principal component is shown in **Figure 3.4**.

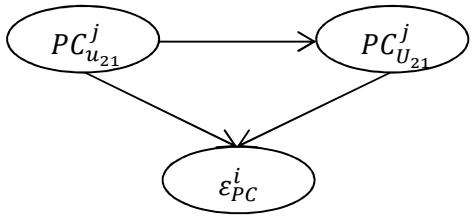

Figure 3.4 Bayesian network using the j^{th} principal component

Once the network is built, impose $\varepsilon^i_{PC} = 0$ and update the distribution of $PC^i_{u_{21}}$. Prior to PCA, there was one BN for the entire problem containing all the correlated coupling

variables in one direction. After applying PCA, we have a few principal components that are uncorrelated. As a result, we have a smaller BN with all the principal components in one network, or if the above approximation is invoked, a few separate BNs for the principal components, each with only 3 nodes as shown in **Figure 3.4**. Thus in the example in Section 3.4.2 , if 10 or 20 principal components are used to implement the proposed methodology, the monolithic BN with 774 nodes is either reduced to a smaller size BN with 30 or 60 nodes, or based on the above approximation, decomposed into 10 or 20 independent BNs, each with only 3 nodes. Therefore, by using PCA we can reduce a large BN in two ways and drastically improve the efficiency in solving high-dimensional problems. The updated samples of the first few principal components are converted to the original correlated space using Eq. (3.7) to get the joint distribution of the coupling variables under interdisciplinary compatibility condition.

Note that PCA is applied in this research in a manner different from previous applications of PCA in the context of MDA. In previous applications, PCA is used to identify the principal components among the inputs and outputs, and then a reduced-order model is built in terms of the principal components [78]. However, in this research, we use PCA only to reduce the dimension of the Bayesian network; the training samples for the Bayesian network are generated from the analysis of the full model, not a reduced-order model.

In summary, the proposed BNC-MDA methodology has four elements: (1) a Bayesian network is built using the samples of the coupling variables from 2 consecutive iterations. (2) The distributions of the coupling variables are estimated using a Bayesian network by enforcing the interdisciplinary compatibility condition, in a manner similar to updating the

Bayesian network with observed data. (3) A vine copula-based sampling technique is adopted for efficient sampling from the joint distribution. (4) Principal component analysis is used to reduce the dimension of the Bayesian network for further efficiency of the BNC-MDA methodology. Note that the coupled multi-disciplinary analysis (only a few iterations) is only required in the first element and dominates the computational effort. The effort in the other three elements is negligible compared to that for the first element, as will be demonstrated in the aeroelasticity example below (in **Table 3.5** and **Table 3.6**). The more iterations the coupled physics analysis requires for convergence, and the longer each individual disciplinary analysis takes, the more time will be saved by using BNC-MDA. The steps are summarized in the flowchart in **Figure 3.5**.

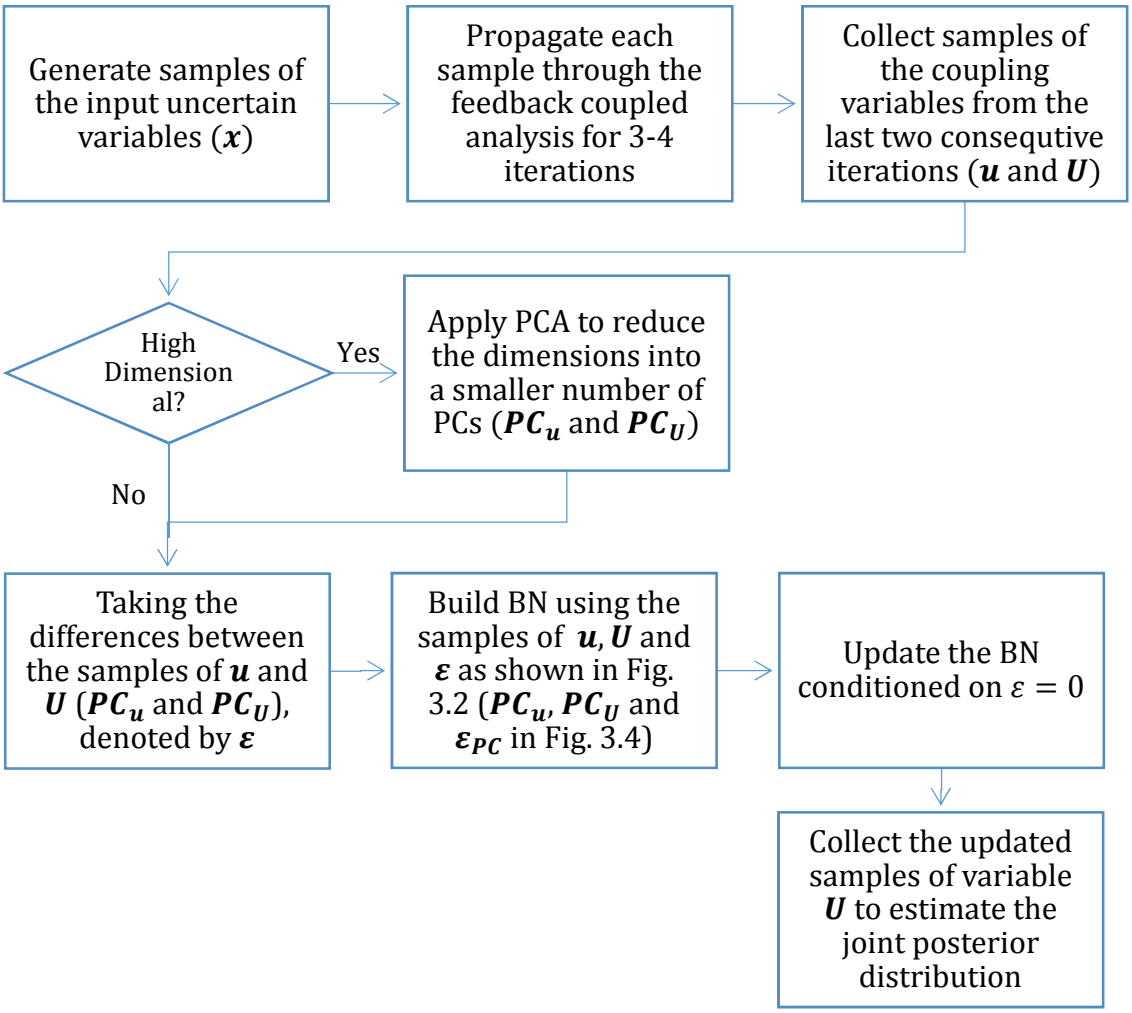

Figure 3.5. Flowchart of BNC-MDA approach

It is also worth noting that the proposed BNC-MDA framework is a sample-based methodology. This method includes two stages of sampling: (1) generating samples as training points for the Bayesian network, and (2) after the BN is built, samples are generated conditioned on the compatibility condition; this is a separate step from (1). The input distributions come into play in the first stage, while generating training points for the BN. The input distributions can be correlated or uncorrelated; the training samples should

be generated accordingly. It is significant to realize that generating samples of the input variables is the step prior to constructing the Bayesian network.

3.4. NUMERICAL EXAMPLES

In this section, a mathematical problem with two coupling variables in each direction is first presented to compare the previous methods (SOFPI, FORM-based LAMDA) and the proposed BNC-MDA method. A multidisciplinary aeroelastic analysis of an aircraft wing is then used to demonstrate the effectiveness of the proposed approach to higher dimensional problems.

3.4.1 MATHEMATICAL MDA PROBLEM

The numerical example in [11] is modified to include two coupling variables in each coupling direction. This is an extension of the problem discussed in Du and Chen [79], and later in [10] where only two analyses were considered. The functional relationships are shown in **Figure 3.6**. The input variables $\boldsymbol{x} = [x_1, x_2, x_3, x_4, x_5]$ are assumed to be normally distributed: $N(1,1)$ and independent of each other. The independent and normal input assumption does not affect the proposed BNC-MDA methodology. If some of the input variables are correlated, we need to jointly sample these variables, then propagate them through one iteration of the coupled analysis to calculate the corresponding coupling

variable values. But the Bayesian network is only built after the training samples are generated. These training samples could be generated in a correlated or independent manner, depending on the problem data.

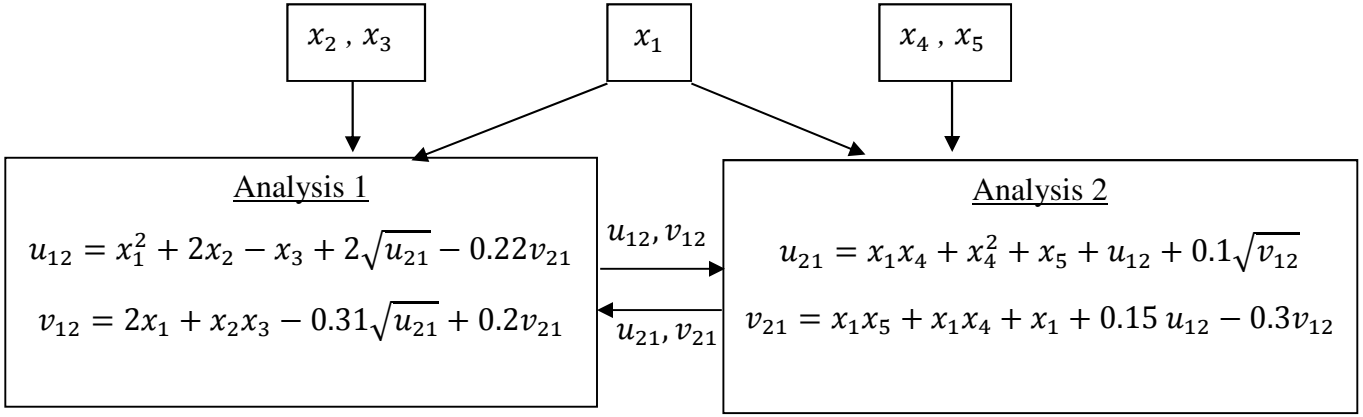

Figure 3.6. Mathematical example of two-discipline coupled analysis

In **Figure 3.6**, the coupling variables are u_{12}, v_{12} from "Analysis 1" to "Analysis 2", and u_{21}, v_{21} in the opposite direction. For the purpose of illustration, only the joint distribution of $u_{21}$and v_{21} is estimated and the joint distribution of u_{12} and v_{12} can be calculated using the same method. In this example, we focus on calculating the PDFs of the coupling variables and do not calculate any further system output.

Once the joint distribution of the coupling variables $u_{21}$and v_{21} is obtained, one can propagate Monte Carlo samples of this joint distribution through one iteration of the feedback coupled analysis similar to **Figure 2.3**, to obtain the corresponding samples of the coupling variables in the other direction, as well as the disciplinary and system level output (which are not assumed in this example). The dependence relations among the output and the coupling variables are preserved, because the connections between the two disciplinary analyses are not completely severed.

Three different approaches, i.e. SOFPI, LAMDA and BNC-MDA are implemented to solve this problem. 10,000 samples of inputs are generated to execute the SOFPI method, which requires 107,421 function evaluations in total. A 2-D kernel density estimation technique is adopted to build the joint distribution. The resultant joint distribution of the coupling variables is used as the benchmark solution.

In the LAMDA method, 10 integration values are chosen in Eq. (2.3) for each coupling variable. Therefore, a total of 100 likelihood values need to be evaluated; and an overall 14,619 function evaluations are required. A cubic spline interpolation is then exploited to construct the entire joint distribution.

In the BNC-MDA method, 1,000 samples of the input and output of the function in **Figure 3.1(b)** are generated. The training points for building the Bayesian network are

generated by samples of the input variables x_1 to x_5 and coupling variables u_{21}, v_{21} to run through one iteration of the coupled analysis to calculate U_{21}, V_{21}. Samples of the outputs after the first and second iterations of the coupled MDA are collected; the number of function evaluations is twice the number of the samples, which in this case is 2,000. The computational cost of the three approaches is summarized in **Table 3.1**. The outputs from the two iterations together with their differences are used to construct the Bayesian network shown in **Figure 3.4**. Note that PCA is not used within BNC-MDA in this examples, since there are only two coupling variables in each direction. The results using the three approaches are listed in **Table 3.2**, and the marginal distributions are compared in **Figure 3.7**.

Table 3.1. Comparison of computational cost

Approach	Number of input samples	Integration values for $u_{21}\backslash v_{21}$	Total number of function evaluations
SOFPI	10,000	N\A	107,421
LAMDA	N\A	8:0.5:15\0:0.25:3.5	14,619
BNC-MDA	1000	N\A	2,000

Table 3.2. Results using SOFPI, LAMDA and BNC-MDA

	U_{21}		V_{21}		$\rho_{U_{21}V_{21}}$
	μ	σ	μ	σ	
SOFPI	11.65	0.69	1.6	0.16	0.24
LAMDA	11.48	0.67	2.02	0.17	0.52
BNC-MDA	11.59	0.69	1.59	0.15	0.24

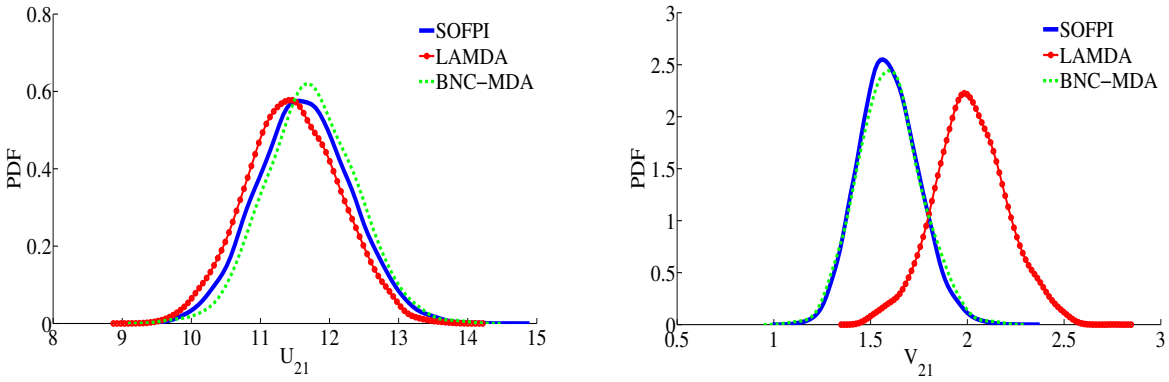

Figure 3.7 Marginal PDFs of coupling variables

It can be concluded from **Table 3.2** and **Figure 3.7** that the proposed BNC-MDA method is able to capture the probability distribution of V_{21} and the value of the $\rho_{U_{21}V_{21}}$ better than the original LAMDA, even though the mean and standard deviation of the marginal distribution of U_{21} calculated by LAMDA and BNC-MDA are both quite close to the benchmark solution. The Kullback-Leiber (K-L) divergence [80] is estimated for the marginal distributions of U_{21} for further comparison of accuracy.

The K-L divergence of distribution q from distribution p, denoted by $D_{KL}(p||q)$, is a measure of the information lost when p is approximated by q. A smaller value of the K-L divergence indicates a greater similarity between the two distributions. For continuous distributions p and q, the K-L divergence is defined as:

$$D_{KL}(p||q) = \int_{-\infty}^{+\infty} p(x)\ln(\frac{p(x)}{q(x)})dx \tag{3.9}$$

In practice, the PDFs are evaluated numerically, and the K-L [80] divergence is calculated as:

$$D_{KL}(p||q) = \sum_{i=1}^{n} \ln(\frac{p(x_i)}{q(x_i)})p(x_i) \tag{3.10}$$

where p and q represent the PDF values at x_i and n is the number of points at which the PDF are evaluated; in this chapter, $n = 1{,}000$. The K-L divergence is only defined if areas of p and q each sums to 1, and $p(x_i) > 0$ and $q(x_i) > 0$ simultaneously. The K-L divergence value with respect to SOFPI is 0.033 for LAMDA and 0.016 for BNC-MDA; thus the BNC-MDA method results in a better approximation to the benchmark solution than the LAMDA approach (also confirmed by **Figure 3.7**). The large error produced by the LAMDA approach is mostly due to its adoption of the first-order approximation.

This mathematical example demonstrates the advantage of the proposed BNC-MDA method for bivariate coupling in each direction. The method achieves an accurate result while requiring much fewer function evaluations compared with both SOFPI and LAMDA. The next example illustrates the benefits of BNC-MDA in the case of high-dimensional coupling.

3.4.2 MDA FOR AIRCRAFT WING

In this section, a three-dimensional aeroelastic analysis of an aircraft wing is used to illustrate the proposed BNC-MDA method. A cantilevered wing with a NACA 0012 airfoil is adopted [81]. We use ANSYS to perform the fluid-structure interaction analysis of the wing. The fluid and structure meshes are shown in **Figure 3.8**.

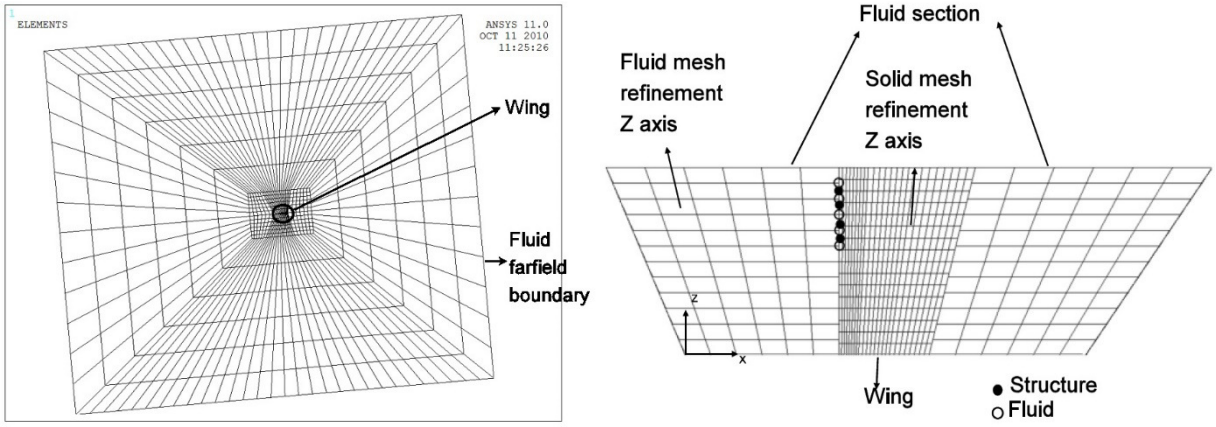

(a) Overall view (b) Fluid and structure meshes

Figure 3.8 Fluid and structure meshes and refinement parameters

This problem consists of hundreds of coupling quantities in each direction. In this case, the computational effort of LAMDA — even if combined with PCA (LAMDA+PCA) — will still be very high while the accuracy will be worsened (due to the use of finite difference and the construction of a joint probability distribution with a sparse grid of integration points and using FORM). The total number of function evaluations in the LAMDA method assuming 10 integration values for each coupling variable is $10^n \times (2n + 1) \times m$ (n: number of coupling variables, m: average number of function evaluations for each FORM analysis). If n is too large and only 20 principal components are used, 'LAMDA+PCA' approach still needs $10^{20} \times 21 \times m$ function evaluations, which is an enormous amount of computing effort. Therefore, the 'LAMDA+PCA' approach is not affordable and not pursued here. BNC-MDA, which requires much fewer training samples of the input and coupling variables (and not fully convergent analysis) to construct the

Bayesian network, is very efficient in solving the problem; its accuracy will be compared with the SOFPI approach below.

This example is run with two different mesh sizes (258 nodes and 1218 nodes) below. The backsweep angle *bw* is chosen to be the input variable with natural variability, and is assumed to be normally distributed as $N(0.4,0.04)$ without loss of generality. 110 realizations of the backsweep angle are sampled to perform the coupled FSI analysis. The values of nodal pressure oscillate drastically in the first and second iterations; typically a large bias between the PDFs of the coupling variables will occur, and the resulting difference term ε will be either all positive or all negative. If the empirical CDF of ε for the copula is computed using all positive (or all negative) values, the conditional sampling will need an extrapolation to calculate the conditional joint distribution given $\varepsilon = 0$. This will significantly decrease the accuracy the proposed approach. To balance the solution accuracy and the computational efficiency, the FSI analysis is terminated after 3 iterations, the Bayesian network is built with the nodal pressure results of the 2nd and 3rd iterations.

Table 3.3. Cumulative distribution of the first 30 principal components

No. of PCs	258 Nodes	1218 Nodes	No. of PCs	258 Nodes	1218 Nodes
1	0.7412	0.7095	16	0.9909	0.9931
2	0.8344	0.7825	17	0.9919	0.9943
3	0.9007	0.8400	18	0.9929	0.9954
4	0.9237	0.8871	19	0.9937	0.9962
5	0.9389	0.9160	20	0.9944	0.9969
6	0.9501	0.9349	21	0.9949	0.9976
7	0.9604	0.9473	22	0.9954	0.9980
8	0.9677	0.9584	23	0.9959	0.9983
9	0.9736	0.9669	24	0.9963	0.9986
10	0.9788	0.9739	25	0.9966	0.9989

11	0.9818	0.9804	26	0.9969	0.9991
12	0.9845	0.9842	27	0.9972	0.9992
13	0.9865	0.9872	28	0.9974	0.9993
14	0.9882	0.9894	29	0.9977	0.9994
15	0.9896	0.9914	30	0.9978	0.9995

It can be seen from **Table 3.3** that, after applying PCA, the first 30 PCs can cover more than 99.99% or the variances from the original samples. Therefore, six cases are discussed here: (1) BNC-MDA method using first 10 principal components. (2) BNC-MDA method using 15 principal components. (3) BNC-MDA method using 20 principal components. (4) BNC-MDA method using 30 principal components. (5) Output collected after 2 iterations. (6) Output collected after 3 iterations. For Cases 1, 2, 3 and 4, 5,000 samples are generated using the BN to estimate the coupling variable distributions. The result of SOFPI is used as the benchmark solution.

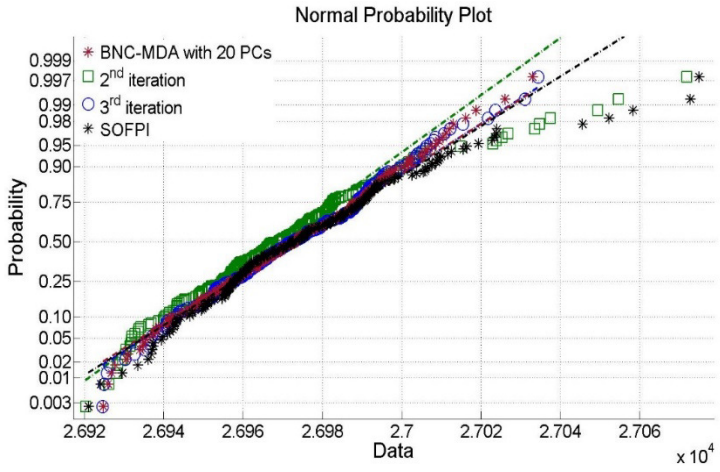

Figure 3.9 Normal probability plot of pressure from four cases at Node 1

Figure 3.9 shows the normal probability plot of Cases 3, 5, 6 as well as the benchmark solution (SOFPI) at Node 1. Cases 3 and 6 are closer to the SOFPI distribution compared with case 5. For an *n*-variable distribution, the K-L divergences for all marginal distributions are computed, and an average value is estimated using Eq. (3.11).

$$\text{Average } D_{KL} = \frac{\sqrt{\Sigma_{i=1}^{n}\left(D_{KL}^{i}(p||q)\right)^{2}}}{n} \tag{3.11}$$

where D_{KL}^{i} denotes the K-L divergence of the marginal distribution for the i^{th} node, and n is the total number of the nodes. For the sake of comparison, the Student's t-copula is also used to implement the BNC-MDA approach. **Table 3.4** summarizes the average K-L divergences for all six cases, using both Gaussian and t copulas.

Table 3.4. Kullback-Leiber divergence for different scenarios (258 nodes)

	BNC-MDA				FSI	
	10 PCs	**15 PCs**	**20 PCs**	**30 PCs**	**2^{nd}Iter**	**3^{rd}Iter**
Average D_{KL}^{Gauss}	0.25	0.19	0.16	0.16	0.21	0.18
Average D_{KL}^{t}	0.24	0.21	0.20	0.19		

The following observations are made:

1. The results using the Gaussian and t copulas are similar for this problem.
2. Case 1, Case 2, Case 3 and Case 4: As the number of utilized principal components increases, the K-L divergence becomes smaller and converges after 20 PCs. As more principal components are taken, more variance of the original data is captured, and the results are refined; however, for this example, 20 PCs are seen to be sufficient.

3. Case 5 and Case 6: Case 6 approaches the converged results better than Case 5. As the iteration number (of the physics analysis) increases, the stability of the solution is enhanced, and the differences between the results from consecutive iterations will become smaller. Also, the 3rd iteration of FPI achieves similar accuracy as the BNC-MDA result in the wing problem; therefore, very few further iterations of FPI are needed for convergence. The proposed BNC-MDA approach saves the computational effort by reducing the total number of iterations in the feedback coupled analysis. Therefore, the more iterations the FPI analysis requires for convergence, and the longer each individual disciplinary analysis takes, the more time will be saved by using BNC-MDA.
4. In the implementation of BNC-MDA in this example, the large BN is broken into several separated small BNs for sampling, as in **Figure 3.4**. This is an approximation since 'uncorrelated' does not imply 'independent'. To verify the accuracy of this approximation, we have also considered an unseparated network with 20 principal components connected to each other as shown in **Figure 3.10**.

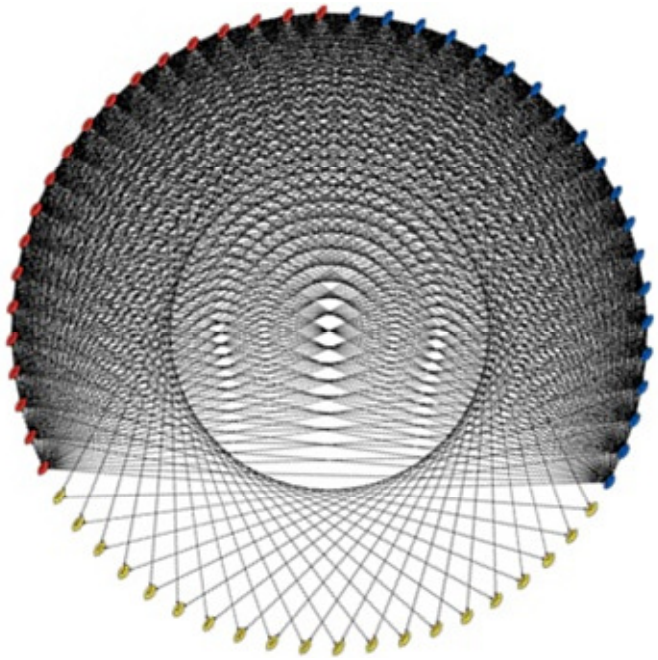

Figure 3.10 Unseparated Bayesian network with 20 principal components

Each node in the network represents a random variable. The 40 nodes on the top left and top right denote the principal components of the nodal pressure after the 2nd and 3rd iterations respectively. The bottom 20 nodes, each connected to 2 nodes, represent the differences between the corresponding values. This unseparated BN is costly to build, and requires care in connecting the nodes correctly since it is particular to each problem, whereas the separated network is generic and only consists of 3-node networks as in **Figure 3.4**. Thus the separated network although approximate, is easy to implement for high-dimensional problems, but its accuracy needs to be verified. The average D_{KL} is computed between the results of the unseparated network and the independent network, and found to be 0.063, which indicates very similar solutions given by both methods. Therefore, the

approximation of individual separated BNs improves the efficiency of the BNC-MDA methodology for this example without too much sacrifice of the accuracy.

5. To demonstrate the scalability of the proposed BNC-MDA approach, the same aeroelasticity problem is considered with a finer mesh of 1218 nodes. Thus the number of coupling variables in each direction is increased to 1218 (nodal pressures) and 3654 (nodal displacements). The same 110 realizations of the input variables (as in the coarse mesh model) are used to perform both BNC-MDA and fixed-point-iteration for this scaled-up problem. The FPI for the finer mesh model takes an average of 6 iterations and 750 seconds for convergence corresponding to each single realization of the input variables. Disciplinary analysis results (i.e., CFD and FEA) after the 3rd and 4th iterations are recorded and used to implement the proposed BNC-MDA methodology. It takes the desktop PC about 550 seconds to complete a 4-iteration analysis for each realization of the input variable. The computational cost of FPI and BNC-MDA, just for the coupled physics analysis, are compared in **Table 3.5**.

Table 3.5 Computational effort comparison between FPI and BNC-MDA

Number of Nodes	**FPI** (secs)	**BNC-MDA** (secs)	**Time saved** (secs)
258	14,300	9,350	4,950
1218	82,500	60,500	22,000

It can be concluded from **Table 3.5** that the computational savings with BNC-MDA improves with the size of the problem. The main reason for the savings in computational effort is that the coupled physics analysis is not run till full convergence; only a few iterations are used to build the Bayesian network (3 iterations for the coarse mesh case, and 4 iterations for the fine mesh case). The CPU time reported in **Table 3.5** also includes the time to build the model for each sample of input realization, which actually takes up 50% of the computational effort for a fully converged analysis. That is, for the 258-node model, it takes about 1 minute to build the model and 1 more minute to converge in about 6 iterations. Thus the BNC-MDA approach takes 1.5 minutes (on average) per sample, compared to 2 minutes per sample for SOFPI. In terms of function evaluations, the savings is 50% in this problem. The savings will be more impressive if the fixed-point iteration took many more iterations to converge. So the computational savings is problem-dependent. In the earlier mathematical example (Section 3.4.1), BNC-MDA needed only 2000 function evaluations compared to 107,421 by SOFPI, thus giving a 98% savings in computational effort.

6. The number of principal components only comes into the picture in sampling the Bayesian network, after generating training samples from the coupled physics analysis. The time required for sampling by BNC-MDA with different numbers of principal components is shown in **Table 3.6.**

Table 3.6 Time required for sampling (seconds) by BNC-MDA

Number of Nodes	10 pcs	15 pcs	20 pcs	30 pcs
258	12.77	18.90	26.52	37.89
1218	11.29	16.58	21.95	32.38

It is seen that for the same number of principal components, there is no significant difference in the sampling effort between the coarser and finer physics models, because the Bayesian network has the same dimension between the two cases for the same number of principal components. The number of principal components will affect the accuracy of the result, but the effect on computational cost is insignificant compared to the cost of the physics (fluid-structure interaction) analysis. This is because the principal components only affect the dimension of the Bayesian network.

7. A very important observation is the comparison of computational effort between **Table 3.5** and **Table 3.6**. **Table 3.6** shows that the computational effort in building the Bayesian network and subsequent sampling is negligible compared to the physics analysis effort shown in **Table 3.5**.
8. In addition to the proposed BNC-MDA approach, the interdisciplinary compatibility can also be imposed using a sample-based conditioning strategy. After building the BN, a large number of unconditional samples of the variables are generated at first. Then the difference term ε are conditioned by a small interval around 0, i.e., $[-\delta_\varepsilon, \delta_\varepsilon]$. Then, the corresponding samples of the coupling variables are collected to estimate the joint distribution under compatibility condition. This approach slightly

relaxes the compatibility condition using a tolerance value, which better agrees with the deterministic MDA.

3.5. SUMMARY

This chapter proposed a new approach for uncertainty propagation in high-dimensional feedback-coupled multidisciplinary analysis. The Bayesian network technique is exploited for this purpose and the joint probability distribution of the coupling variables given interdisciplinary compatibility is computed using conditional sampling of the Bayesian network. A vine copula-based sampling technique, which is not restrained by the type of marginal distributions of the variables, is introduced for efficient sampling of the BN. The joint probability distribution of the coupling variables is estimated using conditional sampling with the copula. Principal component analysis is adopted to decrease the dimensionality of the Bayesian network. A mathematical MDA example and an aeroelastic wing analysis example are used to demonstrate the efficiency and accuracy of BNC-MDA.

Note that each training sample for constructing the Bayesian network only requires a few iterations of the coupled physics analysis instead of a fully converged solution as in FPI. Thus the proposed BNC-MDA approach is promising for high-dimensional problems.

Since the Bayesian network and copula can both incorporate any types of distributions, the proposed BNC-MDA approach can therefore be applied to include epistemic sources of uncertainty. For sparse and interval data, the likelihood-based

approach introduced in Section 2.3 can be used to convert such data into a non-parametric distribution, which can be represented by a random variable node in the BNC approach. For model uncertainty, especially for the stochastic model output, the auxiliary variable method proposed in Section 2.4 can be adopted to represent the model error by an additional random variable (corresponding to the auxiliary variable), which subsequently be included in the proposed BNC-MDA as well. The inclusion of epistemic sources of uncertainty in BNC-MDA will be demonstrated using an example in Section 5.5.2.

In the next two chapters, the Bayesian network and copula-based sampling approach is further investigated as a probabilistic graphical surrogate model for use in multi-objective and multi-disciplinary optimization under uncertainty.

CHAPTER 4

MULTI-OBJECTIVE OPTIMIZATION UNDER UNCERTAINTY

4.1. INTRODUCTION

Chapters 2 and 3 focused on multidisciplinary analysis under uncertainty. Design optimization of multidisciplinary systems under uncertainty brings additional computational burden. Thus, the methodologies proposed in the previous chapters need to be integrated in the optimization framework effectively. Therefore, studies of appropriate optimization techniques are significant for MDO. In this chapter, the optimization technique for single disciplinary analysis (i.e., blackbox analysis) under uncertainty is first investigated. The optimization multidisciplinary systems will be studied in Chapter 5.

A large system is usually designed to meet multiple objectives, which in many cases are conflicting with each other. To improve the overall performance of the system, the conflicting objectives need to be balanced through multi-objective optimization. In multi-objective optimization (MOO) with competing objectives, the multiple solutions are often characterized through a Pareto surface, which is a series of designs describing the tradeoff among different objectives. The decision maker will select the appropriate design alternative based on his/her preferences on the objectives [82]. Four approaches have been studied in the literature to construct the Pareto surface: weighted sum, goal programming, constraint-based methods, and genetic algorithm.

The weighted sum approach assigns weights for each objective based on the stake-holder's preferences, and formulates a single objective optimization. The Pareto front is achieved by trying different weights for the objectives and performing the optimization multiple times. The goal programming approach treats each conflicting objective as an equivalent constraint (one goal), and introduces detrimental deviations for each of the goals. The objective is to minimize the weighted sum of the detrimental deviations. In constraint-based methods [83], one of the objective functions is selected as the only objective, and the remaining objective functions are treated as constraints. The Pareto front can be obtained by systematically varying the constraint bounds. Similarly, multiple optimizations need to be implemented. The genetic algorithm-based approach globally searches for feasible solutions, compares and ranks them based on objectives and constraints, and selects the non-dominated solutions [84]. The first three approaches convert the multi-objective optimization problem into a single objective problem and solve with optimization algorithms, therefore are more efficient. Compared to the first three approaches, a genetic algorithm requires more function evaluations; however, the former three approaches are more likely to result in solutions that do not belong to the Pareto front.

As mentioned earlier, the presence of input uncertainty and model errors introduces uncertainty in the estimation of the system model outputs. As a result, optimization under uncertainty (OUU) requires an extra loop of uncertainty quantification (UQ) or reliability assessment in each optimization iteration. Such stochastic optimization formulation often suffers from intensive computational effort.

Therefore, surrogate modeling techniques, which replace the expensive physics code with an inexpensive model for UQ and reliability analysis, are often used for optimization under uncertainty. However, most surrogate modeling approaches suffer from the curse of dimensionality and may be inaccurate for modeling a system with a large number of input and output variables. Furthermore, multiple outputs need to be considered in multi-objective optimization. If the surrogate models are built for individual analyses, the correlations between the outputs are likely to be missed. To overcome this challenge, surrogate modeling that considers output dependence has been proposed using techniques such as co-kriging [85]. However, the size of the co-kriging covariance matrix grows rapidly as the number of outputs considered increases; thus one can incorporate dependence between only a small number of output variables at present.

As mentioned in Section 1.1, optimization under uncertainty can be addressed by reliability-based design optimization (RBDO) and robustness design optimization (RDO). This chapter addresses multi-objective optimization in terms of RBDO; however, the proposed approach can also be extended to RDO problems.

Reliability assessment, which needs to calculate the probability of the output being less (or greater) than a threshold, is often applied to individual outputs. However, given a set of design values, due to common uncertainty sources propagating through the model, the outputs are inherently correlated with each other. To enhance the system-level reliability, the joint probability of success (or failure) should be introduced in the optimization formulation. This requires the consideration of output dependencies. Inclusion of dependence between the objectives has been proposed in [86], and using the joint probability as a constraint has been considered in [87]. Both studies use first-order

approximation and consider the input variability as the only uncertainty source. Joint probabilities of only 2 objectives in [86] and 3 objectives in [87] are considered. As the number of output variables increases, the accuracy of the first-order approximation gets worse, whereas the number of function evaluations increases many times more than the number of variables [88].

Review of the existing work reveals current limitations of surrogate modeling for large and dependent systems. Therefore, it is important to develop effective OUU methods that can handle a large number of design variables and multiple objectives, while still preserving the correlations between the objectives. Also, a more efficient and accurate method is essential to evaluate the joint probability for a large number of variables. Towards this end, the Bayesian network and vine copula-based sampling technique described in Appendix II is explored as a probabilistic graphical surrogate modeling tool in this chapter.

A BN is first trained using the samples of the input and output variables of the original codes. In optimization under uncertainty, given the values of the design inputs, the Gaussian copula can be conditionally sampled [67] to estimate the conditional joint distribution of all the output variables. The concepts of Bayesian network and copula-based sampling are combined for MOO in this research, and referred to as BNC-MOO. The proposed approach is used with an optimization algorithm to accomplish design under uncertainty. Since the proposed approach is efficient in sampling, genetic algorithms is hence affordable. A Non-dominated Sorting Genetic Algorithm-II (NSGA-II) [84] that specifically solves multi-objective optimization is applied for identifying the Pareto front in this research.

Since the Bayesian network is used as a surrogate model in this research, its predictive capability largely relies on the selection of useful and informative training points. Selection of training points for enhancing the performance of surrogate models in optimization, referred to as Efficient Global Optimization (EGO), has been studied using Gaussian process surrogate models [89], where an expected improvement function is built to select the location at which new training points should be added. Previous research only focuses on the improvement of a single function. However, this is not sufficient when multiple objectives that share the same inputs need to be improved simultaneously. This is because different training points need to be added to improve different objectives. If the EGO-based approach is used, then co-Kriging will have to be adopted to properly account for dependence among the objectives; this is computationally burdensome in the presence of multiple objectives. In this chapter, a novel optimal training point selection technique is proposed based on the inverse propagation capability of the Bayesian network. A sample-based 'sculpting' technique [90] is exploited to selectively choose the input samples that correspond to multiple outputs in the desired region *simultaneously*. This strategy is found to be effective and efficient in constructing the Pareto surface of solutions.

The contributions of this chapter are as follows:

(1) A new concept of probabilistic surrogate modeling technique based on the Bayesian network is adopted in order to consider large numbers of input variables and preserve the dependence between the objectives.

(2) The BNC approach is developed for multi-objective optimization under uncertainty in the context of an RBDO formulation.

(3) A novel training point selection approach is proposed using sample-based conditioning of the BN, in order to efficiently construct the Pareto surface.

The rest of the chapter is organized as follows. Section 4.2 briefly formulates single objective and multi-objective optimization problems under uncertainty, in the context of RBDO. Section 4.3 develops two innovations: (1) the use of the BNC approach for efficient uncertainty quantification and design optimization, and (2) the use of sample-based conditioning to improve the Pareto surface. The first innovation exploits forward propagation through BN, whereas the second innovation exploits inverse propagation through the BN. An automotive side impact problem is used in Section 4.4 for numerical illustration of the proposed MOUU methodology. Section 4.5 provides concluding remarks.

4.2. OPTIMIZATION UNDER UNCERTAINTY

4.2.1. SINGLE OBJECTIVE OPTIMIZATION

This section formulates the optimization problem used in Chapters 4 and 5. A typical deterministic design optimization formulation can be given as follows.

$$\min_{x} f(\boldsymbol{x}, \boldsymbol{p})$$

s.t.

$$g_i(\boldsymbol{x}, \boldsymbol{p}) \leq 0 \; i = \{1, \ldots, n_q\} \tag{4.1}$$

$$lb_{x_k} \leq x_k \leq ub_{x_k}, k = \{1, \ldots, n_x\}$$

where f is the performance function or objective to be minimized; $\mathbf{x}$ is the vector of design variables; $\boldsymbol{p}$ is the vector of non-design variables (i.e., not controlled by the designer); n_q and n_x are the number of constraints and design variables, respectively; lb_{x_k} and ub_{x_k} are the lower and upper bounds of x_k. When the uncertainties in variables $\boldsymbol{x}$ and $\boldsymbol{p}$ are of the aleatory type, the formulation and solution approaches are rather well-established; a survey is provided in [13]. An RBDO formulation of the above problem combining uncertainty can be given as

$$\min_{\mu_X, \boldsymbol{d}} \mu_f(\boldsymbol{X}, \boldsymbol{d}, \boldsymbol{P}, \boldsymbol{p_d})$$

s.t

$$\begin{gathered} Prob(g_i(\boldsymbol{X}, \boldsymbol{d}, \boldsymbol{P}, \boldsymbol{p_d}) \leq 0) \geq p_t^i \quad i = \{1, \dots, n_q\} \\ Prob(\boldsymbol{X} \geq \boldsymbol{lb_X}) \geq p_{lb}^t \\ Prob(\boldsymbol{X} \leq \boldsymbol{ub_X}) \geq p_{ub}^t \\ \boldsymbol{lb_d} \leq \boldsymbol{d} \leq \boldsymbol{ub_d} \end{gathered} \tag{4.2}$$

where $\boldsymbol{X}$ is the vector of random design variables with bounds $\boldsymbol{lb}_X$ and $\boldsymbol{ub}_X$, respectively; μ_f and $\mu_{\boldsymbol{X}}$ are the mean of f and $\boldsymbol{X}$, respectively; $\boldsymbol{d}$ is the vector of deterministic design variables with bounds $\boldsymbol{lb}_d$ and $\boldsymbol{ub}_d$; $\boldsymbol{P}$ is the vector of random non-design variables; $\boldsymbol{p}_d$ is the vector of deterministic parameters. The upper case notations represent stochastic quantities, whereas the lower case notations denote deterministic quantities. p_t^i is the target reliability required for the i^{th} constraint; p_{lb}^t and p_{ub}^t are the target reliabilities for the design variable bounds. An alternate formulation for the inequality/bound constraints using the concept of feasibility robustness involves narrowing the constraint boundaries by a multiple of their respective standard deviations [91].

Evaluation of the objective and constraints for Eq. (4.2) can be done through Monte Carlo sampling, but it is computationally intensive to implement when the original code is time-consuming. Efficient reliability approaches such as FORM and SORM can significantly reduce the effort, yet still need dozens of function evaluations for a given design value. The total number of function evaluations will accumulate as the number of design cycles increases. Therefore, surrogate modeling techniques are usually pursued to replace the original model with computationally inexpensive models for the objective and constraints estimation.

Based on the single objective optimization formulations, the multi-objective problems are formulated in Section 4.2.2.

4.2.2. MULTI-OBJECTIVE OPTIMIZATION

A generic formulation of deterministic multi-objective optimization for n_{obj} objectives may be written as:

$$\begin{aligned} & \min_{\boldsymbol{x}} \left\{ f_1(\boldsymbol{x}, \boldsymbol{p}), \dots, f_{n_{obj}}(\boldsymbol{x}, \boldsymbol{p}) \right\} \\ \textit{s.t.} \quad & g_i(\boldsymbol{x}, \boldsymbol{p}) \leq 0, \ i = 1 \dots n_{con} \\ & \boldsymbol{lb_x} \leq \boldsymbol{x} \leq \boldsymbol{ub_x} \end{aligned} \tag{4.3}$$

where $\boldsymbol{x}$ and $\boldsymbol{p}$ are the design and non-design variables, and g_i $(i = 1 \dots n_{con})$ are the n_{con} deterministic constraints. $\boldsymbol{lb_x}$ **and** $\boldsymbol{ub_x}$ represent the upper and lower bounds for the design variables $\boldsymbol{x}$. The Pareto front for such a problem indicates the tradeoff between the function values of objectives $f_i, i = 1 \dots n_{obj}$.

In the presence of input variability, data uncertainty, and model uncertainty, the outputs become random variables, which result in stochastic objectives and constraints. In this scenario, the mean values $\mu_{f_1}, \dots, \mu_{f_{n_{obj}}}$ are often considered as the objectives. In the context of RBDO, deterministic constraints $g_1, \dots, g_{n_{con}}$ are rewritten with desired probabilities of satisfaction. Therefore, MOO with probabilistic constraints can be formulated as:

$$\begin{aligned} \min_{\boldsymbol{\mu_X}, \boldsymbol{d}} & \begin{cases} \mu_{f_1}(\boldsymbol{X}, \boldsymbol{P}, \boldsymbol{d}, \boldsymbol{p_d}) \\ \vdots \\ \mu_{f_{n_{obj}}}(\boldsymbol{X}, \boldsymbol{P}, \boldsymbol{d}, \boldsymbol{p_d}) \end{cases} \\ \textit{s.t.} \quad & Prob(g_i(\boldsymbol{X}, \boldsymbol{P}, \boldsymbol{d}, \boldsymbol{p_d}) \leq g_i^t) \geq P_{target}, \ i = 1 \dots n_{con} \\ & \boldsymbol{lb_X} \leq \boldsymbol{\mu_X} \leq \boldsymbol{ub_X} \\ & \boldsymbol{lb_d} \leq \boldsymbol{d} \leq \boldsymbol{ub_d} \end{aligned} \tag{4.4}$$

The joint probability of satisfying all the constraints may also be added as a constraint as:

$$Prob\left(\bigcap_{i=1}^{n_{con}} (g_i(\boldsymbol{X}, \boldsymbol{P}, \boldsymbol{d}, \boldsymbol{p_d}) \leq g_i^t)\right) \geq P_{jt} \tag{4.5}$$

Estimating the joint probability of multiple events using first-order approximation was proposed in [92] and improved in [93, 94]. The first-order approximation was used in [86] to estimate the joint probability distribution of the objectives in MOO. The first-order approximation could become inadequate in the presence of nonlinear objectives and constraints, and when the number of objectives and constraints is large. On the other hand, Monte Carlo sampling can be accurate, but very expensive. Therefore, a surrogate modeling

strategy combining Bayesian network and copula sampling is developed in the next section, to achieve both the desired accuracy and efficiency.

4.3. BAYESIAN NETWORK AND COPULA-BASED SAMPLING

Details of the BNC approach are provided in Appendix II. This section introduces its application as a surrogate modeling tool. For the purpose of illustration, the proposed use of the Bayesian network is shown for a simple optimization problem in **Figure 4.1**. **Figure 4.1(a)** shows a simple model with 2 input variables (a design variable *DV,* and an uncertain variable *UV*) and 2 output variables (constraint variable *Constr,* and objective variable *Obj*). **Figure 4.1(b)** shows a slightly different case with 3 design variables ($DV1$, $DV2$, and $DV3$), which are shown in the top row of the BN. Each design variable is associated with variability (i.e., $UV1$, $UV2$ and $UV3$) shown in the second row. This is the variability introduced in realizing the values of the design variables in the actual system (due to manufacturing factors, for example). The second row also includes two additional uncertain input variables $UV4$ and $UV5$ that are not design variables. The outputs are shown in the 3rd ($Constr1$ and $Constr2$) and 4th rows ($Obj1$ and $Obj2$).

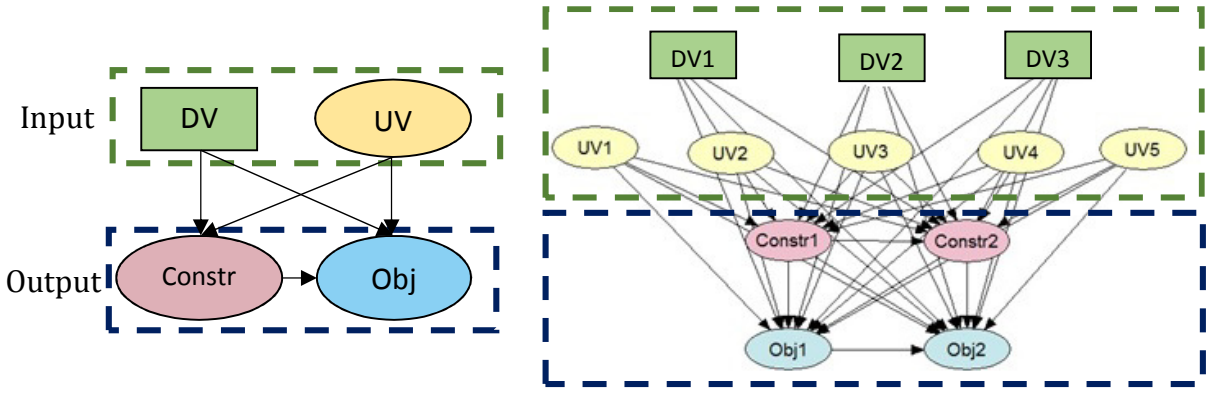

(a) BN for a simple I/O model (b) BN for a model with more variables

Figure 4.1 Bayesian network representation of optimization under uncertainty

In the proposed method, the Bayesian network is used as a probabilistic surrogate model that connects the input and output variables through a joint distribution. (Commonly used surrogate models seek to predict output ***values*** given input values, whereas the BN surrogate model provides the probability distribution of the output given input values).

In each optimization iteration, the design variables are conditioned at the design values, and the posterior joint distribution of the output variables.

$f(Obj1, Obj2, Constr1, Constr2 |\, DV_i = design\ values)$ is estimated. Note that usually the nodes in a BN represent random variables. However, in the context of design optimization, the design variable nodes (DVs, dashed rectangle) are conditioned at specific design values in each iteration, and are therefore deterministic quantities. Once the BN is constructed, it is used for generating conditional samples for both the forward and inverse problems. A vine copula-based strategy is proposed, as explained next. The uncertainty propagation procedure during each design iteration is demonstrated in Section 4 using parallel coordinate plots.

4.3.1 UNCERTAINTY PROPAGATION USING VINE COPULA-BASED SAMPLING

Forward conditioning will be implemented in each optimization iteration, which are illustrated in **Figure 4.2**. During each optimization iteration, the outputs will be conditioned on the values of *DVs* (circles in both figures), then the network is updated using Gaussian copula-based sampling. Samples from the conditional distribution (dashed square on the right figure) are used to estimate the mean of the objectives and the reliability constraints.

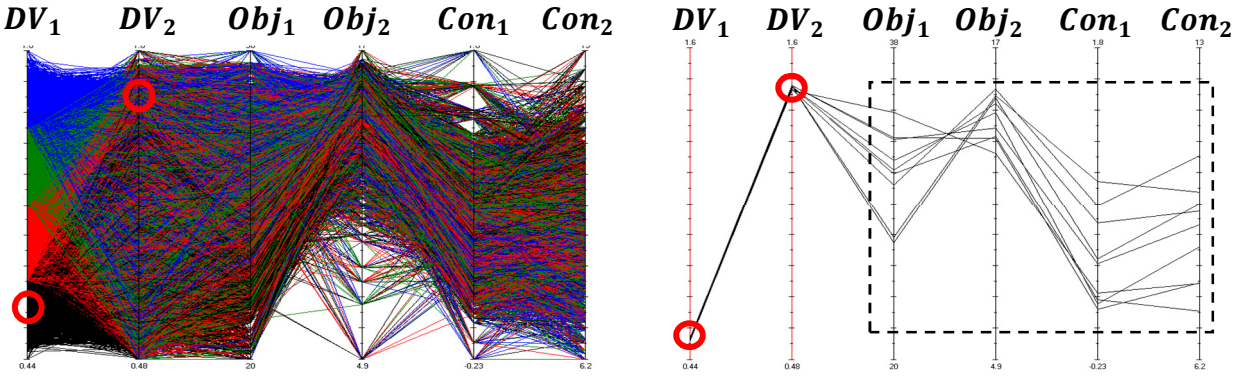

Figure 4.2. Parallel coordinate representation of the model dependencies

4.3.2 TRAINING POINT SELECTION FOR PARETO SURFACE CONSTRUCTION

Based on the performance of the surrogate model, training points can be selectively added to improve the Pareto surface. In MOUU problems, the mean values of several objectives need to be optimized simultaneously. As mentioned in Section 4.1, training point

selection methods in surrogate-based optimization (e.g., EGO) mostly focus on considering a single objective, and little work has been done on multiple objectives simultaneously. In the current section, the Bayesian network is exploited in an inverse way through a sample-based strategy for the purpose of Pareto surface construction. **Figure 4.3** demonstrates the basic concept of this sample-based strategy, which may be referred to as 'sculpting' [90].

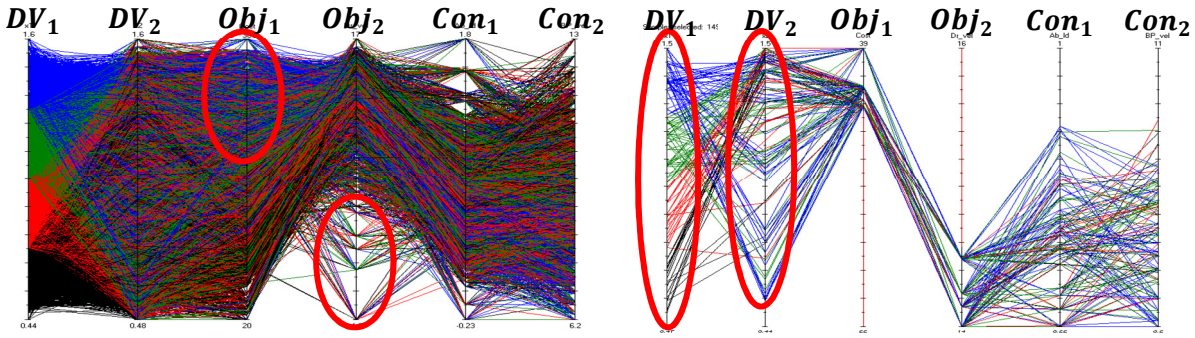

(a) Select samples of the objectives from the desired region **(b) Collect the corresponding samples of the design variables**

Figure 4.3. Sculpting for training points

The proposed strategy for Pareto surface improvement using the Bayesian network-based sculpting is as follows. An initial Bayesian network is first constructed using an initial set of training points (i.e., values of input variables – both design variables and uncertain inputs). Using samples from this BN, the range of values of the objectives in the desired region (often the highest or the lowest values as shown in **Figure 4.3 (a)**) are identified, and the corresponding input variable samples are as shown in **Figure 4.3 (b)**. Then, the input samples identified from **Figure 4.3 (b)** can be used as the new training points and

the corresponding objectives and constraints can be calculated with the original model. Next, a new Bayesian network is built with both the original and additional samples, and the improved Pareto surface is constructed. This 'sculpting strategy' is both efficient and preserves the dependence among different objectives, since the new training points correspond to output samples in the desired region for all objectives simultaneously.

The outcome of the sculpting strategy proposed here is a little different from that described in Ref [90]. In Ref. [90], sculpting is used to identify regions of optimum solution among the available samples generated from the BN. Whereas in this chapter, sculpting is used to identify additional training samples to improve the BN, so that new regions of optimum solutions may be identified. The training point selection and multi-objective optimization processes are summarized in the flowchart as shown in **Figure 4.4**.

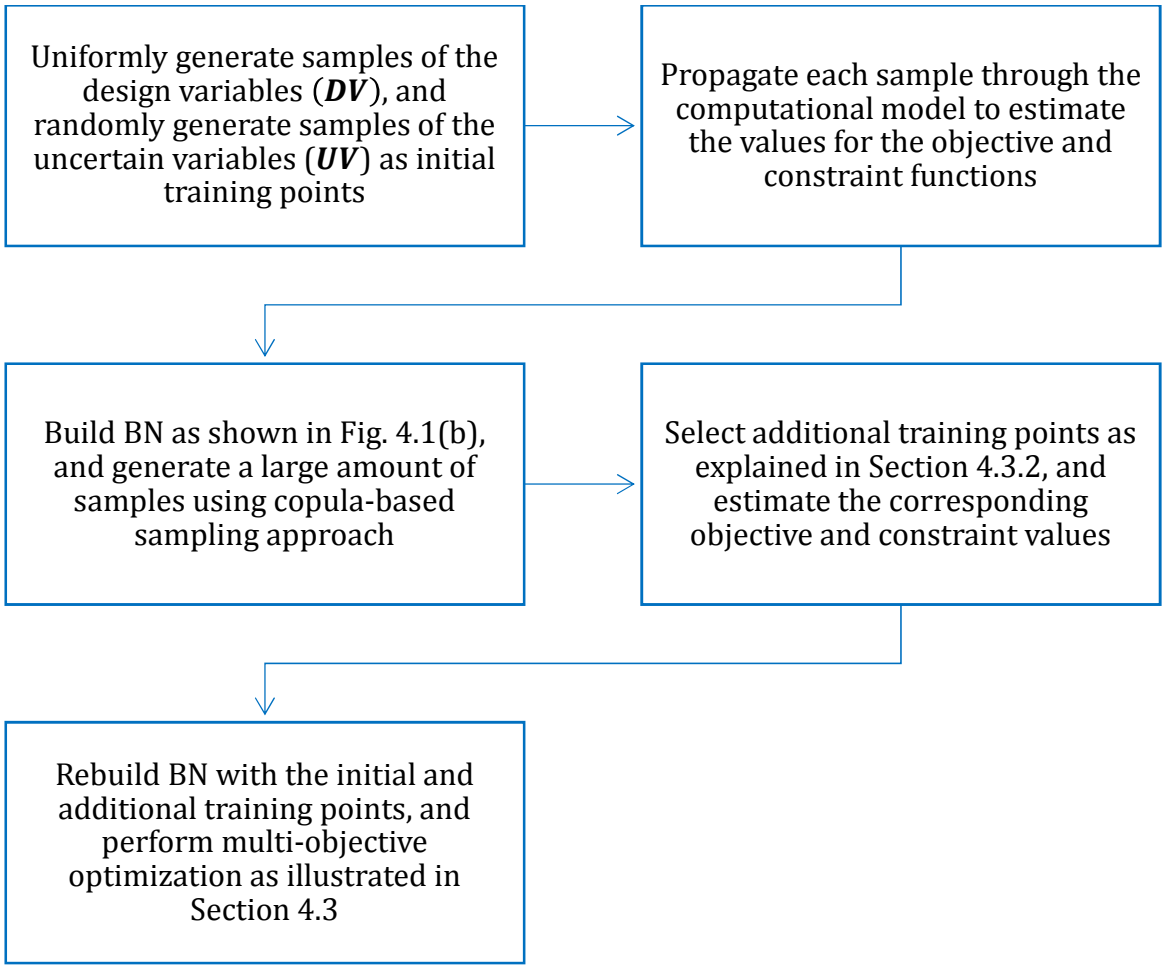

Figure 4.4. Flowchart for the training point selection and multi-objective optimization scheme

4.4. NUMERICAL EXAMPLE

A vehicle side impact model is used to demonstrate the proposed methodology. The model is shown in **Figure 4.5**. A list of input and output variables is provided in Table 1. The uncertainty sources (input variability) are listed in Table 2.

Figure 4.5. Vehicle side impact model [95]

Table 4.1.Input and output variables of the side impact model

No.	Input	Design space	No.	Output
1	B-pillar inner: x_1	[0.5 , 1.5]	1	Weight
2	B-pillar reinforce: x_2	[0.5 , 1.5]	2	Abdomen load: L_{ab}
3	Floor side inner: x_3	[0.5 , 1.5]	3	Upper rib deflection: Rib_u
4	Cross member: x_4	[0.5 , 1.5]	4	Middle rib deflection: Rib_m
5	Door beam: x_5	[0.5 , 1.5]	5	Lower rib deflection: Rib_l
6	Door belt line: x_6	[0.5 , 1.5]	6	Upper viscous criteria: VC_u
7	Roof rail: x_7	[0.5 , 1.5]	7	Middle viscous criteria: VC_m
8	Mat. of B-pillar inner: x_8	[0.192 , 0.345]	8	Lower viscous criteria: VC_l
9	Mat. of floor side inner: x_9	[0.192 , 0.345]	9	Pubic force: F_{Pb}

Table 4.2. Uncertainty sources of the model

No.	Input	Uncertainty Type
1	B-pillar inner	$N(0, 0.03)$
2	B-pillar reinforce	$N(0, 0.03)$
3	Floor side inner	$N(0, 0.03)$
4	Cross member	$N(0, 0.03)$
5	Door beam	$N(0, 0.03)$
6	Door belt line	$N(0, 0.03)$
7	Roof rail	$N(0, 0.03)$
8	Mat. of B-pillar inner	$N(0, 0.03)$
9	Mat. of floor side inner	$N(0, 0.03)$
10	Barrier height	**Data:** 4, -8, 3.5, -0.7, 0.1, 12,[-25,20] [-30,22][-15,31] [-28,28]
11	Barrier hitting	**Data:** 3, -2, 1, 0, -0.5, 0.3,[-4,5][-8,10][-10,7] [-0.1,1]

The variables listed in **Table 4.1** are used as design variables. Due to variability in the manufacturing process, variability is also assumed for each design variable as shown in **Table 4.2**. (This situation corresponds to the case shown in **Figure 4.1(b)**). Note that input variables 10 and 11 were treated as design variables in [34]. In this chapter, they are assumed as uncertain variables, for which sparse observations plus expert-specified ranges are assumed to be available for the sake of illustrating the use of non-parametric empirical distributions in the proposed methodology. The likelihood-based approach introduced in Section 2.3 is used to construct non-parametric PDFs for both variables as shown in **Figure 4.6**.

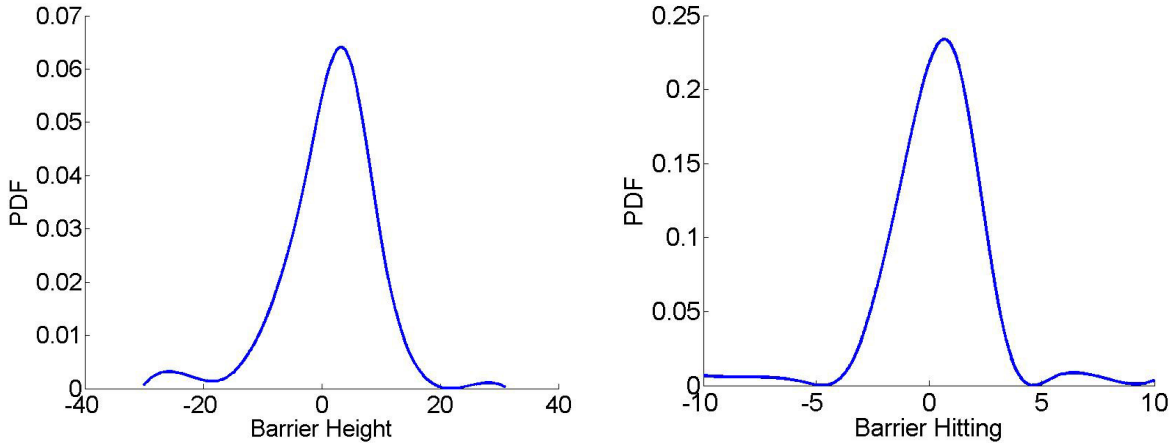

Figure 4.6. Non-parametric PDFs for uncertain parameters

An adequate number of training points first needs to be generated in order to construct the Bayesian network. For the side impact problem, a stepwise regression (SR) model is provided in [95], but the original data used to train the SR model are not available.

Therefore, in this research, the SR model is treated as the "original" model for the sake of illustration, from which input samples are generated to calculate the output. And then the input, uncertain and output variable values are used to train the BN.

The connections (topology) between the nodes can be inferred from the SR model, whereas the required number of samples is identified by the verification technique explained in Appendix II. At first, 100 samples are generated using Latin Hypercube sampling to train the BN. The determinant of the correlation coefficient matrix calculated based on the training samples is $det_{trn}^{100} = 2.07 * 10^{-14}$. After the BN is trained, 100 sets of samples are generated using Guassian copula, the determinants of their correlation coefficient matrices are calculated. The mean and standard deviation of the determinants are: $4.81 * 10^{-15}$ and $7.35 * 10^{-15}$. Thus det_{trn} falls outside the 90% bounds, implying that the number of training samples is not sufficient. Therefore, 15 additional samples are generated and added to the original training samples to build a new BN. The same verification process is implemented, the determinant calculated from the 115 training samples is $det_{trn}^{115} = 3.14 * 10^{-15}$, while the mean and standard deviation of the determinants, which are calculated based on the copula-generated samples, is $1.80 * 10^{-15}$ and $2.17 * 10^{-15}$. Since det_{trn}^{115} lands in the 90% bounds, the new BN and the Gaussian copula assumption is therefore valid.

Next, the 115 samples of the design variables, combined with other uncertain variables, are propagated through the SR model. Samples of the inputs and outputs are then used to build the Bayesian network as shown in **Figure 4.7**. This BN is a probabilistic surrogate model of the side impact problem, i.e., for given values of some variables, it provides the joint probability distribution of the other variables.

Three optimization cases are analyzed. Case I is a single objective optimization problem. Its purpose is to verify the accuracy of the proposed BNC approach with the original SR model. The other two cases consider multi-objective optimization.

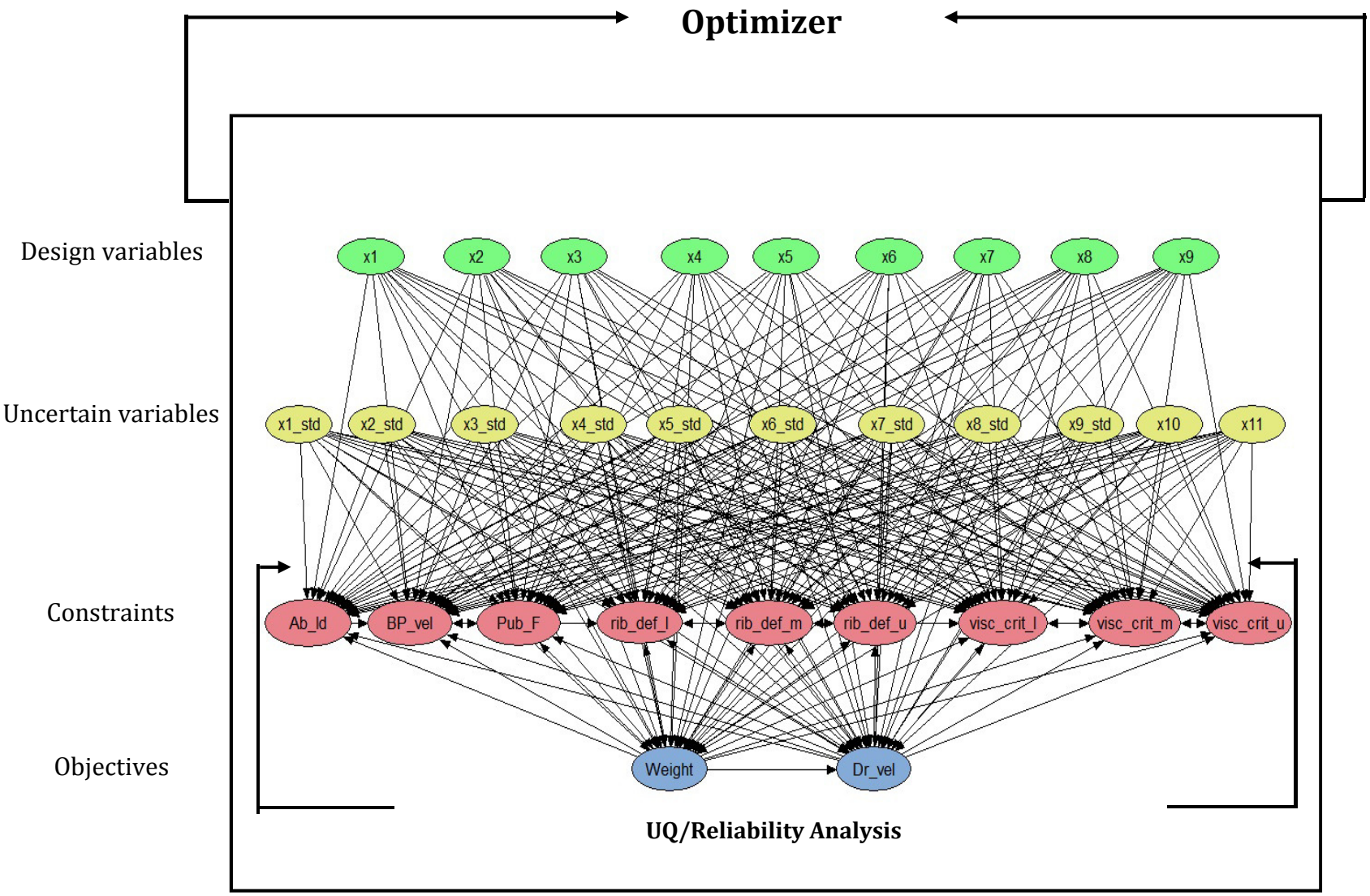

Figure 4.7. Optimization with BN

Table 4.3. Correlations between output variables

	Weight	V_{dr}	L_{ab}	F_{Pb}	Rib_u	Rib_m	Rib_l	VC_u	VC_m	VC_l	VB_P
Weight	1.00	**-0.34**	-0.74	-0.71	-0.38	-0.54	-0.67	-0.58	-0.37	-0.67	-0.62
V_{dr}	**-0.34**	1.00	0.07	0.13	-0.14	0.02	0.01	-0.17	-0.24	0.13	0.01
L_{ab}	-0.74	0.07	1.00	0.86	0.35	0.49	0.64	0.35	0.26	0.67	0.60
F_{Pb}	-0.71	0.13	0.86	1.00	0.04	0.16	0.31	0.16	0.01	0.40	0.27
Rib_u	-0.38	-0.14	0.35	0.04	1.00	0.95	0.80	0.85	0.94	0.56	0.87
Rib_m	-0.54	0.02	0.49	0.16	0.95	1.00	0.93	0.84	0.85	0.74	0.96
Rib_l	-0.67	0.01	0.64	0.31	0.80	0.93	1.00	0.77	0.72	0.87	0.96
VC_u	-0.58	-0.17	0.35	0.16	0.85	0.84	0.77	1.00	0.92	0.53	0.79
VC_m	-0.37	-0.24	0.26	0.01	0.94	0.85	0.72	0.92	1.00	0.43	0.78
VC_l	-0.67	0.13	0.67	0.40	0.56	0.74	0.87	0.53	0.43	1.00	0.77
VB_P	-0.62	0.01	0.60	0.27	0.87	0.96	0.96	0.79	0.78	0.77	1.00

Table 4.3 shows the correlation coefficients between the output variables. It can be seen that the correlation coefficient between the first two objectives (i.e., weight and door velocity) is -0.34, which indicates a competing relationship between the two variables. To simultaneously optimize these two competing quantities, a multi-objective optimization formulation from [86] is adopted, in which car weight and the door velocity are minimized simultaneously. The Pareto front needs to be created to address this relationship. Specifications of different cases are provided as follows:

Case I: Single objective RBDO. In this case, the car weight is used as the sole objective. The probabilities of all other 10 outputs being greater than 0.99 individually are used as the reliability constraints. This is the ϵ-constraint approach. The optimization is solved with both the original SR model and the proposed BNC approach. The purpose of conducting this case is to compare the BNC method with the SR model and study the extent of agreement between the two approaches.

Case II: Multi-objective optimization (RBDO formulation) with 2 objectives and 9 individual probability constraints.

Case III: Multi-objective optimization (RBDO formulation) with 2 objectives, 9 individual probability constraints and an additional joint probability constraint of the 9 outputs.

Case I: Single Objective RBDO

The problem is formulated as:

$$\begin{aligned} & \min_{DV} Weight(DV, nonDV) \\ s.t. \quad & P_i(Con_i < Crit_i) \geq 0.99 \\ & 0.5 \leq x_i \leq 1.5, i = 1 \dots 9 \end{aligned} \tag{4.6}$$

The DIviding RECTangles (DIRECT) algorithm, which is a gradient-free global optimizer, is adopted to solve the optimization problem. The optimum obtained from the BNC approach is compared against the solution of the SR model. The optimization history is shown in **Figure 4.8**, and the optimal solution is listed in **Table 4.4**. The objectives and constraints using the two models are listed in

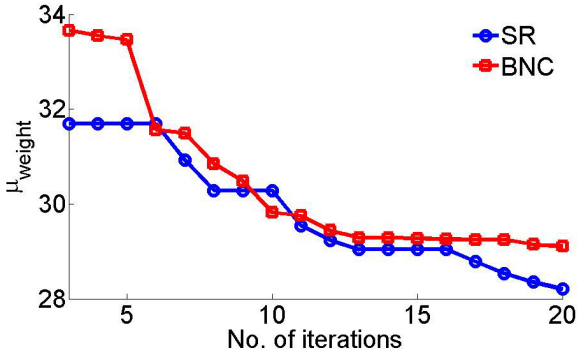

Figure 4.8 Single objective RBDO history for SR and BNC

Table 4.4. Comparison of optimal solutions using SR and BNC

	Design Variables	RBDO with SR	RBDO with BNC	Difference (%)
Design Variables	B-pillar inner	0.96	1	4
	B-pillar reinforce	1.18	1.33	13
	Floor side inner	0.63	0.65	3
	Cross member	1.30	1.33	2
	Door beam	0.89	0.85	4
	Door belt line	1.44	0.96	33
	Roof rail	0.89	0.84	6
	Mat. of B-pillar inner	0.34	0.32	6
	Mat. of floor side inner	0.27	0.32	19

Table 4.5. Performance comparison of the optimal solutions using SR and BNC

	Output Variables (a)	RBDO with SR (b)	RBDO with BNC (c)	Evaluation of BNC with SR (d)	Difference between (b) and (d) %
Objective	Weight	28.20	29.11	29.49	5
Probabilistic Constraints	Abdomen load	1	1	1	0
	Upper rib deflection	1	0.99	1	0
	Middle rib deflection	1	1	1	0
	Lower rib deflection	0.99	1	1	1
	Upper viscous criteria	1	0.99	1	0
	Middle viscous criteria	1	1	1	0
	Lower viscous criteria	1	1	1	0
	Pubic force	0.99	1	**0.97**	2
	B-pillar velocity	1	1	1	0
	Door velocity	1	0.99	**0.97**	3

It can be seen from **Table 4.4** and

Table *4.5* that the overall performances of the SR and BN approaches are quite similar. The differences between the BN and SR results for objective, constraints and most

of the design variables are 5% or less. The probabilistic constraints for pubic symphysis force and door velocity (bold in red) are slightly violated, which may be due to the lack of sufficient samples in training the BN, which will be analyzed later when discussing Pareto surface improvement. Having verified the accuracy of the BNC approach, the next two cases are implemented for multi-objective RBDO.

Cases II/III: Multi-objective RBDO with Individual/Joint Probability Constraints

The optimization with two competing objectives and 9 individual probability constraints (and one additional joint probability constraint for case III) is formulated as shown in Eq. (4.7).

$$\begin{aligned} & \min_{\boldsymbol{\mu_x}} \mu_{Weight} \ \& \ \mu_{Vel_{door}} \\ \textit{s.t.} \quad & P_i(Con_i < Crit_i) \geq 0.99 \\ & P(\cap_{i=1}^{9}(Con_i < Crit_i)) \geq 0.99 \ \text{(case III only)} \\ & 0.5 \leq x_i \leq 1.5, i = 1 \dots 7 \\ & 0.192 \leq x_j \leq 0.345, j = 8 \dots 9 \end{aligned} \tag{4.7}$$

The NSGA-II algorithm is applied to construct the Pareto front. The population size in this genetic algorithm implementation is chosen as 150, probability of crossover is 1 and probability of mutation is 0.15. The total number of iterations is 20. MOO with the SR model is first implemented to identify the effect of the additional joint probability constraint.

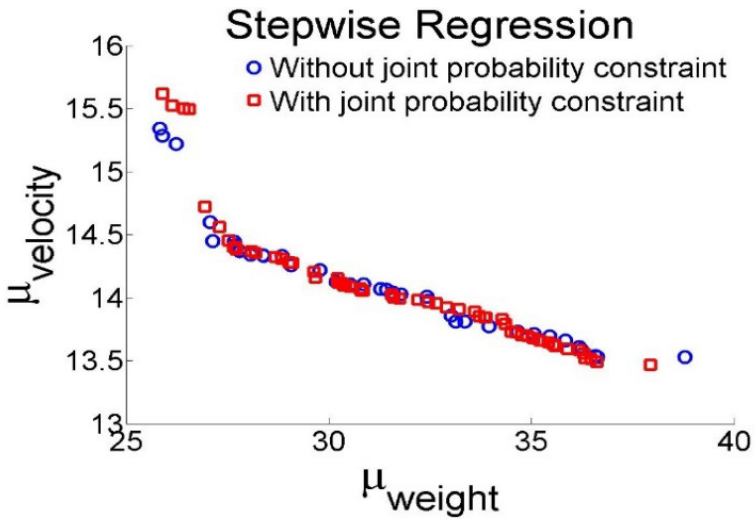

Figure 4.9. Comparison of Pareto fronts with/without joint probability constraints

It can be concluded from **Figure 4.9** that, with the consideration of the joint probability constraint, the designs along the Pareto front with joint probability are generally above those without the joint probability constraint, especially in the region of low weight and high velocity. This is intuitively correct since the objectives are minimized; with an additional constraint, both objectives have higher values.

The proposed BNC approach is next used to construct the Pareto fronts for Cases II and III. At each point of the BNC Pareto front, the objectives are re-evaluated using the SR model. **Figure 4.10** compares the BNC solutions (circles), the BNC solutions re-evaluated using SR (squares) and the SR solutions (triangles) with and without the joint probability constraint.

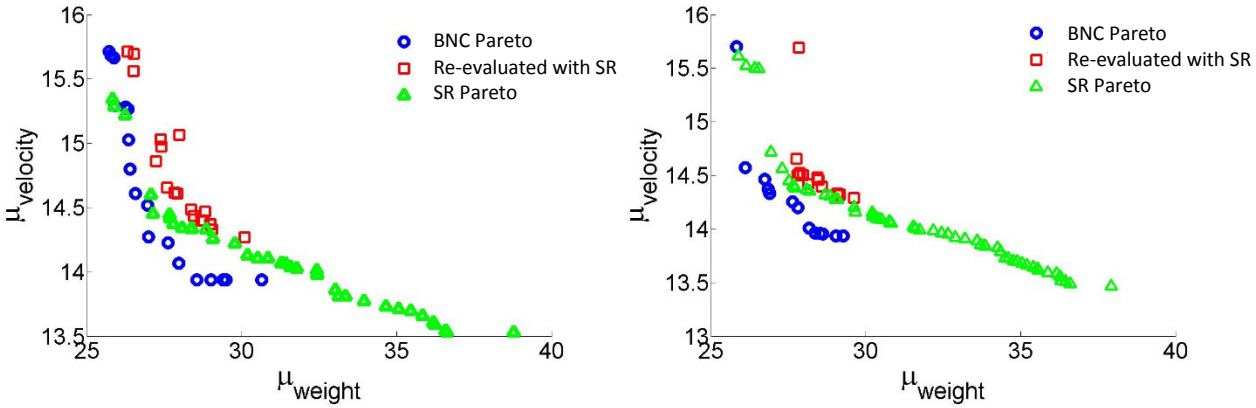

(a) Without joint probability constraint **(b) With joint probability constraint**

Figure 4.10. Pareto fronts with BNC, and SR solutions

It can be observed from both figures that the BNC Pareto surfaces are more optimistic compared to the SR solution, whereas the re-evaluated results using SR (square marks) are more conservative. The figures also show that the initial BNC approach cannot identify solutions at the high weight (greater than 30), low velocity (less than 14) region.

To investigate this issue, scatter plots that characterize the dependence of weight and door velocity samples from the initial 115 training samples (left) and the samples generated from the Gaussian copula (right) are shown in **Figure 4.11**. The dashed squares cover the region which BNC could not detect in **Figure 4.11**. It can be observed from **Figure 4.11(a)** that only 3 of the initial samples land within the dashed area. The Bayesian network will only generate samples based on the training points available; in other words, the training points indicate the joint probability distribution of the variables, and therefore further samples generated by the Bayesian network also reflect this joint distribution. Thus the Bayesian network generates very few samples in the dashed area and is unable to find Pareto solutions in this area.

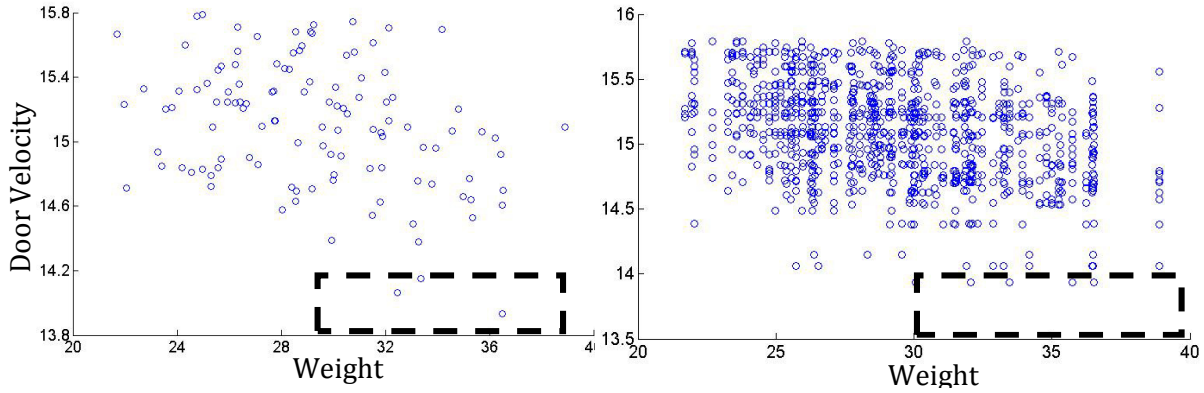

(a) Scatter plots from the original samples (b) Scatter plots from the copula-generated samples

Figure 4.11. Scatter plots of weight and door velocity

To overcome this issue, the training point selection technique proposed in Section 4.3.2 is applied: 20 additional samples of the design variables are generated selectively based on the sculpting strategy. To evaluate this method, Latin Hypercube sampling (LHS) is also used to generate 20 samples of the design variables from uniform distributions based on Tables 1 and 2, and propagated to estimate the outputs. The values of the objectives generated by the two approaches are compared by the scatter plot in **Figure 4.12**.

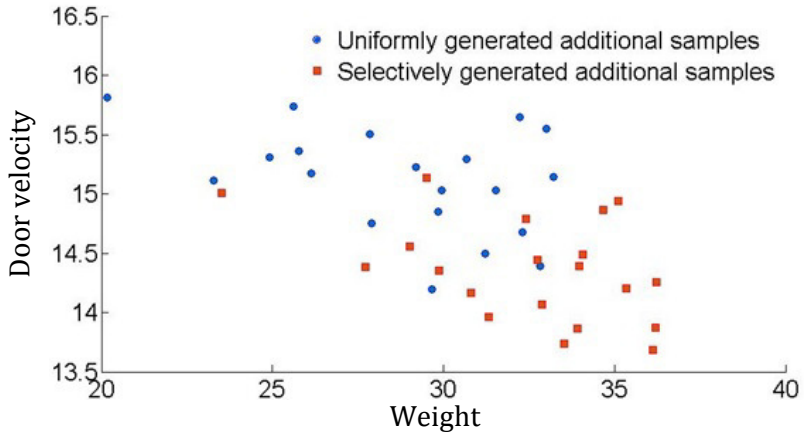

Figure 4.12. Comparison of the outputs from different resampling approaches

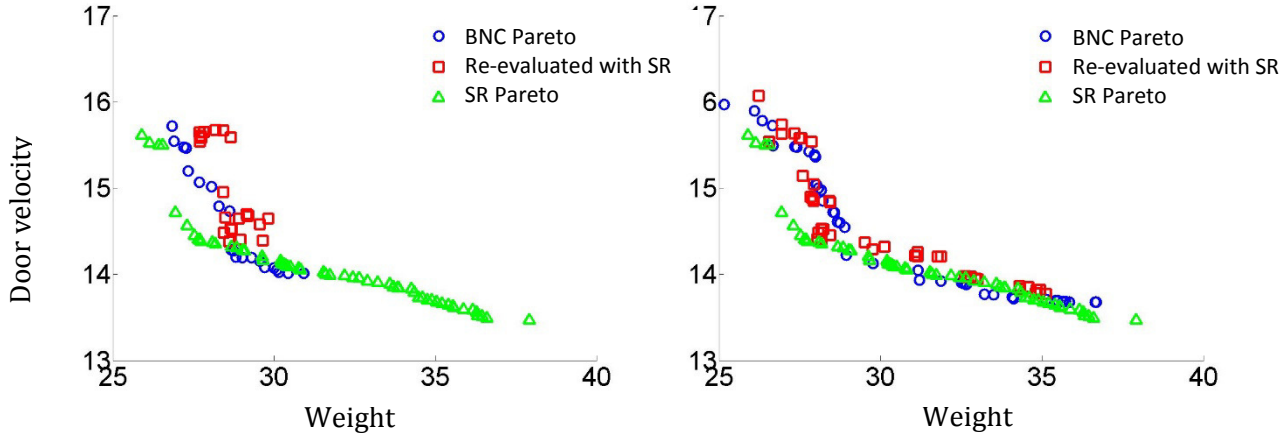

(a) Approach I: uniformly generated samples (b) Approach II: selectively generated samples

Figure 4.13. Comparison of the results between the two resampling

It can be seen from **Figure 4.12** that, the selectively generated samples (squares) focus more on the desired/rectangular region compared with the LHS approach. The additional 20 samples generated in different methods combined with the 115 initial samples are used to build new BN models for Case III (with the joint probability constraint).

The objectives are re-evaluated using the SR model. All results are compared in **Figure 4.13**.

In **Figure 4.13 (a),** the LHS-based solution does not have much improvement compared to **Figure 4.13(b)**. The low door velocity, high weight region is still not covered by the additional uniform samples. However, in **Figure 4.13(b)**, due to the selective resampling based on sculpting, the improved BNC is able to construct the Pareto surface in the high weight and low door velocity region which could not be reached by the original BNC. And the resulting Pareto surface is very close to the SR solution. This shows that the sculpting strategy can be effectively used to improve the Bayesian network model and the Pareto surface.

4.5. SUMMARY

This chapter explored the BNC approach as a probabilistic surrogate model for multi-objective optimization under uncertainty. The Bayesian network is constructed based on input-output samples from the original model, and the vine copula-based sampling technique is generate samples of the outputs conditioned on the design values.

A novel training point selection technique is proposed to further refine the BN model and improve the Pareto surface. Additional samples of training points are generated through a sculpting strategy, which exploits the dependence relations among the inputs and outputs, and the inverse propagation capability of the Bayesian network through conditional sampling.

A vehicle side impact problem is used to demonstrate the proposed methodology. The joint probability of multiple constraints and objectives are efficiently estimated using the proposed BNC approach, by exploiting the forward propagation capability of the Bayesian network. Since the proposed methodology is capable of modeling dependence among large number variables, its application on larger scale problems is very promising.

In the next chapter, both BNC-MDA proposed in Chapter 3 and the BNC surrogate-based optimization addressed in this chapter are combined to formulate an efficient framework for MDO under uncertainty.

CHAPTER 5

MULTIDISCIPLINARY OPTIMIZATION UNDER UNCERTAINTY

5.1. INTRODUCTION

As mentioned in Section 1.1, existing methods for MDA and MDO under uncertainty either require considerable computational effort or introduce several approximations to reduce the computational effort. When high-fidelity models are used for each individual disciplinary analysis of the MDA, all the existing approaches are potentially expensive, even for deterministic analysis. In the presence of uncertainty sources, stochastic MDA can become computationally unaffordable. Further, when MDO under uncertainty is considered, stochastic MDA is required during each design iteration in order to evaluate the probabilistic objectives and constraints, which further magnifies the computational cost. Therefore, the central motivation of this chapter is to reduce the computational burden of MDO under uncertainty.

When high-fidelity models are used for individual disciplinary analyses, typically a large number of coupling variables are present, such as the nodal pressures and displacements in the aeroelasticity example in Section 3.4.2. Existing methods for MDA under uncertainty (such as SOFPI and LAMDA described below) become unaffordable in the presence of high-dimensional coupling. Meanwhile, when the number of input and

output variables of the model becomes larger, training the surrogate model for MDA and MDO requires a large number of training samples, which will also greatly increase the need for computational resources. Therefore this chapter proposes a framework for efficient MDO under uncertainty using the Bayesian network, which is found to be effective for both low and high dimensional problems. The abilities of the BN in both inverse problem (Bayesian inference) and forward problem (uncertainty propagation) are exploited in this chapter.

The forward uncertainty propagation property of the BN is first exploited to consider a novel surrogate modeling technique for efficient optimization under uncertainty. This is similar to the use of BN in Section 4. The ability to obtain the probability distribution of the output for a given specific value of the input makes the BN a *probabilistic* surrogate model, as opposed to deterministic surrogate models that seek to estimate a single value of the output for a given value of the input. Note that algebraic surrogate models such as regression and Kriging models do provide an estimate of the uncertainty in the output for a given input; but this uncertainty is only due to sparse or noisy training data. The central aim in such models is to estimate a single value of the output. As the training data becomes more abundant and less noisy, the uncertainty in the output of such algebraic surrogate models will decrease. The use of BN as a surrogate model is very different; its central aim is to provide the probability distribution of the output for a given value of the input, because the Bayesian network is a probabilistic graphical model that represents the joint probability distribution of the input and output variables.

The inversion capability of the Bayesian network is also exploited to enforce the interdisciplinary compatibility condition in feedback-coupled MDA by setting the difference between the values of the same coupling variable from two successive iterations to zero (as explained in Section 3.3). This approach only requires a few iterations of the feedback coupled analysis (usually 2 to 4 iterations), thus achieving great computational savings by not performing the fully converged physics analysis.

An RBDO formulation is adopted to demonstrate the proposed approach, which can be extended to solve RDO problems as well. In each design iteration, the optimizer generates a new set of design values and sends them to the Bayesian network. Given the value of the design variables, the uncertainty in the outputs can be estimated by forward propagating the uncertain variables through the BN. The resulting output is essentially the conditional probability distribution of the outputs given the design variable values of the inputs. For feedback coupled analysis, the compatibility is enforced as mentioned above. Thus, once the BN is built as a surrogate model, both MDA and design evaluation are achieved simultaneously during each call to the BN by the optimizer, providing tremendous computational advantage. The conditional sampling is achieved using the vine copula-based sampling approach, which further enhances the computational efficiency. Note that the Bayesian network can incorporate different types of random variables.

The proposed methodology can include both aleatory and epistemic uncertainty. The inclusion of aleatory uncertainty is straightforward, since this type of uncertainty can be represented by a random variable node in a BN with known distribution type and parameter. Inclusion of sparse and interval data can also be achieved by using the likelihood-based method in Section 2.3 to construct a non-parametric distribution. The

inclusion of stochastic model error can be accomplished through the auxiliary variable method. Since the auxiliary variable method represents the stochastic model error as a uniformly distributed random variable, it can be denoted as a random node in a BN as well. The inclusion of epistemic uncertainty is not the focus of this chapter, but its inclusion in the proposed methodology is briefly discussed in the electronic packaging example in Section 5.5.2.

The contributions of this chapter are as follows:

(1) The probabilistic surrogate modeling technique based on the Bayesian network and vine copula-based sampling is pursued in order to consider large numbers of input variables and accurately represent the stochastic dependence among the inputs, outputs and coupling variables.

(2) The BNC approach is used to formulate a Bayesian network for efficient and accurate MDO under uncertainty, which simultaneously enforces interdisciplinary compatibility and evaluates the optimization objectives and constraints, without any further evaluations of the original physics models, thus significantly reducing the computational effort in MDO.

The rest of the chapter is organized as follows: Section 5.2 formulates MDO under uncertainty using the RBDO format. Section 5.3 introduces the BNC-MDO approach, which is composed of BNC surrogate modeling and BNC-MDA. Section 5.4 emphasize on the treatment of high-dimensional coupling within BNC-MDO. A mathematical example, an electronic packaging design problem, and an aeroelastic wing design problem are used to illustrate the methodology in Section 5.5. Section 5.6 provides concluding remarks.

5.2. MULTIDISCIPLINARY OPTIMIZATION UNDER UNCERTAINTY

A typical deterministic MDO problem statement is provided in [96] and as shown in Eq. (5.1).

$$\min_{\boldsymbol{x}} f(\boldsymbol{x})$$

s.t.

$$\begin{gathered} g_i(\boldsymbol{x}, \boldsymbol{u}(\boldsymbol{x}), \boldsymbol{v}(\boldsymbol{x})) \leq 0 \; i = \{1, \ldots, n_q\} \\ h_1(\boldsymbol{x}, \boldsymbol{u}, \boldsymbol{v}) = 0 \\ h_2(\boldsymbol{x}, \boldsymbol{u}, \boldsymbol{v}) = 0 \end{gathered} \tag{5.1}$$

where f is the performance function or objective to be minimized; $\boldsymbol{x}$ is the vector of design variables. $\boldsymbol{u}(\boldsymbol{x})$ and $\boldsymbol{v}(\boldsymbol{x})$ are coupling variables, and the interdisciplinary compatibility is defined by h_1 and h_2.

Therefore, if $\boldsymbol{u}(\boldsymbol{x})$ and $\boldsymbol{v}(\boldsymbol{x})$ satisfy Eq. (5.1) simultaneously, then they are said to be compatible, and in practical engineering applications, h_1 and h_2 are implicit functions. For example, in the two disciplinary example shown in **Figure 2.1**, h_1 and h_2 can be written as:

$$\begin{gathered} Analysis\ 1(\boldsymbol{x}, u_{21}) - u_{12} = 0 \\ Analysis\ 2(\boldsymbol{x}, u_{12}) - u_{21} = 0 \end{gathered} \tag{5.2}$$

When uncertainty is considered in the MDO formulation above, the probabilistic variation can be written as:

$$\min_{\boldsymbol{\mu_x}} \mu_f(\boldsymbol{x})$$

s.t.

$$P(g_i\left(\boldsymbol{x}, \tilde{\boldsymbol{\xi}}, \boldsymbol{u}\left(\boldsymbol{x}, \tilde{\boldsymbol{\xi}}\right), \boldsymbol{v}\left(\boldsymbol{x}, \tilde{\boldsymbol{\xi}}\right)\right) \geq 0) \leq \alpha_i \tag{5.3}$$

$$h_1(\boldsymbol{x}, \xi, \boldsymbol{u}, \boldsymbol{v}) = 0$$

$$h_2(\boldsymbol{x}, \xi, \boldsymbol{u}, \boldsymbol{v}) = 0$$

$$i = \{1, \ldots, n_q\}$$

In Eq. (5.3), $\tilde{\boldsymbol{\xi}}$ is a vector of random variables $\tilde{\boldsymbol{\xi}}_{\boldsymbol{1}}, \ldots, \tilde{\boldsymbol{\xi}}_{\boldsymbol{m}}$, that model the uncertainty in the system, whereas ξ is one realization of the random variable $\tilde{\xi}$. α_i represents the desired reliability level for the probabilistic constraint of g_i. It can be seen from the equation that, the MDO under uncertainty requires the interdisciplinary compatibility being satisfied for each realization of the random variable, which can be expensive if the uncertainty assessment is performed with the feedback-coupled iterative analysis.

Therefore, surrogate modeling techniques are usually pursued to replace the original model with computationally economic models for the objective and constraints estimation. For feedback coupled MDA, a sufficient number of training samples need to be obtained by running the fixed-point-iteration method. As the number of model inputs and outputs goes up, the number of training samples needed also increases, and consequently generates a lot of computational burden. Further, when the coupling variables between individual disciplines are large in number, characterizing the dependence among input, coupling and output variables can be very complicated for most of the existing surrogate modeling techniques. To overcome these challenges, a comprehensive framework that combines BNC-MDA and BNC surrogate modeling is proposed for the purpose of efficient MDO under uncertainty. This methodology contains four essential elements: (1) probabilistic graphical surrogate modeling; (2) vine copula-based sampling; (3) interdisciplinary compatibility enforcement; and (4) multidisciplinary design optimization under uncertainty. The proposed methodology is referred to as BNC-MDO. Details of the four elements have been

provided in the previous chapters, thus will not be repeated. Then next section will explain BNC-MDO using an RBDO formulation.

5.3. BNC-MDO WITH LOW-DIMENSIONAL COUPLING

The key idea of the proposed BNC-MDO is as follows: The optimizer calls BNC-MDA at each iteration of the optimization, with specific values of the decision variables; BNC-MDA enforces interdisciplinary compatibility and computes the objectives and constraints *simultaneously* through conditional sampling, and returns the objective and constraint values to the optimizer.

A simple Bayesian network for both design assessment and enforcing interdisciplinary compatibility is shown in **Figure 5.1**.

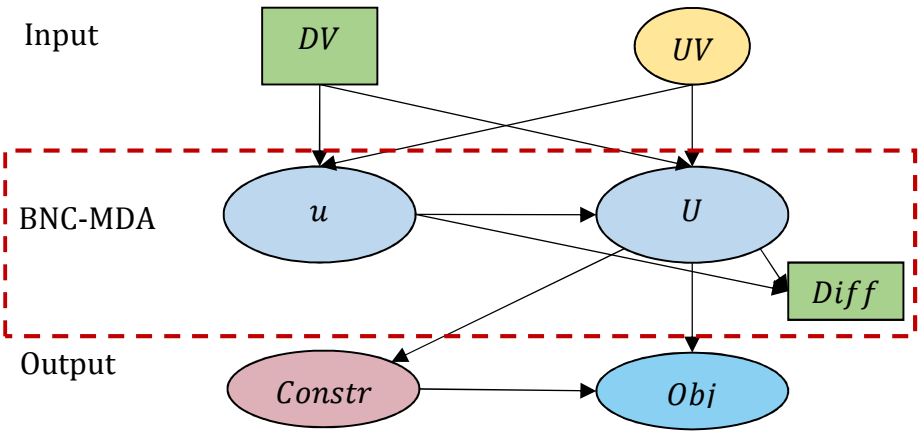

Figure 5.1 A general Bayesian network for MDO

The network contains the design variable (DV), an uncertain variable (UV), coupling variable u from the $(i-1)^{th}$ and U from the i^{th} iterations of the feedback coupled analysis, and the difference between the values of from the two iterations is denoted by the node $Diff$. The model outputs are Obj and $Constr$, which represent the objective and constraint respectively. For MDA, $Diff$ is conditioned to zero, which enforces the interdisciplinary compatibility. Note that usually the nodes in a BN represent random variables. However, in the optimization, the input variable nodes (x_1, x_2) in the BN are conditioned at specific values, and DV are therefore deterministic quantities.

Note that BNC-MDO is composed of two components: (1) BN surrogate modeling, which replaces the computational model with a Bayesian network shown in **Figure 5.1**, and (2) BNC-MDA, which is only part of the MDO and is identified in **Figure 5.1** with the dashed rectangle.

The optimization procedure can be demonstrated using the parallel coordinate plot shown in **Figure 5.2**. In each design iteration, a new value of the design variable (dv) will be generated and passed to the Bayesian network. The distribution of the output variables $Constr$ and Obj will be conditioned given both $DV = dv$ (dashed circle) and $Diff = 0$ (solid circle) *simultaneously*. The resulting conditional samples of the output variables (dashed rectangle) are subsequently delivered to the optimizer for further iteration.

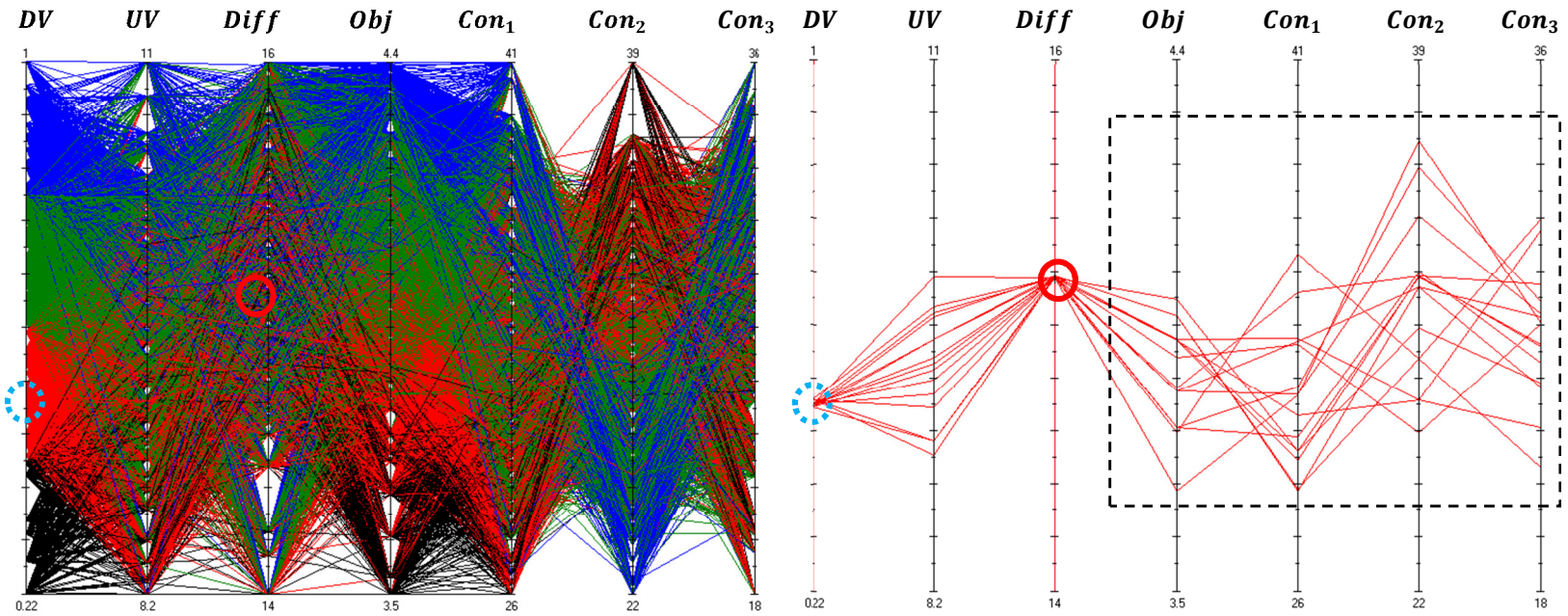

(a) Samples of an unconditioned BN **(b) Conditional samples from the BN**

Figure 5.2 Parallel coordinate representation of MDO

5.4. BNC-MDO WITH HIGH-DIMENSIONAL COUPLING

The size of the Bayesian network (specifically the BNC-MDA component in dashed rectangle) becomes large for a high-dimensional coupled analysis (i.e., a large number of coupling variables between the disciplines). Including all coupling variables in one BN makes the network quite large and unwieldy for training and sampling. Therefore, the dimension reduction of the Bayesian network proposed in Section 3.3.2 can be applied to improve the efficiency of BNC-MDO.

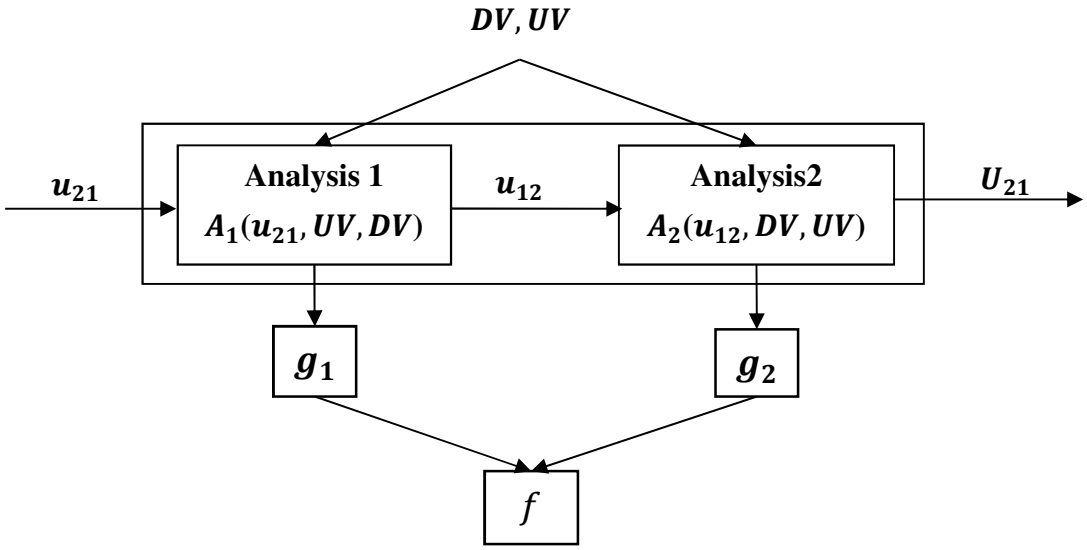

Figure 5.3. One iteration of feedback coupled analysis with high-dimensional coupling

Consider one iteration of the feedback coupled analysis in **Figure 5.3** and assume the coupling variable $\boldsymbol{u_{21}}$ and $\boldsymbol{U_{21}}$ are large vectors of the coupling variable. Given samples of the inputs, the one iteration analysis is executed for each realization of the input, therefore, each coupling variable becomes a random variable, and the corresponding realizations of $\boldsymbol{u_{21}}$ and $\boldsymbol{U_{21}}$ can be organized into matrices. PCA is applied to map the matrices $\boldsymbol{u_{21}}$ and $\boldsymbol{U_{21}}$ into the principal component space. Let l denote the selected number of principal components (PC), then the first l principal components for the inputs and outputs are represented by $PC^j_{\boldsymbol{u_{21}}}$ and $PC^j_{\boldsymbol{U_{21}}}, j = 1 \dots l$. The differences between $PC^j_{\boldsymbol{u_{21}}}$ and $PC^j_{\boldsymbol{U_{21}}}$ are calculated as:

$$\boldsymbol{\varepsilon^j_{PC} = PC^j_{u_{21}} - PC^j_{U_{21}}} \tag{5.4}$$

Given the samples of the design variables, uncertain variables, the coupling variables in the principal component space, and the corresponding difference terms $\boldsymbol{\varepsilon}$, a Bayesian network is built as shown in **Figure 5.4**. In each design iteration, DV is conditioned on the design value, whereas the interdisciplinary compatibility is enforced by imposing $\boldsymbol{\varepsilon^j_{PC} = 0}\ for\ \boldsymbol{j = 1 \dots l}$. Samples of the objective and constraints are then used for further optimization.

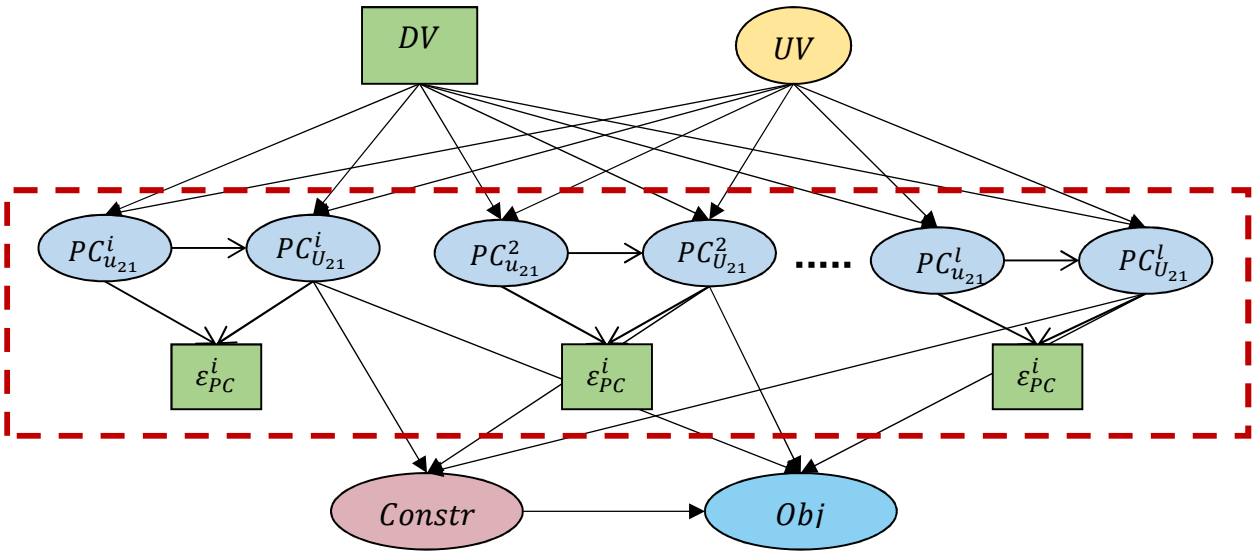

Figure 5.4. Bayesian network with reduced coupling variables

It can be seen from **Figure 5.4** that without PCA, there would have been one BN for the entire problem containing all the correlated coupling variables in one direction. After applying PCA, we have a few principal components that are uncorrelated. As a result, we have a much smaller BN with all the principal components in one network. Thus in the example in Section 5.5.3, if 20 or 30 principal components are used to implement the proposed methodology, the BN with 774 coupling variables and difference nodes is reduced to a smaller size BN with 60 or 90 nodes for the coupling variables and differences, while the nodes of DV, UV, $Constr$ and Obj remain the same. Therefore, by using PCA we can reduce a large BN and drastically improve the efficiency in solving high-dimensional problems. The BNC-MDO approach can be summarized in the flowchart shown in **Figure 5.5**.

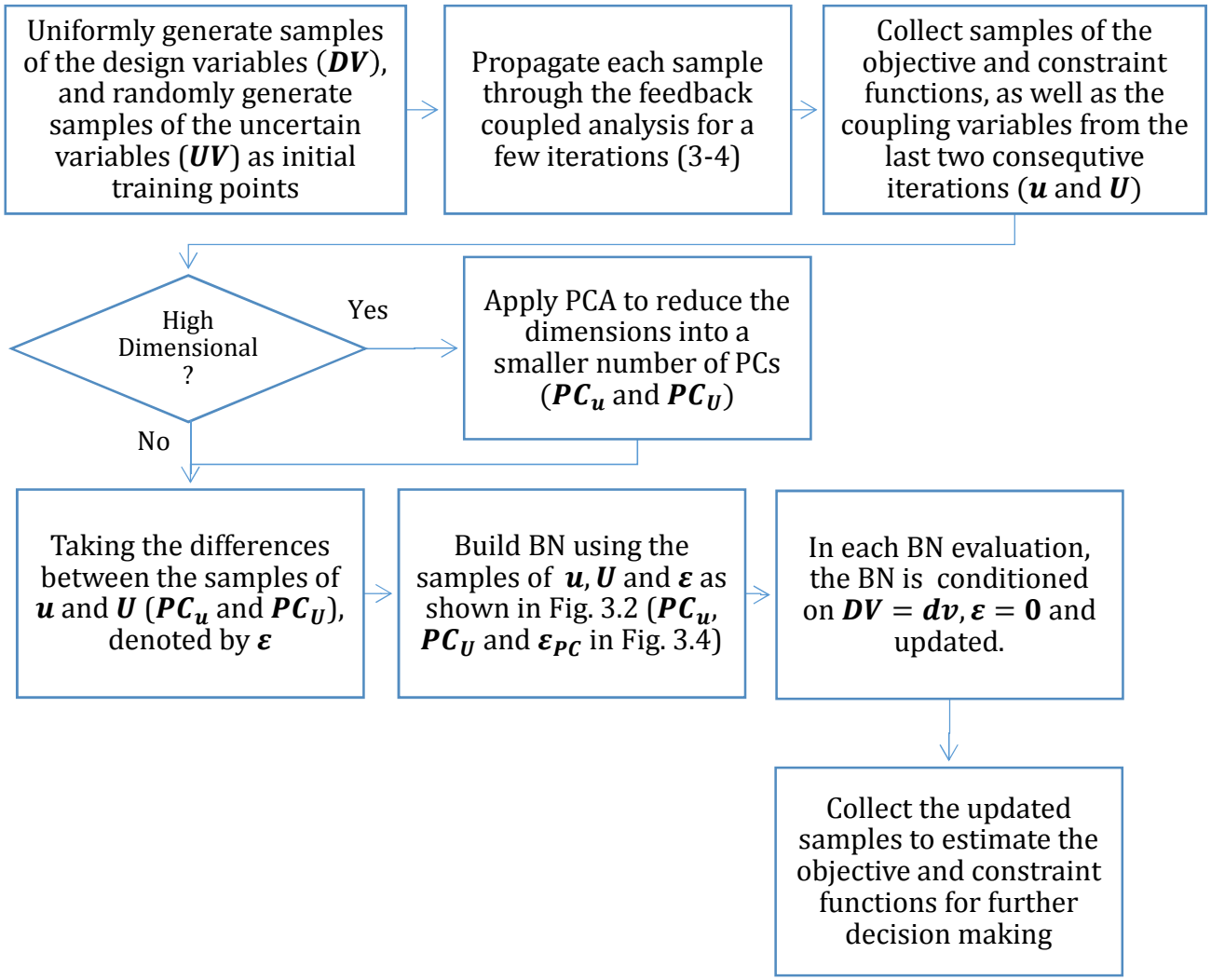

Figure 5.5. Flowchart for BNC-MDO

5.5. NUMERICAL EXAMPLES

In this section, the proposed BNC-MDO methodology is illustrated using a mathematical example, an electronic packaging design problem, and an aero-elastic wing

design problem, all through RBDO formulations. The optimization algorithm Dividing RECTangles (DIRECT) [97] is used as the optimizer in all three problems.

5.5.1 MATHEMATICAL EXAMPLE

The mathematical example in Section 3.4.1 is modified by adding analyses and system level outputs and is shown in **Figure 5.6**. A feedback coupling exists between "Analysis 1" and "Analysis 2", and the coupling variables are denoted as u_{12} and u_{21}. Then the subsystem output g_1 and g_2 are calculated and used as the inputs to analysis 3 to compute the system level output f. The bounds for the design variables x_1 to x_5 are $[0.8, 1.2]$. For the sake of illustration, input variability as normal distribution $N(0, 0.02)$ is assumed for all design variables.

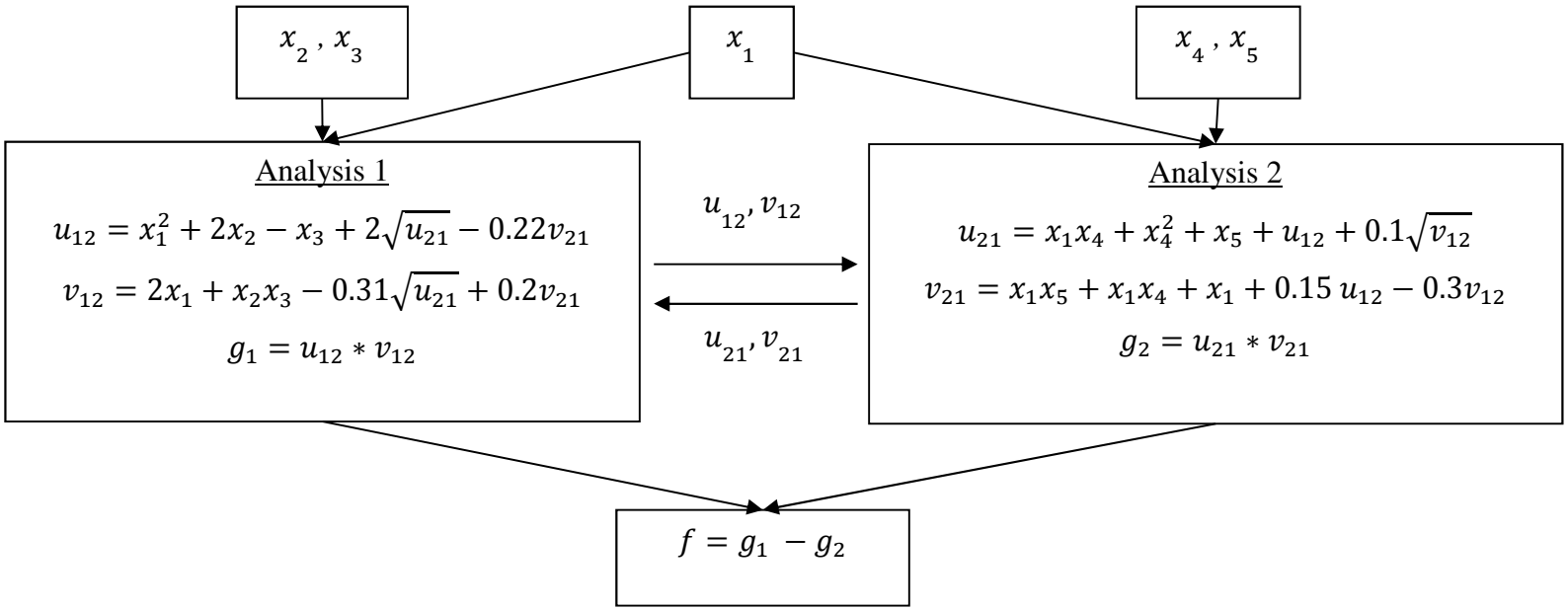

Figure 5.6 Functional relations of the mathematical MDA model

In the context of deterministic optimization, the system level output f is used as the objective, whereas the disciplinary outputs g_1 and g_2 are adopted as constraints. Due to the input variability, the objective and constraints are stochastic quantities. Therefore, an RBDO formulation is constructed as shown in Eq. (5.5):

$$\begin{aligned} & \min_{\mu_{x_i}} \mu_f \\ s.t. \quad & P(g_1 < 24.6) \geq 0.9 \\ & P(g_2 < 48.2) \geq 0.9 \\ & 0.8 \leq \mu_{x_i} \leq 1.2 \\ & P(x_i \geq 0.8) \geq 0.9 \\ & P(x_i \leq 1.2) \geq 0.9 \\ & i = 1, \dots, 5 \end{aligned} \tag{5.5}$$

$$\begin{aligned} U_{12}(\boldsymbol{x}, u_{21}, v_{21}) - u_{12} &= 0 \\ V_{12}(\boldsymbol{x}, u_{21}, v_{21}) - u_{12} &= 0 \\ U_{21}(\boldsymbol{x}, u_{12}, v_{12}) - u_{21} &= 0 \\ V_{21}(\boldsymbol{x}, u_{12}, v_{12}) - v_{21} &= 0 \end{aligned}$$

where the last four equation indicates the interdisciplinary compatibility being satisfied for each realization of $\boldsymbol{x}$. The upper-case letters denote the functions that compute the coupling variables, whereas the lower-cases represent a realization of the corresponding variable. 200 samples of x_1 to x_5 are uniformly generated from their design spaces using Latin Hypercube sampling method. For each realization of $\boldsymbol{x}$, one iteration of the analysis as shown in **Figure 5.7** is executed to calculate samples of the coupling variables u_{12}, v_{12}, U_{21}, V_{21} and output variables , g_1, g_1 and f.

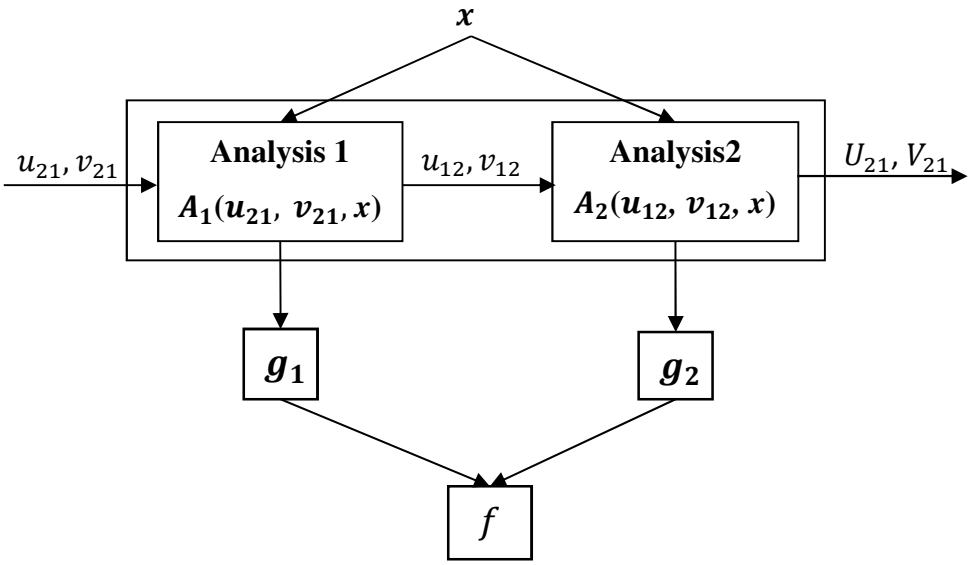

Figure 5.7. One iteration of feedback coupled analysis

The differences between U_{21}, V_{21} and u_{21}, v_{21} are then computed and denoted as $diff_{U_{21}}$ and $diff_{V_{21}}$. Samples of the input, coupling and output variables together with $diff_{U_{21}}$ and $diff_{V_{21}}$ are used to build the Bayesian network as explained in Section 5.3. **Figure 5.8** shows the Bayesian network built using these samples.

After the BN is constructed, the optimization framework is applied on top of the BN, and the DIRECT algorithm is employed as mentioned earlier. The maximum number of iterations for DIRECT is set to be 15. In each design cycle, the optimizer delivers a design value to the network. $x_1 \dots x_5$ are conditionalized at the design values. Meanwhile, $diff_{u_{21}}$ and $diff_{v_{21}}$ need to be enforced as 0 such that the interdisciplinary compatibility condition is satisfied. Update the network using vine copula-based sampling and obtain the posterior distribution of g_1, g_2 and f, based on which the objective and constraints in Eq. (5.5) are calculated.

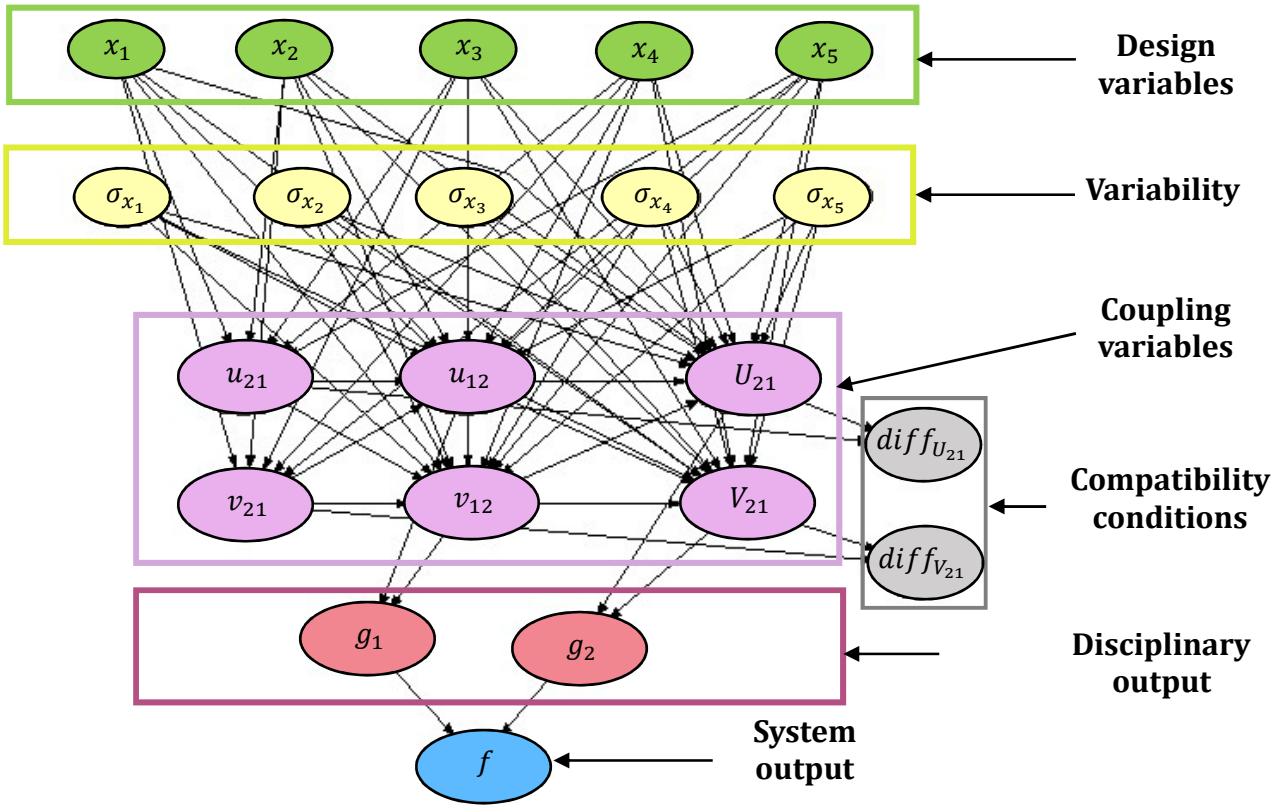

Figure 5.8 BN based on the samples from Fig. 5.7

An optimization using the SOFPI (Monte Carlo sampling outside fixed point iteration) approach is also implemented, and the results are used as the benchmark solution. 10,000 samples are used to estimate the objective and constraint in each design cycle. A total of 6,260,000 function evaluations is required, which is much more beyond the 400 function evaluations that required by BNC-MDO. **Figure 5.9** compares the optimization histories of the two approaches, which agree well with each other.

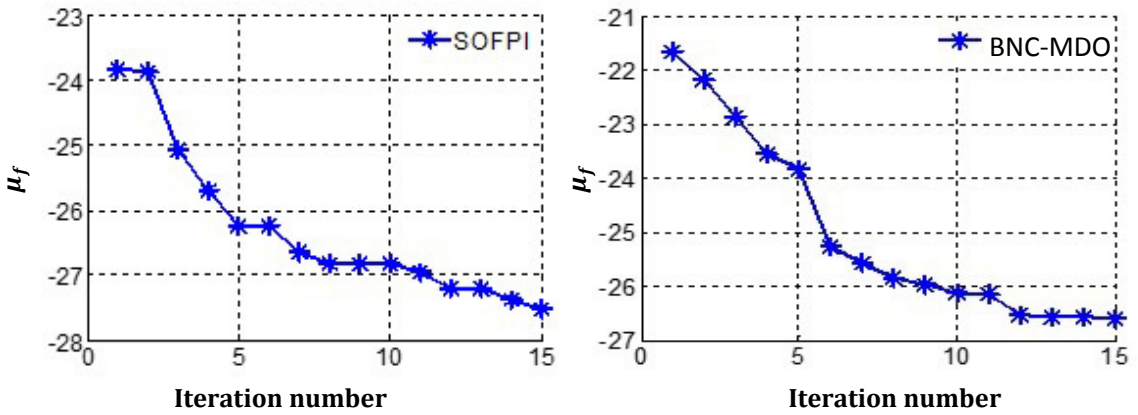

Figure 5.9 Optimization histories of SOFPI and BNC-MDO

Table 5.1 compares the RBDO result of SOFPI (column 3, benchmark) and the proposed BNC-MDO approach (column 4). The optimal solution obtained by BNC-MDO (merged column 4 and 5) is also evaluated by SOFPI (column 5) to check its accuracy.

Table 5.1. Comparison of the optimization results using SOFPI and BNC-MDO

100 Samples	Variable	RBDO using SOFPI	BNC-MDO	Re-evaluated
Design Variables	x_1	1	0.87	
	x_2	0.82	0.80	
	x_3	0.82	0.84	
	x_4	1.19	1.18	
	x_5	1	1.15	
Objective	$\boldsymbol{\mu_f}$	**-27.52**	**-26.60**	**-25.48**
Constraint	$P(g_1 < 24.6)$	1.00	1.00	1.00
	$P(g_2 < 48.2)$	0.93	0.90	1.00

It can be observed from **Table 5.1** that the difference between the optimal objectives obtained by the two methods is only 7.4%, which is quite small considering only 400 function evaluations (i.e., 200 each for Analysis 1 and Analysis 2) are required for the proposed BNC-MDO approach compared to SOFPI which needs more than 6 million.

Also, the differences for x_2, x_3 and x_4 are also very small (less than 5%), but the differences between values for x_1 and x_5 are comparably larger (13% and 15% respectively). This is because optimization with SOFPI uses the fully converged analysis for each design evaluation, whereas the BNC-MDO is trained using only partially converged samples. Next, two engineering examples are used to demonstrate the proposed BNC-MDO approach.

5.5.2 ELECTRONIC PACKAGING DESIGN

The electronic packaging problem [61] described in Section 2.6.2 is used in this sub-section as a design problem to demonstrate the BNC-MDO approach. Coupling variables are heat generated by the electrical analysis, and the heatsink temperature calculated by the thermal analysis. A detailed problem description can be found in Section 2.6.2.

In this chapter, geometric parameters x_1, x_2, x_3 and x_4 are considered as the design variables, of which the upper and lower bounds are ub = [0.15, 0.15, 0.08, 0.05] and lb = [0.05, 0.05, 0.02, 0.01]. The design variables are assumed to have variability as given in where y_2 is the resistance of the resistor at temperature T_1, which is a constant. y_4 and y_5 are the coupling variables between the two analyses. y_4 is the component heat and y_5 is

the heatsink temperature. The design variables are assumed to have variability as given in **Table 5.2**. x_5 and x_6 are additional uncertain variables the same as provided in **Table 2.5**.

The goal of optimization is to maximize the mean power density of the heatsink (ratio between the heat dissipation and the volume of the heat sink) while maintaining the size and working temperature of the heatsink at low values. Therefore, the RBDO formulation is constructed as below:

$$
\begin{aligned}
& x_i^* = argmax\, \mu_{WD}(x_i) \\
& s.t. \\
& P(Temp < 56^oC \cap Volume < 6 \times 10^{-4}\, m^3) \geq 0.95 \\
& lb_i \leq x_i \leq ub_i,\ i = 1, \dots, 4 \\
& Thermal(y_4, \boldsymbol{x}) - y_5 = 0 \\
& y_2 y_5^2 - y_4 = 0
\end{aligned}
\tag{5.6}
$$

where y_2 is the resistance of the resistor at temperature T_1, which is a constant. y_4 and y_5 are the coupling variables between the two analyses. y_4 is the component heat and y_5 is the heatsink temperature.

Table 5.2: Parameters of the electronic packaging system

	Physical meaning	Uncertainty
x_1	Heat sink width (m)	$N(0, 0.01)$
x_2	Heat sink length (m)	$LogN(0, 0.01)$
x_3	Fin length (m)	$N(0, 0.005)$
x_4	Fin width (m)	$N(0, 0.0025)$

The coupling variable heatsink temperatures (Temp in **Figure 5.10**) from two consecutive iterations are computed to implement the BNC-MDO approach. For the sake of comparison, the numbers of the input samples are chosen as 800, 1000 and 1200. Thus, the total number of function evaluations required are 1600, 2000 and 2400 respectively. A Bayesian network is built as shown in **Figure 5.10**.

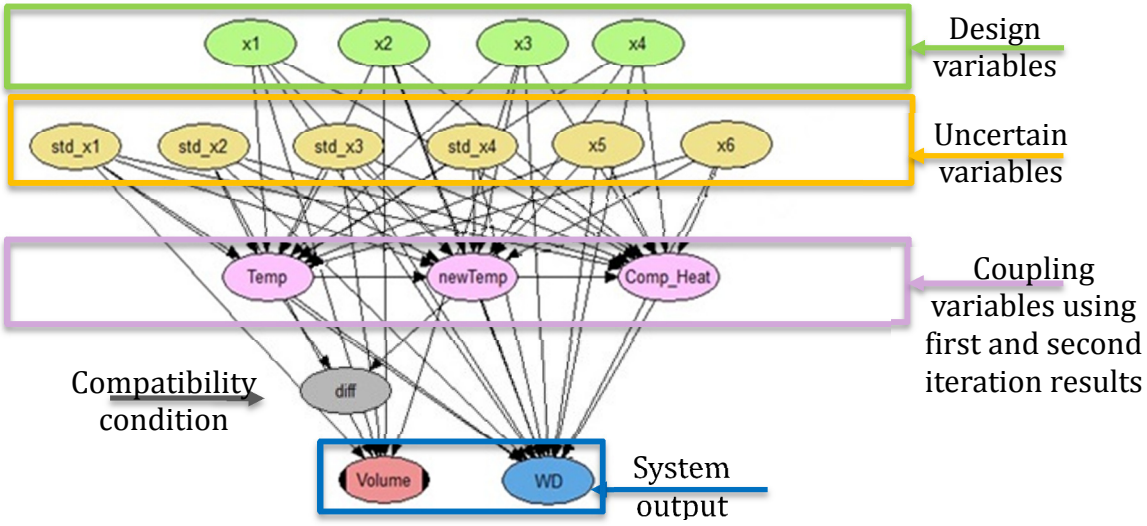

Figure 5.10 BBN for the electronic packaging problem

Optimization with SOFPI is also implemented, and the results are used as the benchmark solution. 10,000 samples are used to estimate the objective and constraint in each design cycle. Fixed-point-iteration (FPI) takes an average of 5 iterations to converge. DIRECT optimization algorithm is applied, and due to the limited computational resource, only 10 iterations is implemented. A total of 6,950,000 function evaluations is required for

optimization with the SOFPI approach, which takes about 4 hours to accomplish on a desktop computer. Whereas once the BN is built with the training samples (obtained from the 1st and 2nd iterations, takes 5 seconds for 800 samples), the average time for the optimization process is less than 5 minutes.

Rows 1- 5 in **Table 5.3** compare the RBDO results with SOFPI (column 2), and with the proposed BNC-MDO approach with different numbers of BN training samples (column 3,4 and 5). Rows 6-7 list the re-evaluation of BNC-MDO result using SOFPI.

Table 5.3. Comparison of the optimization results using SOFPI and BNC-MDO with different number of training samples

		Benchmark	**Number of training points for BN**		
			800	**1000**	**1200**
x_1		0.056	0.052	0.056	0.051
x_2		0.056	0.052	0.052	0.051
x_3		0.021	0.021	0.021	0.020
x_4		0.039	0.024	0.048	0.037
Objective: μ_{WD}		73172	73781	78600	70000
re-evaluate with SOFPI	**objective**	N/A	84997	78749	93131
	constraint		0.962	0.965	0.984

It can be observed from **Table 5.3** that although the optimal values of x_1 to x_4 and the optimum obtained by the proposed BNC-MDO approach with different numbers of training samples are close to the benchmark solution (differences mostly less than 10%), the re-evaluation results shows that the proposed methodology is able to find higher values of the power density (objective is maximized) than the SOFPI approach. Based on the

optimal solutions, it can be seen that the objective values are very sensitive to all four design variables. Therefore, the 'benchmark' solution may be suboptimal due to insufficient number of samples used in the Monte Carlo sampling, and/or insufficient number of optimization iterations, since only 10 iterations of the optimization algorithm are performed, and the number of samples for reliability assessment is only 10,000 as mentioned above.

Inclusion of model error

The solution above already includes data uncertainty (sparse and interval data of x_6). The proposed methodology can also incorporate stochastic model error, through the auxiliary variable method described in Section 2.4.2. The same electronic packaging problem is solved again considering the discretization error (and the stochastic Gaussian process model output as mentioned in Section 2.6.2) as described below.

(1) Generate samples of inputs and initial values of temperature and run through one iteration analysis as in **Figure 5.3**.

(2) For each input realization, the finite difference analysis code (for thermal analysis) with different mesh sizes is executed, and the GP extrapolation technique is used with the three solutions to estimate the 'correct' value (i.e., corrected for discretization error). The output temperature is a normal random variable, of which the mean is the GP estimate of the correct value, and the variance represents the uncertainty associated with this estimate.

(3) To account for the stochastic GP output, an auxiliary variable P_h is introduced. For each normal distribution of the GP prediction, one realization of P_h is randomly generated from a uniform distribution $U[0,1]$. Take the inverse CDF

of the normal distribution with respect to P_h to get a realization of the prediction (temperature).

(4) Use the samples for input, output, coupling and the auxiliary variables to build a BN as shown in **Figure 5.11**.

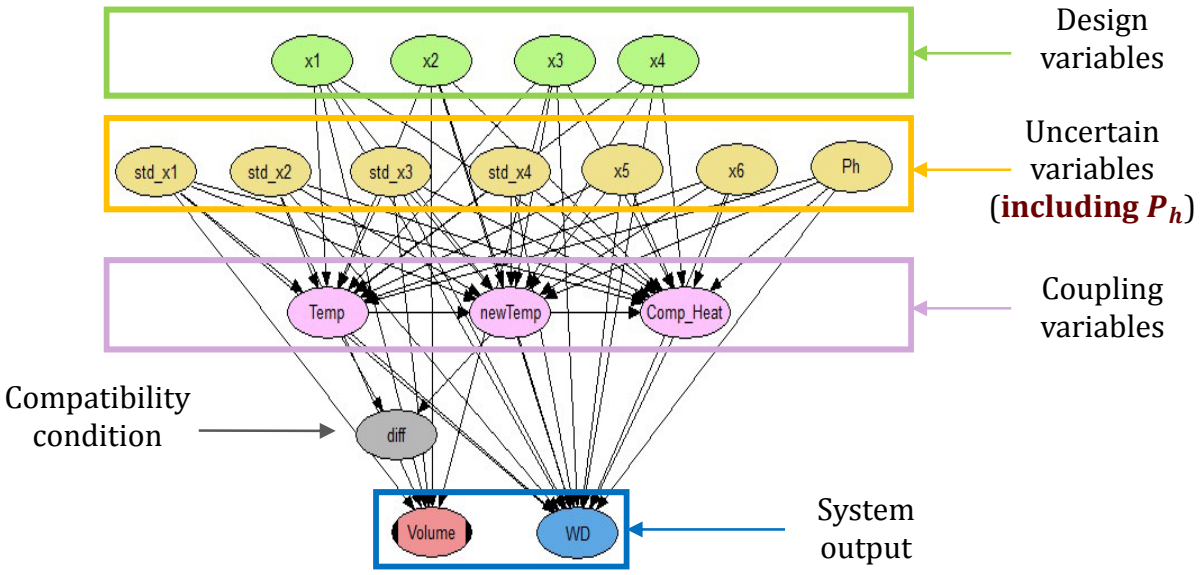

Figure 5.11 BN for MDA with stochastic model error

Then BNC-MDO is implemented with this BN, and the result is shown in **Table *5.4***. When the stochastic model output is considered, the fixed-point-iteration method can barely converge. Therefore, the benchmark solution with SOFPI is unaffordable for this problem. This further shows the advantage of the proposed BNC-MDO approach, which does not required any fully converged analysis from the physics codes.

Thus it can be seen that the BNC-MDO is capable of incorporating stochastic model error since the auxiliary variable method represents the model error as an additional random variable.

Table 5.4 Optimization results considering discretization error and stochastic GP output

x_1	x_2	x_3	x_4	μ_{WD}
0.077	0.149	0.021	0.010	11,170

5.5.3 AERO-ELASTIC WING DESIGN

The design optimization of a three-dimensional aeroelastic wing described in Section 3.4.2 is performed here using the proposed BNC-MDO approach. The backsweep angle is appointed as the design variable with design bounds as [0, 0.5]. The mesh size is chosen such that the total number of nodes on the surface of the structure is 258. 200 realizations of the backsweep angle are uniformly sampled to perform the fluid-structure interaction analysis using the CFD and FEA analyses. For full convergence analysis using fixed point iteration (FPI), the average number of iterations is 8, and the total time for running the converged aeroelastic analyses for all 200 input realizations is 8.5 hours.

Since the values of nodal pressure oscillate drastically in the first and second iterations, in order to balance the solution accuracy and the computational efficiency, the Bayesian network is built with the nodal pressure results of the 3rd and 4th iterations. (This means that in the BNC-MDO approach, the FSI analysis is terminated after 4 iterations). For 200 samples, a total of 5.5 hours is needed, which is 3 hours less and 1600 function evaluations (i.e., 800 each of FEA and CFD analyses) fewer than the performing the full convergence analysis with fixed point iteration. Note that this is the time required for collecting training samples for the BN. Once the samples are collected, the Bayesian network can be built within 10-15 seconds; thus the time for stochastic analysis is negligible compared to the time required for the aeroelastic analysis.

The design optimization problem is to maximize the lift subject to a stress constraint. The backsweep angle is assumed to have variability described by a Gaussian distribution with zero mean and a standard deviation of 0.03 radians. The optimization problem (RBDO) is given in Eq. (5.7).

$$\max_{\mu_{bw}} E[L]$$

s.t

$$P[S \geq 3 * 10^5\ Pa] \leq 10^{-3} \qquad (5.7)$$

$$0 \leq \mu_{bw} \leq 0.5$$

where *bw* is the backsweep angle. To apply the proposed BNC-MDO approach, two successive iteration values of the coupling variables 'Nodal Pressures' are used to build the BN, along with the design and uncertain variables and the objective and constraint. Because the coupling variables are large in number (258 nodal pressures), building the Bayesian network with such data will be problematic. Therefore, the dimension reduction strategy

using PCA introduced is implemented to reduce the dimension of the Bayesian network, such that the building and sampling of the BN is affordable. The PCA is applied on the nodal pressures after 3rd and 4th iterations (denoted by NP_3 and NP_4), and the first 30 principal components are selected since 99.6% of the total variance from the original samples can be covered by them. The BN is built with the input, output and the coupling variables represented by the 30 principal component following the strategy in **Figure 5.4**, and the resulting BN is as shown in **Figure 5.12**.

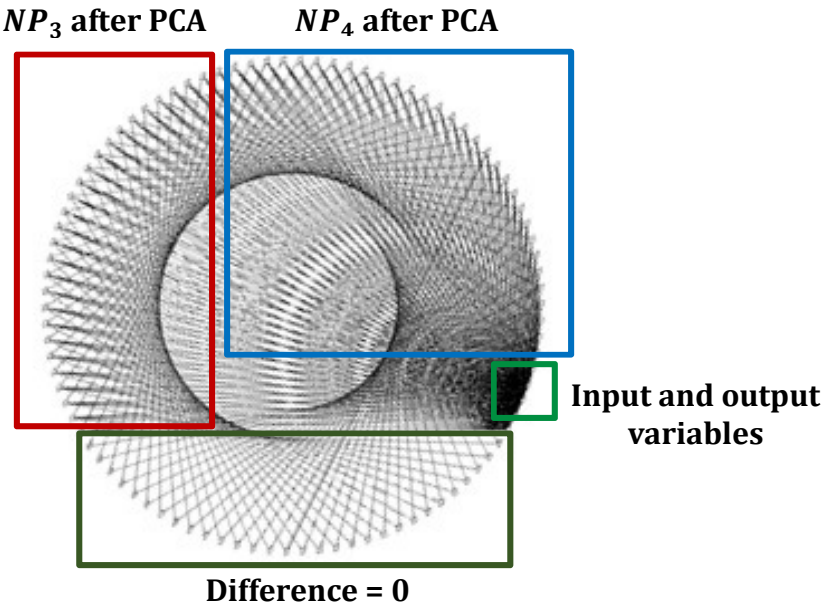

Figure 5.12. BN of the aeroelastic wing with reduced coupling variables

The RBDO is then performed using the BN above. The DIRECT algorithm stops after 10 iterations, requiring 67 calls to the BN surrogate model and 547 seconds of computational time. The BNC-MDO results are shown in **Table 5.5**.

Table 5.5. Optimal solution of the aero-elastic wing design

		BNC-MDO
Design variable	μ_{bw}	0.405
Objective	μ_{lift}	1707.5
Constraint	$P(stress)$	0.998

No benchmark solution is provided for this problem since SOFPI is unaffordable to implement using the aeroelastic codes. Note that MDO can also be performed using other surrogate models, such as Kriging, neural network, regression models, etc. However, the training samples for the other surrogate models require fully converged physics analyses, whereas the training samples for the BN surrogate model only require a few iterations of the feedback-coupled analysis; thus the BN surrogate model approach based on the LAMDA concept achieves much more computational savings. Moreover, as mentioned earlier, the savings will become more prominent when higher fidelity models are used for the individual disciplinary analyses, and when more iterations are needed for MDA convergence.

5.6. SUMMARY

This chapter proposed a novel Bayesian network-based approach for multidisciplinary design optimization under uncertainty. The Bayesian network is constructed for two purposes: (1) as a probabilistic surrogate model based on input-output samples from a few iterations of the original disciplinary analyses, and (2) to perform design evaluation and enforce interdisciplinary compatibility *simultaneously* using conditional sampling. Once the BN is built as a surrogate model, both MDA and design evaluation are achieved simultaneously during each time the BN is called by the optimizer. The proposed methodology only requires a few iterations of the coupled analysis from the physics codes, instead of the full convergence analysis, thus providing tremendous computational advantage

Further computational efficiency is achieved through the vine copula-based sampling technique and the Bayesian network dimension reduction using principal component analysis. A mathematical RBDO example, an electronic packaging design problem, and an aeroelastic wing design problem were used to demonstrate the proposed methodology.

CHAPTER 6

CONCLUSION

The central goal of this dissertation was to develop novel strategies for reducing the computational effort while maintaining accuracy in multidisciplinary analysis and design optimization under uncertainty. To achieve this goal, four objectives were pursued: (1) propagation of epistemic uncertainty — data uncertainty and model error — through multidisciplinary analysis; (2) Investigation of a methodology for uncertainty propagation in a high-dimensional coupled system; (3) Development of a framework to incorporate different sources of uncertainty in single disciplinary design optimization, considering multiple objectives; and (4) Investigation of a Bayesian methodology for the design optimization of multidisciplinary systems with feedback coupled analyses. The main accomplishments are summarized below.

6.1. ACCOMPLISHMENTS

6.1.1 MDA UNDER EPISTEMIC UNCERTAINTY

Chapter 2 presented a new methodology to systematically include both aleatory and epistemic uncertainty in the input variables, and the epistemic uncertainty due to model

errors, within feedback-coupled MDA. This methodology offers a comprehensive framework for the representation and propagation of multiple sources of uncertainty within MDA, using the LAMDA concept, which estimates the probability of the the interdisciplinary compatibility condition being satisfied given a value of the coupling variable.

First, a likelihood-based approach is employed to represent both variability and data uncertainty in the input random variables (due to sparse and/or imprecise data) through non-parametric distributions, which is consequently propagated within the MDA framework using methods such as Monte Carlo sampling, FORM and SORM.

Then, an auxiliary variable method based on the probability integral transform is proposed to include the effect of stochastic model error in coupled MDA. This method brings the epistemic uncertainty to the same level of analysis as input variability such that the propagation of both aleatory and epistemic uncertainty can be implemented in a single loop manner. The proposed methodology provides a general formulation to include both model form error and numerical errors (e.g., discretization error, surrogate model error, etc.) within feedback coupled MDA. A mathematical problem and an electronic packaging application were used to illustrate the proposed methodology.

The auxiliary variable approach also provides a breakthrough in global sensitivity analysis, which previously was only used in the context of aleatory uncertainty and for feed-forward problems.

6.1.2 MDA WITH HIGH-DIMENSIONAL FEEDBACK COUPLING

The original LAMDA approach was implemented using FORM (first-order reliability method), and has difficulty in solving high-dimensional problems, since the accuracy and computational efficiency deteriorate as the number of the coupling variables increases. Therefore, Chapter 3 proposed an efficient implementation of the LAMDA concept using Bayesian network and copula sampling for high-dimensional MDA, in the presence of a large number of coupling variables.

The Bayesian network is adopted to estimate the joint probability distribution of the coupling variables given interdisciplinary compatibility. This is similar to the concept of Bayesian updating, and a Gaussian copula-based sampling technique is adopted to generate samples from the conditioned Bayesian network (i.e., conditioned on zero difference between two successive iteration values of the coupling variables) and to estimate the conditional joint distribution of the coupling variables.

When the dimension of the coupling is so large that incorporating all the coupling variables in one Bayesian network becomes computationally cumbersome, principal component analysis is adopted to decrease the dimensionality of the Bayesian network. A mathematical MDA example and an aeroelastic wing analysis example were used to demonstrate the efficiency and accuracy of this BNC-MDA approach. It can be seen from the example that, the PCA compresses a BN with hundreds or thousands of nodes into a BN with 30 to 60 nodes (i.e., using 10 to 20 principal components) without sacrificing too much accuracy.

In the proposed methodology, each sample only requires a few iterations of the coupled physics analysis instead of a fully converged solution as in fixed point iteration. Thus the proposed BNC-MDA approach is promising for high-dimensional problems.

6.1.3 MULTI-OBJECTIVE OPTIMIZATION UNDER UNCERTAINTY

Chapter 4 further develops the use of Bayesian network and vine copula sampling as a probabilistic surrogate model for multi-objective optimization under uncertainty and BN training point selection.

The first innovation is to construct the Bayesian network as a probabilistic surrogate model based on input-output samples from the original model. A vine copula-based sampling technique is used for efficient uncertainty propagation. A vehicle side impact problem is used to demonstrate the proposed methodology. For a given set of design values, the joint probability of multiple constraints and objectives are efficiently estimated using the proposed BNC approach, by exploiting the forward propagation capability of the Bayesian network.

The second novelty is the training point selection technique to construct the Bayesian network. Additional training points are generated in the desired region based on sculpting, which exploits the dependence relations among the inputs and outputs, and the inverse propagation capability of the Bayesian network. This sculpting further refines the BN model and improves the Pareto surface for multi-objective optimization.

6.1.4 MULTIDISCIPLINARY OPTIMIZATION UNDER UNCERTAINTY

Chapter 5 developed a comprehensive framework for multidisciplinary design optimization under uncertainty. The BNC-MDA technique proposed in Chapter 3 and probabilistic graphical surrogate modeling introduced in Chapter 4 were integrated for the optimization of feedback coupled MDA under uncertainty.

In this framework, the Bayesian network is pursued for two purposes: (1) as a probabilistic surrogate model based on the dependence relations among the input, output and the coupling variables, and (2) to perform stochastic MDA/MDO with samples from only a few iterations of the feedback coupled analysis, without the fully converged physics analysis. The BNC approach simultaneously enforces interdisciplinary compatibility and evaluates the optimization objectives and constraints through conditional sampling, without any further evaluations of the original physics models. Further efficiency is achieved by adopting the vine copula-based technique for generating samples from the conditioned Bayesian network efficiently. A mathematical RBDO example, an electronic packaging design problem and an aeroelastic wing design problem were used to demonstrate the proposed methodology.

6.2. LIMITATIONS OF THE RESEARCH

In this research, the Bayesian network with Gaussian copula-based sampling is heavily used. The Gaussian copula adopts a linear correlation assumption for the CDFs of different random variables. However, since correlation does not imply causation, the proposed approach has confronted challenges especially when dealing with non-monotonic function analysis. To overcome such challenge, different copula assumptions may need to be applied on different correlations among each pair of the random variables, and the vine-based strategy needs to be investigated for the purpose of efficient sampling.

6.3. FUTURE WORK

Future research based on this dissertation can be pursued in the following directions:

(1) The performance of the BNC-MDA approach for realistic problems with higher dimensions needs to be evaluated. The proposed approach has been shown effective for the aero-elastic wing example with 1218 nodes; however, in reality, the dimension of the coupling variables can be of the order of several thousands. The scalability of the proposed methodology thus needs to be investigated by solving larger problems.

(2) The extension of the BNC-MDA methodology needs to be investigated for multi-level analyses, and multi-disciplinary feedback coupled analyses for more than two

disciplines. The adaptability of the proposed methodology for more complex configurations of coupled systems also needs to be investigated.

(3) More sources of uncertainty should be included in the proposed methodology. The probabilistic graphical model estimates the distribution with the marginal distributions of variables, and the correlations between them. The marginal distributions can be discrete, continuous and empirical distributions. This means that the graphical model is capable of incorporating different forms of uncertainty. Therefore, future study should extend the proposed methodology to incorporate model and data uncertainty sources.

(4) The optimization methods explored in this dissertation used a reliability-based formulation (RBDO). The extension of the Bayesian network-based approach to robustness-based design optimization under both aleatory and epistemic uncertainty also needs to be explored in the future.

(5) In the optimization problems, sample-based strategy was used to compute the constraint probabilities (for RBDO problems). Future work can incorporate analytical multi-normal integration of the Gaussian copula instead of the sampling-based strategy, thus further improving the efficiency of reliability assessment and optimization.

(6) The proposed methods have been currently implemented using the Gaussian copula assumption. If the Gaussian copula assumption is not justified, then non-Gaussian copulas need to be used. Efficiency improvements in the presence of non-Gaussian copulas need to be studied, since sampling with non-Gaussian copula is very time-consuming.

(7) All the problems considered in this dissertation were time-independent. Future work needs to investigate the extension of the proposed techniques to time-dependent problems.

BIBLIOGRAPHY

[1] Cramer, E. J., Dennis, J. E., Frank, P. D., and Shubin, G. R., "Problem Formulation for Multidisciplinary Optimization Problem Formulation for Multidisciplinary Optimization," *Siam Journal Optimization*, vol. 4, pp. 754–776, 1993.

[2] Kroo, I., Altus, S., Braun, R., Gage, P., and Sobieski, I., "Multidisciplinary optimization methods for aircraft preliminary design," *NASA Technical Report*, 1994.

[3] Belytschko, T., "Fluid-structure interaction," *Computers & Structures*, vol. 12, pp. 459–469, 1980.

[4] Thornton, E. a., "Thermal structures - Four decades of progress," *Journal of Aircraft*, vol. 29, pp. 485–498, 1992.

[5] Wieting, A. R., Dechaumphai, P., Bey, K. S., Thornton, E. a., and Morgan, K., "Application of integrated fluid-thermal-structural analysis methods," *Thin-Walled Structures*, vol. 11, pp. 1–23, 1991.

[6] Sobieszczanski-Sobieski, J., and Haftka, R., "Multidisciplinary aerospace design optimization: survey of recent developments," *Structural optimization*, vol. 14, pp. 1–23, 1997.

[7] Rebba, R., Mahadevan, S., and Huang, S., "Validation And Error Estimation Of Computational Models," *Reliability Engineering & System Safety*, vol. 91, pp. 1390–1397, 2006.

[8] Haldar, A., and Mahadevan, S., *Probability, Reliability, And Statistical Methods In Engineering Design*, John Wiley, 2000.

[9] Du, X., and Chen, W., "Collaborative Reliability Analysis under the Framework of Multidisciplinary Systems Design," *Optimization and Engineering*, vol. 6, pp. 63–84, 2005.

[10] Mahadevan, S., and Smith, N., "Efficient First-Order Reliability Analysis of Multidisciplinary Systems," *International Journal of Reliability and Safety*, vol. 1, pp. 137–154, 2006.

[11] Sankararaman, S., and Mahadevan, S., "Likelihood-Based Approach to Multidisciplinary Analysis Under Uncertainty," *Journal of Mechanical Design*, vol. 134, p. 031008, 2012.

[12] Liang, C., Sankararaman, S., and Mahadevan, S., "Stochastic Multi-Disciplinary Analysis under Epistemic Uncertainty," *Journal of Mechanical Design*, vol. 137, pp. 1–38, 2015.

[13] Valdebenito, M. a., and Schuëller, G. I., "A survey on approaches for reliability-based optimization," *Structural and Multidisciplinary Optimization*, vol. 42, pp. 645–663, 2010.

[14] Du, X., and Chen, W., "Sequential Optimization and Reliability Assessment Method for Efficient Probabilistic Design," *Journal of Mechanical Design*, vol. 126, p. 225, 2004.

[15] Noh, Y., Choi, K. K., and Du, L., "Reliability-based Design Optimization of Problems with Correlated Input Variables using A Gaussian Copula," *Structural and Multidisciplinary Optimization*, vol. 38, pp. 1–16, 2008.

[16] Chen, W., Garimella, R., and Michelena, N., "Robust Design for Improved Vehicle Handling Under a Range of Maneuver Conditions," *Engineering Optimization*, vol. 33, pp. 303–326, 2001.

[17] Zaman, K., McDonald, M., Mahadevan, S., and Green, L., "Robustness-based design optimization under data uncertainty," *Structural and Multidisciplinary Optimization*, vol. 44, pp. 183–197, 2011.

[18] Gu, L., Yang, R., Tho, C., Makowskit, M., Faruquet, O., and Li, Y., "Optimisation and robustness for crashworthiness of side impact," *International Journal of Vehicle Design*, vol. 26, p. 348, 2001.

[19] Gu, X., Renaud, J. E., Batill, S. M., Brach, R. M., and Budhiraja, A. S., "Worst Case Propagated Uncertainty of Multidisciplinary Systems in Robust Optimization," *Structural Optimization*, vol. 20, pp. 190–213, 2000.

[20] Li, M., and Azarm, S., "Multiobjective Collaborative Robust Optimization With Interval Uncertainty and Interdisciplinary Uncertainty Propagation," *ASME Journal of Mechanical Design*, vol. 130, 2008.

[21] Jiang, Z., Li, W., Apley, D. W., and Chen, W., "A System Uncertainty Propagation Approach With Model Uncertainty Quantification in Multidisciplinary Design," *ASME 2014 International Design Engineering Technical Conferences and Computers and Information in Engineering Conference*, 2014, pp. V02BT03A029–V02BT03A029.

[22] Huang, H.-Z., and Zhang, X., "Design Optimization With Discrete and Continuous Variables of Aleatory and Epistemic Uncertainties," *Journal of Mechanical Design*, vol. 131, p. 031006, 2009.

[23] Zhang, X., and Huang, H.-Z., "Sequential Optimization and Reliability Assessment for Multidisciplinary Design Optimization under Aleatory and Epistemic Uncertainties," *Structural and Multidisciplinary Optimization*, vol. 40, pp. 165–175, 2009.

[24] Agarwal, H., Renaud, J. E., Preston, E. L., and Padmanabhan, D., "Uncertainty Quantification using Evidence Theory in Multidisciplinary Design Optimization," *Reliability Engineering & System Safty*, vol. 85, pp. 281–294, 2004.

[25] Giunta, A., "Aircraft multidisciplinary design optimization using design of experiments theory and response surface modeling methods," p. 185, 1997.

[26] Kokkolaras, M., Mourelatos, Z. P., and Papalambros, P. Y., "Design Optimization of Hierarchically Decomposed Multilevel Systems Under Uncertainty," *Journal of Mechanical Design*, vol. 128, p. 503, 2006.

[27] Liu, H., Chen, W., Kokkolaras, M., Papalambros, P. Y., and Kim, H. M., "Probabilistic Analytical Target Cascading: A Moment Matching Formulation for Multilevel Optimization Under Uncertainty," *Journal of Mechanical Design*, vol. 128, p. 991, 2006.

[28] Simpson, T. W., Mauery, T. M., Korte, J. J., and Mistree, F., "Kriging Models for Global Approximation in Simulation-Based Multidisciplinary Design Optimization," *AIAA Journal*, vol. 39, pp. 2233–2241, 2001.

[29] Simpson, T. W., Poplinski, J. D., Koch, P. N., and Allen, J. K., "Metamodels for

Computer-based Engineering Design: Survey and recommendations," *Engineering With Computers*, vol. 17, pp. 129–150, 2001.

[30] Liang, C., and Mahadevan, S., "Stochastic Multidisciplinary Analysis with High Dimensional Coupling," pp. 1–6, 2013.

[31] Felippa, C. a., Park, K. C., and Farhat, C., "Partitioned analysis of coupled mechanical systems," *Computer Methods in Applied Mechanics and Engineering*, vol. 190, pp. 3247–3270, 2001.

[32] Michler, C., and Hulshoff, S., "A Monolithic Approach to Fluid–Structure Interaction," *Computers & fluids*, 2004.

[33] Park, K. C., Felippa, C. A., and DeRuntz, J. A., "Stabilization of Staggered Solution Procedures for Fluid-structure Interaction Analysis," *Computational methods for fluid-structure interaction problems*, pp. 95–124, 1977.

[34] Sankararaman, S., and Mahadevan, S., "Likelihood-based representation of epistemic uncertainty due to sparse point data and/or interval data," *Reliability Engineering & System Safety*, vol. 96, pp. 814–824, 2011.

[35] Agarwal, H., Renaud, J. E., Preston, E. L., and Padmanabhan, D., "Uncertainty Quantification using Evidence Theory in Multidisciplinary Design Optimization," *Reliability Engineering & System Safety*, vol. 85, pp. 281–294, 2004.

[36] Helton, J. C., Johnson, J. D., Oberkampf, W. L., and Storlie, C. B., "A sampling-based computational strategy for the representation of epistemic uncertainty in model predictions with evidence theory," *Computer Methods in Applied Mechanics and Engineering*, vol. 196, pp. 3980–3998, 2007.

[37] Du, L., Choi, K. K., Youn, B. D., and Gorsich, D., "Possibility-Based Design Optimization Method for Design Problems with Both Statistical and Fuzzy Input Data," *Journal of Mechanical Design*, vol. 128, pp. 928–935, 2006.

[38] Zhang, X., and Huang, Z., "Sequential Optimization and Reliability Assessment for Multidisciplinary Design Optimization under Aleatory and Epistemic Uncertainties," *Structural and Multidisciplinary Optimization*, vol. 40, pp. 165–175, 2010.

[39] Zadeh, L., "Toward a perception-based theory of probabilistic reasoning with imprecise probabilities," *Journal of statistical planning and inference*, vol. 105, pp. 233–264, 2002.

[40] Ferson, S., Kreinovich, V., Ginzburg, L., Myers, D. S., and Sentz, K., "Constructing Probability Boxes and Dempster-Shafer Structures," 2003.

[41] Matsumura, T., and Haftka, R. T., "Reliability Based Design Optimization Modeling Future Redesign With Different Epistemic Uncertainty Treatments," *Journal of Mechanical Design*, vol. 135, p. 091006, 2013.

[42] Zaman, K., Rangavajhala, S., McDonald, M. P., and Mahadevan, S., "A probabilistic approach for representation of interval uncertainty," *Reliability Engineering and System Safety*, vol. 96, pp. 117–130, 2011.

[43] Du, L., Choi, K. K., Youn, B. D., and Gorsich, D., "Possibility-Based Design Optimization Method for Design Problems with Both Statistical and Fuzzy Input Data," *Journal of Mechanical Design*, vol. 128, p. 928, 2006.

[44] Zadeh, L. A., "Toward a perception-based theory of probabilistic reasoning with imprecise probabilities," vol. 105, pp. 233–264, 2002.

[45] Sankararaman, S., "Significance, interpretation, and quantification of uncertainty in prognostics and remaining useful life prediction," *Mechanical Systems and Signal Processing*, vol. 52-53, pp. 228–247, 2013.

[46] Mahadevan, S., and Liang, B., "Error and Uncertainty Quantification and Sensitivity Analysis in Mechanics Computational Models," *International Journal for Uncertainty Quantification*, vol. 1, pp. 147–161, 2011.

[47] Kennedy, M. C., and O'Hagan, A., "Bayesian calibration of computer models," *Journal of the Royal Statistical Society: Series B (Statistical Methodology)*, vol. 63, pp. 425–464, 2001.

[48] Zaman, K., Rangavajhala, S., McDonald, M. P., and Mahadevan, S., "A Probabilistic Approach for Representation of Interval Uncertainty," *Reliability Engineering & System Safety*, vol. 96, pp. 117–130, 2011.

[49] Saltelli, A., Ratto, M., Andres, T., Campolongo, F., Cariboni, J., Gatelli, D., Saisana, M., and Tarantola, S., *Global sensitivity analysis: the primer*, Wiley-Interscience, 2008.

[50] McKeeman, W. M., "Algorithm 145: Adaptive Numerical Integration by Simpson's Rule," *Communications of the ACM*, vol. 5, p. 604, 1962.

[51] Mahadevan, S., and Rebba, R., "Inclusion of Model Errors in Reliability-Based Optimization," *Journal of Mechanical Design*, vol. 128, p. 936, 2006.

[52] Chen, W., Baghdasaryan, L., Buranathiti, T., and Cao, J., "Model validation via uncertainty propagation and data transformations," *AIAA journal*, vol. 42, pp. 1403–1415, 2004.

[53] Sankararaman, S., Ling, Y., Shantz, C., and Mahadevan, S., "Inference of equivalent initial flaw size under multiple sources of uncertainty," *International Journal of Fatigue*, vol. 33, pp. 75–89, 2011.

[54] Huang, S., Mahadevan, S., and Rebba, R., "Collocation-based stochastic finite element analysis for random field problems," *Probabilistic Engineering Mechanics*, vol. 22, pp. 194–205, 2007.

[55] Clarke, S. M., Griebsch, J. H., and Simpson, T. W., "Analysis of Support Vector Regression for Approximation of Complex Engineering Analyses," *Journal of Mechanical Design*, vol. 127, p. 1077, 2005.

[56] Wang, G. G., and Shan, S., "Review of Metamodeling Techniques in Support of Engineering Design Optimization," *Journal of Mechanical Design*, vol. 129, p. 370, 2007.

[57] Hombal, V., and Mahadevan, S., "Bias Minimization in Gaussian Process Surrogate Modeling for Uncertainty Quantification," *International Journal for Uncertainty Quantification*, vol. 1, pp. 321–349, 2011.

[58] Zhu, P., Zhang, S., and Chen, W., "Multi-point objective-oriented sequential sampling strategy for constrained robust design," *Engineering Optimization*, pp. 1–21, 2014.

[59] Pearson, E., "The probability integral transformation for testing goodness of fit and combining independent tests of significance," *Biometrika*, vol. 30, pp. 134–148, 1938.

[60] Sankararaman, S., and Mahadevan, S., "Separating the contributions of variability and parameter uncertainty in probability distributions," *Reliability Engineering & System Safety*, vol. 112, pp. 187–199, 2012.

[61] Padula, S., Alexandrov, N., and Green, L., "MDO test suite at NASA Langley Research Center," *AIAA Paper*, pp. 1–13, 1996.

[62] Rangavajhala, S., Sura, V., Hombal, V., and Mahadevan, S., "Discretization Error Estimation in Multidisciplinary Simulations," *AIAA journal*, vol. 49, pp. 2673–2683.

[63] Zhang, R., and Mahadevan, S., "Model Uncertainty and Bayesian Updating in Reliability-Based Inspection," *Structural Safety*, vol. 22, pp. 5–9, 2000.

[64] Mahadevan, S., and Rebba, R., "Validation of Reliability Computational Models using Bayes Networks," *Reliability Engineering & System Safety*, vol. 87, pp. 223–232, 2005.

[65] Jiang, X., and Mahadevan, S., "Bayesian Probabilistic Inference for Nonparametric Damage Detection of Structures," *Journal of Engineering Mechanics*, vol. 134, pp. 820–831, 2008.

[66] Jiang, X., and Mahadevan, S., "Bayesian Hierarchical Uncertainty Quantification by Structural Equation Modeling," *International Journal for Numerical Methods in Engineering*, vol. 80, pp. 717–737, 2009.

[67] Cooke, R., and Kurowicka, D., "Continuous/Discrete Non-Parametric Bayesian Belief Nets With Unicorn and Uninet," *Proceedings of Mathematical Methods in Reliability MMR*, 2007.

[68] Ale, B. J. M., Bellamy, L. J., van der Boom, R., Cooper, J., Cooke, R. M., Goossens, L. H. J., Hale, A. R., Kurowicka, D., Morales, O., Roelen, A. L. C., and Spouge, J., "Further Development of A Causal Model for Air Transport Safety (CATS): Building the Mathematical Heart," *Reliability Engineering & System Safety*, vol. 94, pp. 1433–1441, 2009.

[69] Doucet, A., Godsill, S., and Andrieu, C., "On Sequential Monte Carlo Sampling Methods for Bayesian Filtering," *Statistics and Computing*, pp. 197–208, 2000.

[70] Friedman, N., "The Bayesian Structural Em Algorithm," *Proceedings of the Fourteenth Conference on Uncertainty in Artificial Intelligence*, Morgan Kaufmann Publishers Inc., 1998.

[71] Nelsen, R. B., *An introduction to copulas*, Springer, 1999.

[72] Bouyé, E., and Durrleman, V., "Copulas for Finance-A Reading Guide and Some Applications," *Available at SSRN 1032533*, 2000.

[73] Choi, K., Noh, Y., and Lee, I., "Reliability-Based Design Optimization with Confidence Level for Problems with Correlated Input Distributions," *6th China-Japan-Korea Joint Symposium on Optimization of Structural and Mechanical Systems*, 2010.

[74] Kurowicka, D., and Cooke, R. M., "Vines and Continuous Non-parametric Bayesian Belief Nets with Emphasis on Model Learing," *Rethinking Risk Measurement and Reporting I*, 2010, pp. 295–330.

[75] Jolliffe, I. T., "Principal Component Analysis and Factor Analysis," *Principal Component Analysis*, 2002, pp. 150–166.

[76] Ditlevsen, O., "Narrow Reliability Bounds for Structural Systems," *Journal of*

Structural Mechanics, vol. 7, pp. 453–472, 1979.

[77] Jiang, X., and Mahadevan, S., "Bayesian Inference Method for Model Validation and Confidence Extrapolation," *Journal of Applied Statistics*, vol. 36, pp. 659–677, 2009.

[78] Coelho, R., Breitkopf, P., and Knopf-Lenoir, C., "Model Reduction for Multidisciplinary Optimization-Application to a 2D Wing," *Structural and Multidisciplinary Optimization*, vol. 37, pp. 29–48, 2008.

[79] Du, X., and Chen, W., "Efficient Uncertainty Analysis Methods for Multidisciplinary Robust Design," *AIAA journal*, vol. 40, pp. 545–552, 2002.

[80] Kullback, S., and Leibler, R. A., "On Information and Sufficiency," *The Annals Of Mathematical Statistics*, vol. 22, pp. 79–86, 1951.

[81] Abbott, I., and Doenhoff, A. Von, *Theory of Wing Sections: Including A Summary of Airfoil Data*, Dover Publications, Inc, 2012.

[82] Marler, R. T., and Arora, J. S., "Survey of Multi-Objective Optimization Methods for Engineering," *Structural and Multidisciplinary Optimization*, vol. 26, pp. 369–395, 2004.

[83] Mavrotas, G., "Effective implementation of the ??-constraint method in Multi-Objective Mathematical Programming problems," *Applied Mathematics and Computation*, vol. 213, pp. 455–465, 2009.

[84] Deb, K., Pratap, A., Agarwal, S., and Meyarivan, T., "A Fast and Elitist Multiobjective Genetic Algorithm: NSGA-II," *IEEE Transactions on Evolutionary Computation*, vol. 6, pp. 182–197, 2002.

[85] Knotters, M., Brus, D. J., and Oude Voshaar, J. H., "A Comparison of Kriging, Co-Kriging and Kriging Combined with Regression for Spatial Interpolation of Horizon Depth with Censored Observations," *Geoderma*, vol. 67, pp. 227–246, 1995.

[86] Rangavajhala, S., and Mahadevan, S., "Joint Probability Formulation for Multiobjective Optimization Under Uncertainty," *Journal of Mechanical Design*, vol. 133, p. 051007, 2011.

[87] Zhang, Y., Monder, D., and Fraser Forbes, J., "Real-time Optimization under Parametric Uncertainty: A Probability Constrained Approach," *Journal of Process Control*, vol. 12, pp. 373–389, 2002.

[88] Liang, C., and Mahadevan, S., "Stochastic Multidisciplinary Analysis with High-Dimensional Coupling," *10th World Congress on Structural and Multidisciplinary Optimization*, 2013.

[89] Jones, D., Schonlau, M., and Welch, W., "Efficient global optimization of expensive black-box functions," *Journal of Global optimization*, vol. 13, pp. 455–492, 1998.

[90] Roger M. Cooke, Thomas A. Zang, Dimitri N. Mavris, J. C. T., "Sculpting: A Fast, Interactive Method for Probabilistic Design Space Exploration and Margin Allocation," *16th AIAA/ISSMO Multidisciplinary Analysis and Optimization Conference*, 2015.

[91] Liu, Y., Chen, W., Arendt, P., and Huang, H.-Z., "Toward a Better Understanding of Model Validation Metrics," *Journal of Mechanical Design*, vol. 133, p. 071005, 2011.

[92] Hohenbichler, M., and Rackwitz, R., "First-Order Concepts in System Reliability," *Structural Safety*, vol. 1, pp. 177–188, 1983.

[93] Gollwitzer, S., and Rackwitz, R., "An Efficient Numerical Solution to the Multinormal Integral," *Probabilistic Engineering Mechanics*, vol. 3, pp. 98–101, 1988.

[94] Smith, N., and Mahadevan, S., "Integrating system-level and component-level designs under uncertainty," *Journal of spacecraft and rockets*, vol. 42, 2005.

[95] Youn, B. D., Choi, K. K., Yang, R. J., and Gu, L., "Reliability-Based Design Optimization for Crashworthiness of Vehicle Side Impact," *Structural and Multidisciplinary Optimization*, vol. 26, pp. 272–283, 2004.

[96] Chiralaksanakul, A., and Mahadevan, S., "Decoupled Approach to Multidisciplinary Design Optimization under Uncertainty," *Optimization and Engineering*, vol. 8, pp. 21–42, 2007.

[97] Björkman, M., and Holmström, K., "Global optimization using DIRECT algorithm in matlab," *Advanced Modeling and Optimization*, vol. 1, pp. 17–37, 1999.

[98] Rangavajhala, S., Liang, C., Mahadevan, S., "Design Optimization Under Aleatory and Epistemic Uncertainties," *Proceedings of 14TH AIAA/ISSMO Multidisciplinary Analysis and Optimization Conference*, 2012.

[99] Cooke, R. M., "Markov and entropy properties of tree-and vine-dependent variables.," *Proceedings of the ASA Section of Bayesian Statistical Science.*, 1997.

[100] Bedford, T., and Cooke, R. M., "Probability Density Decomposition for Conditionally Dependent Random Variables Modeled by Vines," *Annals of Mathematics and Artificial Intelligence*, vol. 32, pp. 245–268, 2001.

[101] Hanea, A., "Non-Parametric Bayesian Belief Nets versus Vines," *Dependence Modeling: Vine Copula Handbook*, 2010, p. 281.

[102] Yule, G. U., and Kendall, M. g., *An Introduction to the Theory of Statistics*, Belmont,CA: Charles Griffin & Co, 1965.

APPENDIX I. GAUSSIAN PROCESS SURROGATE MODEL

The GP modeling technique has been used in a wide range of applications such as data regression and model calibration. A GP regression or interpolation models the underlying covariance within the data instead of the actual function form. With a set of training points $\boldsymbol{X_T} = \{x_1, x_2, \dots x_n\}$ and the corresponding model outputs: $\boldsymbol{y}_T = \{y_1, y_2, \dots y_n\}$, it is assumed that the true response function is modeled by function:

$$G(\boldsymbol{x}) = \boldsymbol{h}(\boldsymbol{x})^{\boldsymbol{T}}\boldsymbol{\beta} + Z(\boldsymbol{x}) \tag{A1.1}$$

where $\boldsymbol{h}$ is a trend of the model, $\boldsymbol{\beta}$ is the vector of trend coefficients, and Z is a stationary Gaussian process with zero mean, which indicates the deviation of the model from the trend. The trend function is usually assumed as a constant, and $\boldsymbol{\beta}$ is taken as the mean of the training data $\boldsymbol{y_T}$. The covariance between outputs of the GP Z at two points $\boldsymbol{a}$ and $\boldsymbol{b}$ is defined as:

$$Cov[Z(\boldsymbol{a}), Z)(\boldsymbol{b})] = \sigma_Z^2 \boldsymbol{R}(\boldsymbol{a}, \boldsymbol{b}) \tag{A1.2}$$

where σ_Z^2 is the process variance and $\boldsymbol{R}$ is the correlation function. A squared-exponential function is commonly chosen as the correlation function as below.

$$\boldsymbol{R}(\boldsymbol{a}, \boldsymbol{b}) = exp\left[-\sum_{i=1}^{d} \theta_i (a_i - b_i)^2\right] \tag{A1.3}$$

where d represents the number of the input variables, and θ_i is a length scale parameter that implies the correlation between the points in the i^{th}dimension. A large θ_i value

indicates a stronger correlation. The GP model estimates the mean and variance at point $\boldsymbol{x}$ as:

$$\mu_G(\boldsymbol{x}) = \boldsymbol{h}(\boldsymbol{x})^{\boldsymbol{T}}\boldsymbol{\beta} + \boldsymbol{r}(\boldsymbol{x})^{\boldsymbol{T}}\boldsymbol{R}^{-1}(\boldsymbol{y_T} - \boldsymbol{F\beta}) \tag{A1.4}$$

$$\sigma_G^2(\boldsymbol{x}) = \sigma_z^2 - [\boldsymbol{h}(\boldsymbol{x})^{\boldsymbol{T}} \quad \boldsymbol{r}(\boldsymbol{x})^T]\begin{bmatrix}\boldsymbol{0} & \boldsymbol{F^T}\\ \boldsymbol{F} & \boldsymbol{R}\end{bmatrix}^{-1}\begin{bmatrix}\boldsymbol{h}(\boldsymbol{x})\\ \boldsymbol{r}(\boldsymbol{x})\end{bmatrix} \tag{A1.5}$$

where $\boldsymbol{R}$ is the $t \times t$ matrix of the covariances between $\boldsymbol{X}_T$; $\boldsymbol{F}$ are the $p \times t$ matrix of covariances between $\boldsymbol{X}_P$ and $\boldsymbol{X}_T$ and its transpose.

The parameters σ_Z^2 and $\boldsymbol{\theta}$ are calculated using the maximum likelihood estimation in a log-likelihood format as below:

$$\log[p(\boldsymbol{y_t}|\boldsymbol{R})] = -\frac{1}{n}\log(|\boldsymbol{R}|) - \log(\hat{\sigma}_Z^2) \tag{A1.6}$$

where $|\boldsymbol{R}|$ is the determinant of $\boldsymbol{R}$ and $\hat{\sigma}_Z^2$ is calculated as:

$$\hat{\sigma}_Z^2 = \frac{1}{n}(\boldsymbol{y_T} - \boldsymbol{F\beta})^T\boldsymbol{R}^{-1}(\boldsymbol{y_T} - \boldsymbol{F\beta}) \tag{A1.7}$$

Function evaluations with the GP surrogate model are inexpensive; therefore it can be used to replace an expensive high-fidelity computational model in activities such as model calibration [47] and optimization [98].

APPENDIX II. PROBABILISTIC SURROGATE MODELING WITH BAYESIAN NETWORKS

Bayesian network

A Bayesian network is a directed acyclic graph that represents a multivariate joint probability distribution of random variables using their marginal distributions (nodes) and the conditional probabilities (arrows). The Bayesian network is capable of incorporating heterogeneous marginal distributions (e.g., continuous, discrete, binomial and empirical), and is also able to include functional relationships between the nodes if available. A common usage of the Bayesian network is to infer the posterior distribution of the parameters $\boldsymbol{\theta}$, given the measurement data D, which depends on the parameters $\boldsymbol{\theta}$. The posterior probability of $\boldsymbol{\theta}$ given data D could be evaluated using Bayes' theorem as:

$$f''(\boldsymbol{\theta}) = \frac{\mathcal{L}(\boldsymbol{\theta}) f'(\boldsymbol{\theta})}{\int \mathcal{L}(\boldsymbol{\theta}) f'(\boldsymbol{\theta}) d\boldsymbol{\theta}} \tag{A2.1}$$

where $f'(\boldsymbol{\theta})$ and $f''(\boldsymbol{\theta})$ denote the prior and posterior distributions of $\boldsymbol{\theta}$, whereas $\mathcal{L}(\boldsymbol{\theta})$ represents the likelihood function of $\boldsymbol{\theta}$, which is proportional to $P(D|\boldsymbol{\theta})$.

In this research, the Bayesian network is used as a probabilistic surrogate model that connects the input and output variables through a joint distribution. A simple model shown in **Figure A2. 1(a)** is used to illustrate the proposed approach. The model M has 2 input variables: X_1 and X_2; and 2 output variables: Y_1 and Y_2. Assume that there is correlation between inputs X_1 and X_2, and the outputs Y_1 and Y_2 are correlated as well. Based on the model in **Figure A2. 1(a)**, a Bayesian network is built as shown in **Figure A2. 1(b)**. Each node represents a variable, and the edges denote the dependence relations.

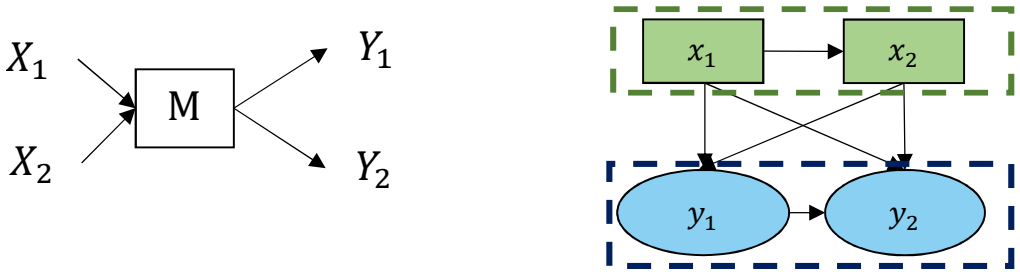

(a) Two-input-two-output model M **(b) BN representation of the model**

Figure A2. 1 Bayesian network representation of a model with input and output variables

In forward uncertainty propagation, for a given realization of the input values (x_1, x_2), the conditional joint distribution of the output variables: $f(Y_1, Y_2 | X_1 = x_1, X_2 = x_2)$ is estimated. This joint distribution is often evaluated using sampling approaches such as MCMC, slice sampling, etc. as mentioned in the introduction. These sampling approaches may be time consuming or even fail to converge when the Bayesian network contains a large number of variables. A vine copula-based strategy is therefore adopted to efficiently generate conditional samples.

Vine copula-based sampling

The vine approach is a way to identify a set of conditional bivariate joint distributions that represent the joint distribution of all the variables in the problem. Detailed theory on vines can be found in [74, 99, 100, 101]. Consider the model shown in **Figure A2. 1(a)**, and assume that samples of X_1, X_2, Y_1 and Y_2 are available. A vine structure can be constructed as shown in **Figure A2. 2**.

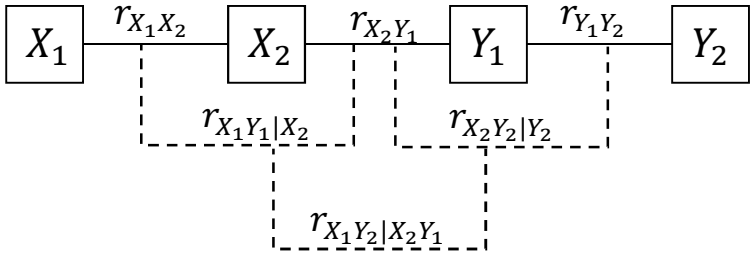

Figure A2. 2 Vine representation of the BN shown in Figure A2. 1

where r_{ij} represent the rank correlations and conditional rank correlations between two variables. The rank correlations represented by the 6 edges in the BN in **Figure A2. 1(b)** are mapped to three non-partial bivariate correlations (solid lines) and three conditional bivariate correlations (dashed lines) in the vine structure. It has been proved that these 6 correlations along with the marginal distributions are able to uniquely define the joint distribution of all the variables in the BN in **Figure A2. 1(b)** [101].

Since the vine approach uniquely represents the multivariate joint distribution using the marginal distributions of the variables and the six correlation terms shown in **Figure A2. 2**, only a *bivariate copula* function C needs to be assumed for each of the bivariate distributions. Note that the choice of copula can be different for different edges in a vine structure. Now, suppose we generate samples of 4 independent uniform random variables u_1, u_2, u_3 and u_4 from the interval [0,1]. The CDF values of each variable in the BN, which are correlated, can be obtained using Eq. A2.2 [74].

$$u_{x_1} = u_1 \tag{A2.2.1}$$

$$u_{x_2|u_{x_1}} = C^{-1}_{U_{X_2}U_{X_1}|u_{x_1}}(u_2) \tag{A2.2.2}$$

$$u_{y_1|u_{x_2}u_{x_1}} = C^{-1}_{U_{Y_1}U_{X_2}|u_{x_2}}\left(C^{-1}_{U_{Y_1}U_{X_1}|u_{x_1}u_{x_2}}(u_3)\right) \tag{A2.2.3}$$

$$u_{y_2|u_{y_1}u_{x_2}u_{x_1}} = C^{-1}{}_{U_{Y_2}U_{Y_1}|u_{y_1}}\left\{C^{-1}_{U_{Y_2}U_{X_2}|u_{y_1}u_{x_2})}\left[C^{-1}_{U_{Y_2}U_{X_1}|u_{y_1}u_{x_2}}(u_4)\right]\right\} \quad \text{(A2.2.4)}$$

where C are bivariate copula functions between the CDF of two variables. Given a realization of u_i, $C^{-1}_{ij|j}$ computes the CDF of i^{th} variable given the CDF(s) of j^{th} variable(s).

$$C_{U_{X_1}U_{X_2}} = P(u_{X_1} \le u_1, u_{X_2} \le u_2) \quad \text{(A2.3)}$$

For the sake of illustration, consider the copula function between X_1 and X_2 in Eq. A2.3:

Given a realization of u_2, and the value of u_{X_1} already generated in Eq. A2.2.1, the CDF of X_2 can be calculated as

Similarly, the CDF values of Y_1 and Y_2, namely u_{Y_1} and u_{Y_2}, can be generated using

$$u_{X_2} = C^{-1}_{U_{X_1}U_{X_2}|u_{X_1}}(u_2) \quad \text{(A2.4)}$$

the bi-variate copulas in Eqs. A2.2.3 and A2.2.4. Once the <u>*correlated*</u> CDF values are generated, the inverse CDF estimation is subsequently taken to obtain the samples of the corresponding variables, as shown in Eq. A2.5.

$$x_1 = F^{-1}_{X_1}(u_{x_1}) \quad \text{(A2.5.1)}$$
$$x_2 = F^{-1}_{X_2}(u_{x_2|u_{x_1}}) \quad \text{(A2.5.2)}$$
$$y_1 = F^{-1}_{Y_1}(u_{y_1|u_{x_2}u_{x_1}}) \quad \text{(A2.5.3)}$$
$$y_2 = F^{-1}_{Y_2}(u_{y_2|u_{y_1}u_{x_2}u_{x_1}}) \quad \text{(A2.5.4)}$$

When the number of variables within the BN (hence the vine structure) is large, this series of inverse copula estimations can be computationally intensive. The assumption of a Gaussian copula provides an analytical solution and avoids the sequential bivariate

estimation, thus making the sampling inexpensive. A Gaussian copula represents the joint CDF of all marginal CDFs using a multivariate Gaussian distribution.

To apply the Gaussian copula, the Spearman's rank correlations between all the pairs of variables are first computed, denoted as r_{ij}. Then, a Pearson's transform is applied to get the conditional linear product moment correlations:

$$\rho_{ij} = 2\sin(\frac{r_{ij}\pi}{6}) \tag{A2.6}$$

As mentioned earlier, the vine structure is a saturated graph, which is not necessarily true for BN. A missing link in the BN can be expressed in a vine structure by setting the corresponding rank correlation (conditional or unconditional) as zero. Subsequently, the conditional product moment ρ also equal to zero. Therefore, the bivariate unconditional linear correlations need to be recalculated with the recursive formula [102]:

$$\rho_{12;3\ldots n} = \frac{\rho_{12;3\ldots,n-1} - \rho_{1n;3,\ldots,n-1} * \rho_{2n;3,\ldots,n-1}}{\sqrt{1-\rho^2_{1n;3,\ldots,n-1}}\sqrt{1-\rho^2_{2n;3,\ldots,n-1}}} \tag{A2.7}$$

A Gaussian copula representing the relationships in Fig. A.1 can be written as:

$$c_R(\boldsymbol{u}) = \frac{1}{\sqrt{\det(R)}}\exp\left(-\frac{1}{2}\begin{pmatrix}\Phi^{-1}(u_1)\\ \Phi^{-1}(u_2)\\ \Phi^{-1}(u_3)\\ \Phi^{-1}(u_4)\end{pmatrix}\cdot(R^{-1}-I)\cdot\begin{pmatrix}\Phi^{-1}(u_1)\\ \Phi^{-1}(u_2)\\ \Phi^{-1}(u_3)\\ \Phi^{-1}(u_4)\end{pmatrix}\right) \tag{A2.8}$$

where Φ^{-1} represents the inverse CDF of a standard normal random variable. $\boldsymbol{u}$ are independent uniform random variables from the interval [0,1]. I is an identity matrix. $\boldsymbol{R}$ is the covariance matrix of the four variables, and since the marginals of the Gaussian copula

are standard normals, $\boldsymbol{R}$ is essentially the correlation coefficient matrix composed of the unconditional product moment correlations ρ_{ij}.

The multivariate Gaussian distribution in Eq. A2.8 can be used to rapidly generate a large number of samples of correlated normal random variables. In this case, samples of 4 variables from this joint normal distribution are generated and denoted as X_1', X_2', Y_1', Y_2'. For each sample of the variables, compute the CDF with respect to the marginal distributions of standard normal distribution, and denote the CDF values as $u_{X_1}, u_{X_2}, u_{Y_1}$ and u_{Y_2}. Samples of X_1, X_2, Y_1 and Y_2 are then obtained by taking the inverse CDFs of $u_{X_1}, u_{X_2}, u_{Y_1}$ and u_{Y_2} with respect to their marginal distributions as shown in Eq. A2.5.

Conditional sampling

The combination of Bayesian network and vine copula-based sampling technique (BNC) helps to formulate a methodology for efficient modeling and sampling of a multivariate joint distribution. To use this framework as a surrogate model, the conditional distributions of outputs $\boldsymbol{y}$ for given values of input $\boldsymbol{x}$ needs to be estimated. Conditionally sampling with the Gaussian copula assumption is very easy to implement since Eq. A2.8 can be converted to conditional Gaussian copula analytically. The procedure is as follows:

For example, the conditional samples of Y_1 and Y_2 need to be generated given $X_1 = x_1, X_2 = x_2$. The equivalent normals corresponding to $X_1 = x_1, X_2 = x_2$ are first calculated as $x_1' = \Phi^{-1}\left(F_{X_1}(x_1)\right), x_2' = \Phi^{-1}\left(F_{X_2}(x_2)\right)$.

Let μ be the mean vector of X_1, X_2, Y_1 and Y_2 in the equivalent normal space $[X_1', X_2', Y_1', Y_2']$; μ is a vector of zeros with 4 entries, and $\boldsymbol{R}$ is the covariance matrix:

$$\boldsymbol{R} = \begin{bmatrix} \overbrace{\begin{matrix} 1 & \rho_{12} \\ & 1 \end{matrix}}^{\boldsymbol{\Sigma_3}} & \overbrace{\begin{matrix} \rho_{13} & \rho_{14} \\ \rho_{23} & \rho_{24} \end{matrix}}^{\boldsymbol{\Sigma_1}} \\ \begin{matrix} & \\ & \end{matrix} & \underbrace{\begin{matrix} 1 & \rho_{34} \\ & 1 \end{matrix}}_{\boldsymbol{\Sigma_2}} \end{bmatrix} \tag{A2.9}$$

Then the conditional joint distribution of Y_1' and Y_2' given $X_1' = x_1', X_2' = x_2'$ is denoted as: $f(Y_1', Y_2' | X_1' = x_1', X_2' = x_2') \sim N(\tilde{\boldsymbol{\mu}}, \tilde{\boldsymbol{\Sigma}})$, where the conditioned mean vector $\tilde{\boldsymbol{\mu}}$ and covariance matrix $\tilde{\boldsymbol{\Sigma}}$ are

$$\tilde{\boldsymbol{\mu}} = \boldsymbol{\Sigma_1 \Sigma_3^{-1}} * \begin{bmatrix} x_1' \\ x_2' \end{bmatrix} \tag{A2.10.1}$$

$$\tilde{\boldsymbol{\Sigma}} = \boldsymbol{\Sigma_2 - \Sigma_1 \Sigma_3^{-1} \Sigma_1^{T}} \tag{A2.10.2}$$

Samples Y_1' and Y_2' are jointly generated from a multivariate normal distribution, of which the mean and covariance matrix are calculated as in Eq. A2.10. The CDF values of each Y_1' and Y_2' sample with respect to the standard normal distribution (u_{Y_1}, u_{Y_2}) are computed, and the inverse CDF is taken to obtained the conditional samples of Y_1 and Y_2 as shown in Eq. A2.5. Thus sampling from the Gaussian copula avoids the evaluation of the series of inverse copula functions in Eq. A2.2, and is very efficient.

Note that the Gaussian copula assumption is only for connecting the CDFs of the random variables, which is less restrictive than assuming a joint Gaussian distribution for the variables themselves. The individual variables can have any arbitrary distribution. Connections between the nodes (i.e. network topology) could be based on the analyst's underlying knowledge of the analysis flow of the model, whereas marginal and conditional probability distributions (and unknown connections) could be learned from data (samples). Therefore, the number of samples needs to be sufficient for an accurate BN model.

A verification approach has been proposed in [101] to test the Gaussian copula assumption. In this verification, samples from the Gaussian copula are generated 100 times. The determinant of the normal rank correlation coefficient matrix is calculated for each set of samples, and the determinants are denoted as $detmat_i,\ i = 1 \ldots 100$. If the determinant based on the original training samples $detmat_{ori}$ lands within 90% of the probability bounds of $detmat_i,\ i = 1 \ldots 100$, the Gaussian copula is assumed valid. Otherwise, the Gaussian copula does not hold, and other copulas need to be investigated. However, if other copulas are chosen, the sampling efficiency of the stochastic analysis will be downgraded since the inverse bivariate copula needs to be evaluated for each sample, and thus the vine approach will become much less efficient. In Chapters 3 to 5, Gaussian copula is adopted in the BNC approach but verified for each numerical example.